AD-A070 362 ARMY ENGINEER WATERWAYS EXPERIMENT STATION VICKSBURG MS F/G 13/2
LIQUEFACTION POTENTIAL OF DAMS AND FOUNDATIONS. REPORT 6. LABOR--ETC(U)
MAR 79 F C TOWNSEND, J P MULILIS

UNCLASSIFIED WES-RR-S-76-2 NL

| OF |
AD
A070362

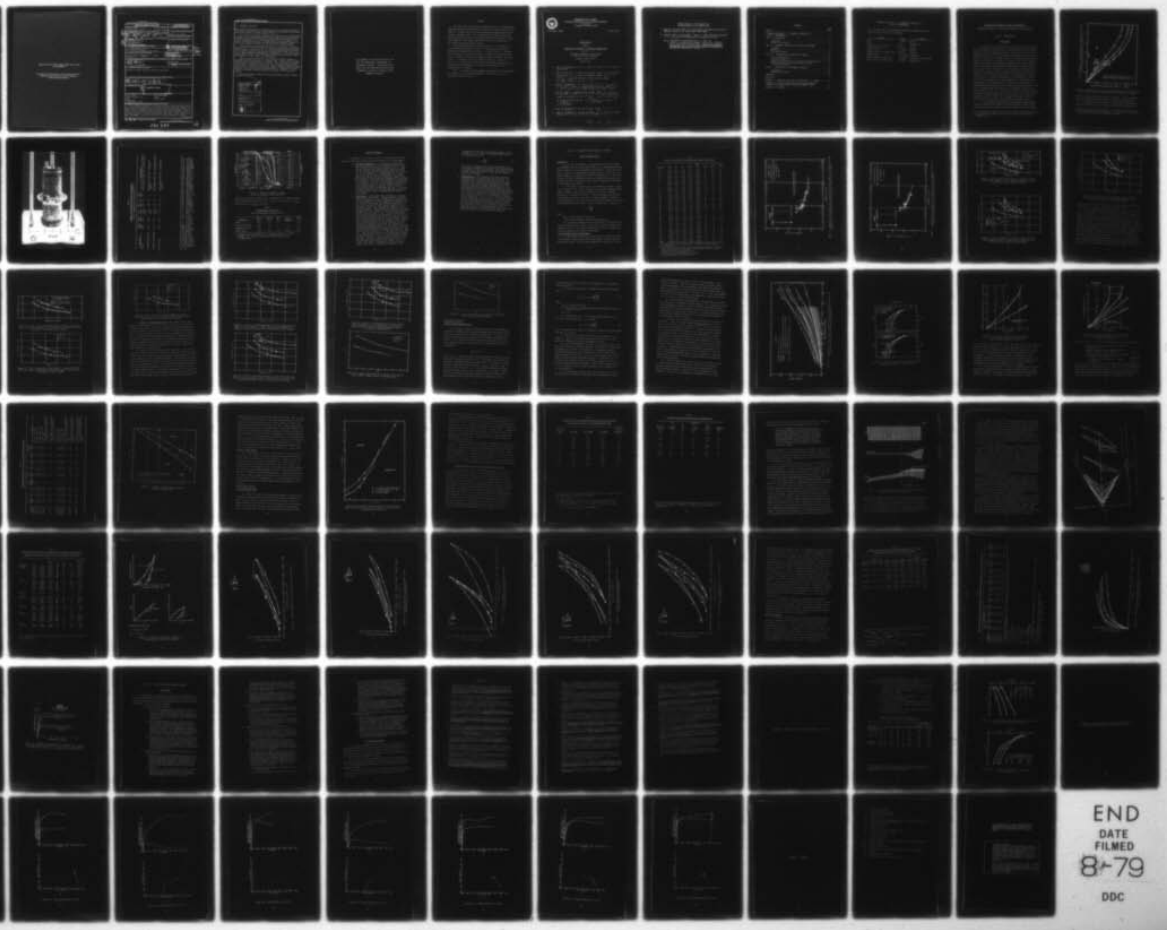

END
DATE
FILMED
8-79
DDC

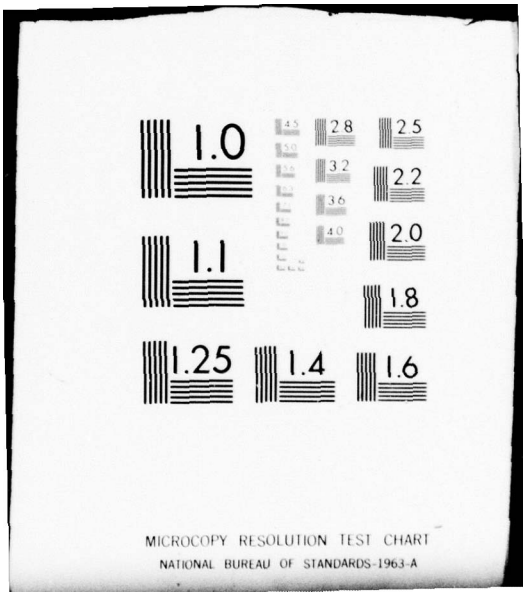
1.0
1.1
1.25
1.4
1.6
1.8
2.0
2.2
2.5
2.8
3.2
3.6
4.0
4.5
MICROCOPY RESOLUTION TEST CHART
NATIONAL BUREAU OF STANDARDS-1963-A

RESEARCH REPORT S-76-2

LIQUEFACTION POTENTIAL OF DAMS AND FOUNDATIONS

Report 6

LABORATORY STRENGTH OF SANDS UNDER STATIC AND CYCLIC LOADINGS

by

Frank C. Townsend, John P. Mulilis

Geotechnical Laboratory
U. S. Army Engineer Waterways Experiment Station
P. O. Box 631, Vicksburg, Miss. 39180

March 1979
Report 6 of a Series

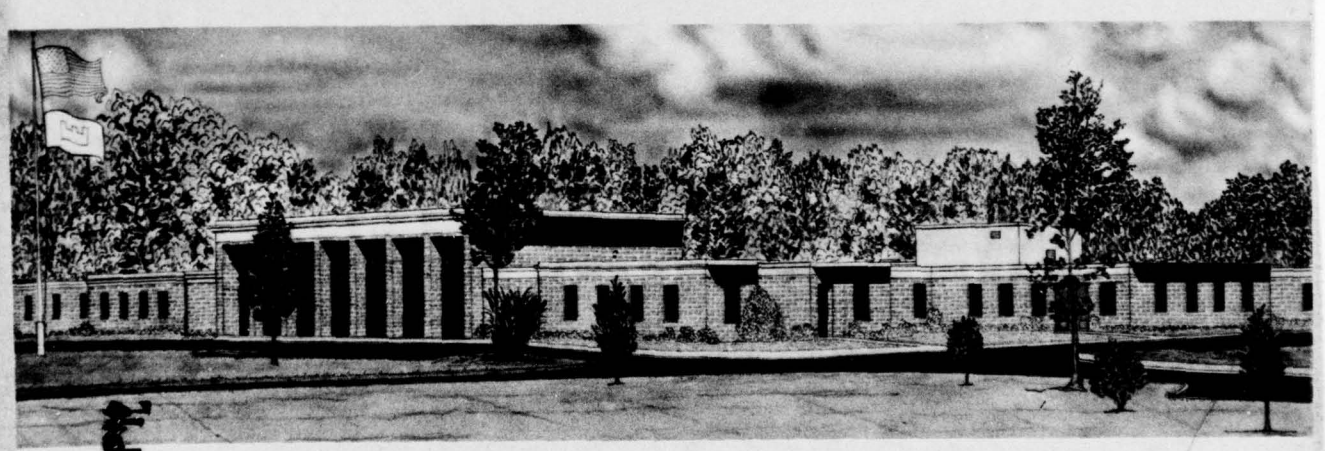

Prepared for Office, Chief of Engineers, U. S. Army
Washington, D. C. 20314

Under Project 4A161102B52E
Task 04, Work Unit CWIS 31145

Destroy this report when no longer needed. Do not return it to the originator.

The findings in this report are not to be construed as an official Department of the Army position unless so designated by other authorized documents.

Unclassified

SECURITY CLASSIFICATION OF THIS PAGE (When Data Entered)

REPORT DOCUMENTATION PAGE

READ INSTRUCTIONS BEFORE COMPLETING FORM

1. REPORT NUMBER: Research Report S-76-2

2. GOVT ACCESSION NO.

3. RECIPIENT'S CATALOG NUMBER

4. TITLE (and Subtitle): LIQUEFACTION POTENTIAL OF DAMS AND FOUNDATIONS; Report 6, Laboratory Strength of Sands Under Static and Cyclic Loadings.

5. TYPE OF REPORT & PERIOD COVERED: Report 6 of a series

6. PERFORMING ORG. REPORT NUMBER

7. AUTHOR(s): Frank C. Townsend, John P. Mulilis

8. CONTRACT OR GRANT NUMBER(s)

9. PERFORMING ORGANIZATION NAME AND ADDRESS: U. S. Army Engineer Waterways Experiment Station, Geotechnical Laboratory, P. O. Box 631, Vicksburg, Miss. 39180

10. PROGRAM ELEMENT, PROJECT, TASK AREA & WORK UNIT NUMBERS: Project 4A161102B52E, Task 04, Work Unit CWIS 31145

11. CONTROLLING OFFICE NAME AND ADDRESS: Office, Chief of Engineers, U. S. Army, Washington, D. C. 20314

12. REPORT DATE: March 1979

13. NUMBER OF PAGES: 93

14. MONITORING AGENCY NAME & ADDRESS (if different from Controlling Office): 94 p.

15. SECURITY CLASS. (of this report): Unclassified

15a. DECLASSIFICATION/DOWNGRADING SCHEDULE

16. DISTRIBUTION STATEMENT (of this Report)

Approved for public release; distribution unlimited.

17. DISTRIBUTION STATEMENT (of the abstract entered in Block 20, if different from Report)

WES-RR-S-76-2

18. SUPPLEMENTARY NOTES: Research rept.

19. KEY WORDS (Continue on reverse side if necessary and identify by block number)

Cyclic loads
Cyclic triaxial tests
Dams
Foundations
Liquefaction (Soils)
R tests (Soils)
Sands
Static loads

20. ABSTRACT (Continue on reverse side if necessary and identify by block number)

The strength decrease due to increased pore pressure, previously referred to as liquefaction potential, of four sands, for which laboratory Standard Penetration Tests (SPT) had previously been performed, was evaluated by cyclic triaxial tests at comparable relative densities and confining pressures. Stress-controlled monotonic R tests were performed on one sand to compare potential for strength loss due to increasing pore pressure under static versus cyclic loading. The object of both test series was to develop correlations between

(Continued)

DD FORM 1 JAN 73 1473 EDITION OF 1 NOV 65 IS OBSOLETE

Unclassified

SECURITY CLASSIFICATION OF THIS PAGE (When Data Entered)

038 100

20. ABSTRACT (Continued).

CONT'

SPT-N values and potential for strength loss due to increasing pore pressure. In addition, material constants for evaluating an elastic-plastic constitutive model were obtained during the monotonic $\bar{R}$ tests.

The results of the cyclic triaxial tests revealed that as the mean grain diameter, D_{50}, and uniformity coefficient decreased, so did the resistance to achieving 100 percent pore pressure response (previously referred to as initial liquefaction), i.e., fine uniform sands are most susceptible to 100 percent pore pressure response. Increasing confining pressures decrease the stress ratio required for achieving 100 percent pore pressure response.

Values of C_N for correcting SPT N-values to an effective overburden pressure of 1 tsf (95.76 kPa) vary with relative density, sand type, and overburden pressure. The value of C_r for correcting isotropically consolidated cyclic triaxial results to estimated field behavior varied from 0.41 to 0.63 for specimens prepared by moist tamping. Nevertheless, a first approximation between cyclic triaxial tests and laboratory SPT N-values was used to extend the data base of τ/σ'_o versus N_1 relationships.

Cyclic triaxial tests produce 100 percent pore pressure response in specimens denser than critical, i.e. dilative sands. However, for this condition to occur, two criteria must be satisfied: (a) a stress reversal through the hydrostatic condition must occur, and (b) a sufficient number of cycles must be applied. Failure in cyclic tests occurs in extension, usually several cycles prior to 100 percent pore pressure response. The same effective stress parameters in monotonic and cyclic triaxial tests are appropriate to define failure; the primary difference between the two tests is the stress path followed.

The elastic-plastic constitutive model qualitatively predicts behavior in monotonic $\bar{R}$ tests.

THE CONTENTS OF THIS REPORT ARE NOT TO BE USED FOR ADVERTISING, PUBLICATION, OR PROMOTIONAL PURPOSES. CITATION OF TRADE NAMES DOES NOT CONSTITUTE AN OFFICIAL ENDORSEMENT OR APPROVAL OF THE USE OF SUCH COMMERCIAL PRODUCTS.

PREFACE

The study reported herein was performed by the U. S. Army Engineer Waterways Experiment Station (WES) as part of the Office, Chief of Engineers, U. S. Army (OCE), Civil Works and Military Engineering and Construction Research effort. This investigation was authorized by OCE under the CWIS 31145 Work Unit entitled "Liquefaction Potential of Dams and Foundations" and Project 4A161102B52E, Task 04, "Liquefaction of Soils Under Static and Dynamic Loads."

The laboratory tests were conducted by Mr. R. D. Barnette with instrumentation assistance from Mr. H. B. Dent under the technical direction and responsibility of Drs. J. P. Mulilis and F. C. Townsend. The verification of the elastic-plastic constitutive equation was done by Dr. B. Rohani. The work was conducted under the general supervision of Mr. C. L. McAnear, Chief, Soil Mechanics Division. Messrs. J. P. Sale and R. G. Ahlvin were Chief and Assistant Chief, respectively, of the Geotechnical Laboratory. This report was prepared by Drs. F. C. Townsend and J. P. Mulilis.

COL J. L. Cannon, CE, was Commander and Director of the WES during the conduct of the study and preparation of this report. Mr. F. R. Brown was Technical Director.

DEPARTMENT OF THE ARMY
WATERWAYS EXPERIMENT STATION, CORPS OF ENGINEERS
P. O. BOX 631
VICKSBURG, MISSISSIPPI 39180

IN REPLY REFER TO: WESGV

14 June 1979

Errata Sheet

No. 1

LIQUEFACTION POTENTIAL OF DAMS AND FOUNDATIONS

Report 6

LABORATORY STRENGTH OF SANDS UNDER
STATIC AND CYCLIC LOADINGS

Research Report S-76-2

March 1979

1. Page 51, paragraph 48, line 10: Change $\tilde{K}'$ and K' to $\tilde{K}$ and K, respectively.

2. Page 53, Figure 32: In lower left drawing, change J_1 (abscissa description) to J_1'; in lower left drawing, change $M/3\sqrt{3} = \alpha$ to $M/3\sqrt{3} = \alpha_1$; and to the left above figure caption, change $J_2' = \frac{1}{2}\left(\sigma_1^2 + 2\sigma_3^2\right)$ to $J_2' = \frac{1}{3}(\sigma_1 - \sigma_3)^2$.

3. Page 59, paragraph 51: In line 3, change K_o', $\tilde{K}'$, K' and K_i' to K_o, $\tilde{K}$, K and K_i, respectively; in line 5, change α to α_1 (twice); and in line 6, change deviation to deviator (twice).

4. Page 61, Table 11: Change column headings K_o'**, $\tilde{K}'$+, K'++, K_i' and α§§ to K_o**, K+, K++, K_i and α_1§§, respectively; change (6th footnote) ‡‡ $W = P/\tilde{K} - \frac{1}{K_o} =$. to ‡‡ $W = P'/\tilde{K} - \frac{1}{K_o}$. ; and change (8th footnote) §§ $\alpha = \frac{2 \sin \phi'}{(3 - \sin \phi')\sqrt{3}}$ to §§ $\alpha_1 = \frac{2 \sin \phi'}{(3 - \sin \phi')\sqrt{3}}$.

5. Page 63, paragraph 51, top line of page: Change ν^1 to ν'.

6. Page 63, paragraph 52: In line 8, change $1/\alpha$ to $1/\alpha_1$; in line 9, change $1/\alpha$ to $1/\alpha_1$; and in line 10, change α to α_1.

Errata Sheet No. 1 (Continued) for
Research Report S-76-2, March 1979

7. Page 63, title for Table 12: Title should read "Numerical Values of Material Constants for Reid-Bedford Model Sand*"

8. Page 64, Table 12 (Concluded): Change α under "Material Constants" to α_1 ; and add the following under closing line of table:

Note: See Table 11 for definitions of W and D_1 .
* After G. Y. Baladi and B. Rohani. April 1979. "Elastic-Plastic Model for Saturated Sands," Journal, Geotechnical Engineering Division, American Society of Civil Engineers, Vol 105, No. GT4, Table 1, p 474.

CONTENTS

CONVERSION FACTORS, U. S. CUSTOMARY TO METRIC (SI)
UNITS OF MEASUREMENT

U. S. customary units of measurement used in this report can be converted to metric (SI) units as follows:

Multiply	By	To Obtain
feet	0.3048	metres
inches	25.4	millimetres
inches of mercury (60° F)	3376.85	pascals
pounds (force)	4.448222	newtons
pounds (force) per square inch	6894.757	pascals
pounds (mass)	0.4535924	kilograms
pounds (mass) per cubic foot	16.01846	kilograms per cubic metre
tons (force) per square foot	95.76052	kilopascals

LIQUEFACTION POTENTIAL OF DAMS AND FOUNDATIONS

LABORATORY STRENGTH OF SANDS UNDER STATIC AND CYCLIC LOADINGS

PART I: INTRODUCTION

Background

1. Evaluation of the potential for strength loss due to increase in pore pressure of cohesionless soil deposits based upon field performance is obviously a meritorious method. In the case of flow slides, Casagrande[1] and Castro[2] have relied upon establishing the critical void ratio as a function of confining pressure to evaluate the contractive or dilative response of a sand deposit. Recently, Seed[3,4] has suggested using a semiempirical procedure for estimating the liquefaction potential for seismically induced ground failure of level ground deposits due to cyclic stress applications. This procedure, guided by earlier studies,[4-8] correlates field performance with in situ characteristics determined by the Standard Penetration Test (SPT) and cyclic stress ratio, which is an indirect measurement of ground shaking. Reliance on the SPT is an extension of early evaluations of the potential for seismically induced ground failure[9] based upon relative density and relationships between penetration resistance and relative density. However, recognizing that most factors (soil structure, coefficient of earth pressure at rest K_o,* as well as density) which tend to improve resistance to ground failure also tend to increase the standard penetration resistance, it might well be expected that an in situ test would be useful as an index of the potential for ground failure.

2. In evaluating the potential for seismically induced ground failure, a design chart (Figure 1) has been prepared in which cyclic stress ratios likely to cause failure are plotted versus SPT N-values

---

* For convenience, symbols are listed and defined in the Notation (Appendix C).

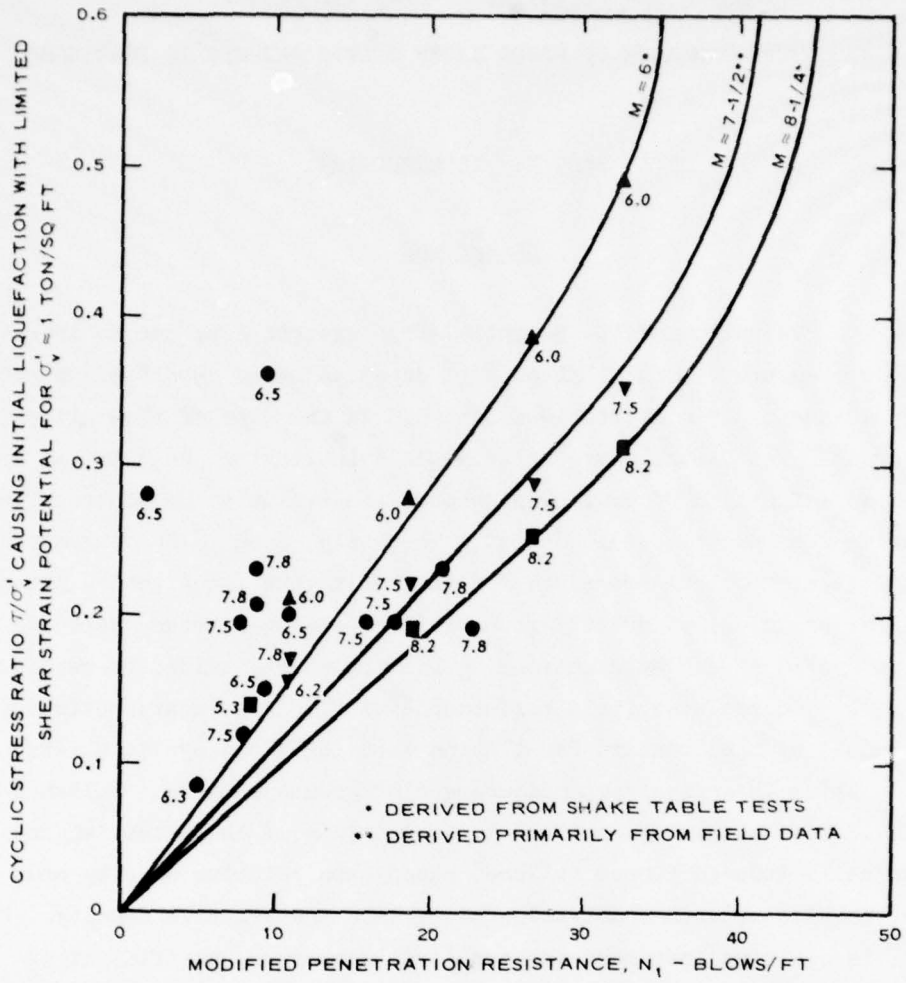

Figure 1. Correlation between field liquefaction behavior of sands for level ground conditions and penetration resistance (from Seed[3])

corrected to an overburden pressure of 1 tsf* N_1. No such correlation has been published for failure caused by monotonic load increases.

3. Introduction of liquefaction in loose sand deposits is not solely restricted to cyclic stresses, as evidenced by numerous flow

---

* A table of factors for converting U. S. customary units of measurement to metric (SI) units is presented on page 4.

slides which have occurred in the absence of earthquakes.[10] Castro,[2] Durham and Townsend[11] have demonstrated in the laboratory that liquefaction under monotonic loadings is highly dependent upon relative density and confining pressure. For relative densities greater than the critical void ratio, dilation occurs; while for densities below the critical void ratio, contraction and liquefaction (100 percent pore pressure response), i.e. flow, can occur. Conversely, cyclic loading in the laboratory has produced 100 percent pore pressure response in test specimens denser than the critical void ratio. Nevertheless, a design chart similar to Figure 1, but for monotonic loading, may be possible.

4. Regardless of the loading condition, understanding liquefaction problems in saturated sands can be assisted by examining the stress-strain pore pressure response, i.e. constitutive properties. In this context, Baladi and Rohani[12] have proposed a preliminary elastic-plastic constitutive relationship for saturated sands for use in boundary value problems. Characterization of their model requires: four material constants, K_i , K_o , K_1 , K_2 , from isotropic compression tests; the elastic shear modulus G ; and slope of the failure envelope M .

Objectives and Scope

5. With the above factors in mind, the objectives of the investigation described herein are:

a. To determine the undrained cyclic triaxial response of Reid-Bedford Model, Ottawa, Platte River, and Standard Concrete sands in order to evaluate relationships between standard penetration resistance of these sands[13,14] and their potential for strength loss due to increased pore pressure.

b. Since the four sands vary to some extent in gradation, mineralogy, particle-shape, and size, to investigate the effect of these variables on the potential of these sands to lose strength because of increasing pore pressures.

c. To determine the undrained cyclic triaxial response of Reid-Bedford Model sand at various densities and confining pressures and to investigate the effects of these

variables on the potential of this sand to lose strength because of increasing pore pressures.

d. To determine the undrained monotonic $\bar{R}$ triaxial response of Reid-Bedford Model sand at various densities and confining pressures, to investigate the effects of these variables on the liquefaction potential of this sand, and to evaluate the critical void ratio.

e. To characterize the confining pressures under monotonic loading and the material parameters, according to Baladi and Rohani's constitutive relationship,[12] for Reid-Bedford Model sand under various densities.

PART II: EQUIPMENT, MATERIALS, AND TESTING PROCEDURES

Equipment

6. In this investigation, sinusoidal cyclic or stepwise increasing monotonic axial loads were applied by a MTS closed-loop testing system. All tests were performed in the load control mode.

7. For the cyclic triaxial test a constant sinusoidal cyclic deviator stress σ_{cd} was applied at a frequency of 1 Hz to fully saturated specimens under undrained conditions until the specimen deformed to a peak-to-peak axial strain of approximately 10 percent. In the monotonically loaded tests, axial load increments of 8 lb were applied at 1-min intervals until an axial compressive strain from 10 to 20 percent was achieved, depending upon whether the specimen dilated or liquefied.

8. In both the cyclic triaxial and monotonic $\bar{R}$ tests, four variables were continuously monitored during each test: axial load, axial deformation, pore pressure, and chamber pressure. An additional variable, radial deformation, was monitored by an LVDT lamp placed at the specimen midheight during the monotonic loading tests to provide data for characterizing the elastic-plastic constitutive model (Figure 2). The variables were monitored with electronic sensors and recorded with a high-speed continuous line recorder. The equipment was carefully calibrated prior to testing. All tests were isotropically consolidated and conducted undrained on remolded specimens approximately 2.8 in. in diameter by 6 in. high.

Materials

9. The majority of all tests were performed on four sands: Reid-Bedford Model, Ottawa, Platte River, and Standard Concrete. The gradation curves of these sands are shown in Figure 3, the pertinent mechanical properties are summarized in Table 1, and the mineralogical compositions are shown in Table 2. In addition to these sands, two check

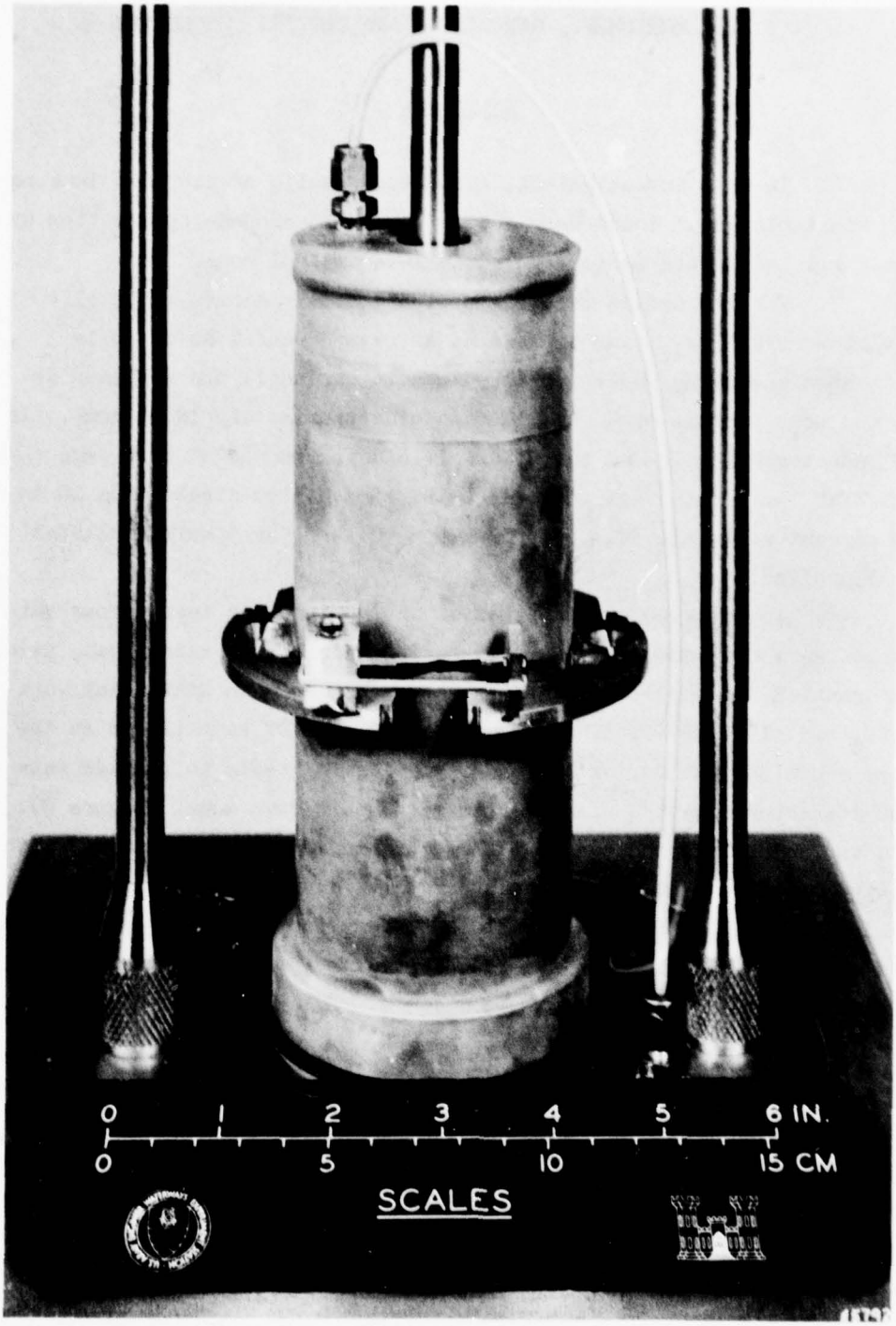

Figure 2. Photograph of LVDT clamp positioned to measure radial deformations

Table 1

Summary of Pertinent Mechanical Properties

(After Bieganousky and Marcuson[13,14])

Material	$\gamma_{d\text{-max}}$ pcf	$\gamma_{d\text{-min}}$ pcf	G_s*	D_{50} mm	C_u	%-#200	Description
Ottawa	109.1	93.0	2.65 (est.)	0.20	1.6	0	Uniform white sand (SP), rounded grains
Reid-Bedford Model	107.1	88.7	2.65 (est.)	0.23	1.8	2	Uniform tan sand (SP), subangular grains
Standard Concrete**	120.6	103.7	2.65 (est.)	0.51	2.5	4	Gap graded sand (SP), subrounded grains
Platte River	122.7	102.8	2.66	2.00	5.3	0	Well graded sand (SP), subrounded grains

* G_s for this investigation: Ottawa = 2.67, Reid-Bedford Model = 2.66, Standard Concrete = 2.66, and Platte River = 2.68.

** A different stockpile of the same Standard Concrete sand used by Bieganousky and Marcuson,[14] was used in this investigation, and the physical properties of this stockpile varied somewhat from the one used by Bieganousky and Marcuson. The properties of the stockpile used in this investigation are as follows: γ_{max} = 116.6 pcf , γ_{min} = 98.2 pcf , D_{50} = 0.42 mm , C_u = 2.2 , %-#200 = 0 , G_s = 2.66 .

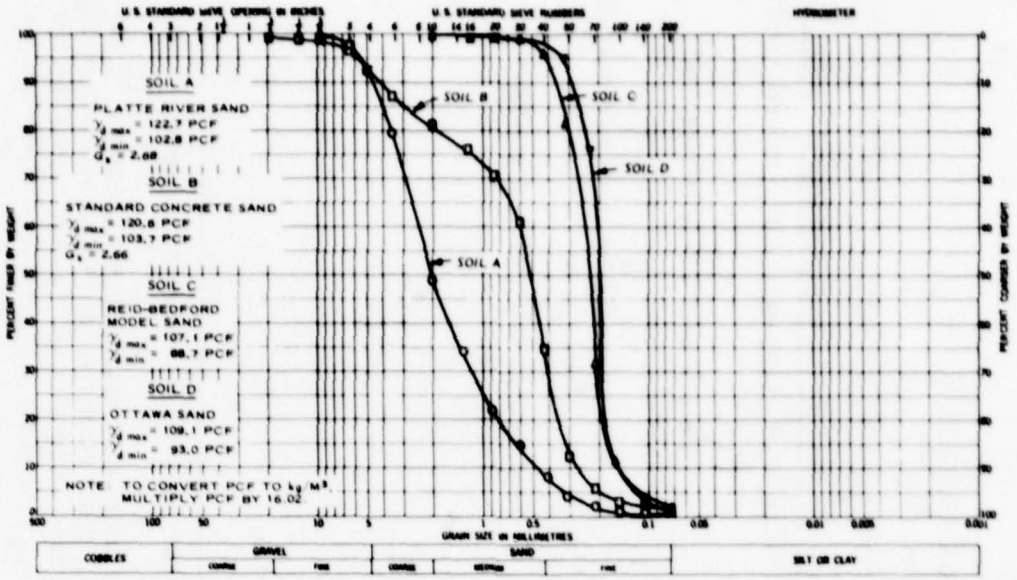

Figure 3. Summary of gradation curves
(after Bieganousky and Marcuson[13,14])

tests were performed on Monterey No. 0 sand, which is a clean, uniform beach and dune sand ($D_{50} \approx 0.36$ mm , $C_u \approx 1.5$, $G_s \approx 2.65$, $\gamma_{d\text{-max}} \approx 105.7$ pcf and $\gamma_{d\text{-min}} \approx 89.3$ pcf) .

Table 2

Mineralogical Composition

(After Bieganousky and Marcuson[13,14])

Material	Quartz %	Feldspar %	Mica %	Rock Fragments	Other* %
Ottawa	98.0	--	--	--	2.0
Reid-Bedford Model	89.1	9.4	--	--	1.5
Standard Concrete	80.3	6.0	--	11.3	2.6
Platte River	53.0	25.3	0.5	18.0	3.2

* Includes calcite, "heavies" (i.e. minerals with $G_s > 2.85$), "opaques (i.e. minerals that do not transmit light), and ferromagnesium.

Testing Procedures

10. Regardless of the type of test to be performed, all specimens were compacted, saturated, and consolidated in the same manner:

a. Specimen preparation. All specimens were remolded to the desired density by a moist-tamping method of compaction described in detail by Mulilis et al.[15] After the specimen had been compacted and sealed by placing the top cap and securing the membrane with an O-ring, 10.2 in. of vacuum (5.0 psi) were applied to the specimen through the top cap. Subsequently, the forming jacket was removed, and the specimen was supported by the vacuum while the height and diameter of the specimen were measured. The height was measured with a dial gage to the nearest 0.001 in., and the diameter was measured to the nearest 0.001 in. at three equally spaced locations (approximately the quarter points) along the specimen with a steel circumferential tape. In the case of the monotonic R tests, an LVDT clamp was positioned at midheight and fixed to the membrane with Devcon 5-min epoxy.

b. Saturation. All specimens were saturated by a process consisting of two phases: seepage saturation and back-pressure saturation. After determining the dimensions of the specimen, the triaxial chamber was assembled, and the vacuum on the sample was gradually increased to 28.5 in. of mercury (14 psi) while a vacuum of 18.3 in. of mercury (9 psi) was simultaneously applied to the triaxial chamber. Thus, although a large vacuum (14 psi) was applied to the specimen, the net effective confining pressure was still only 5 psi. A line containing de-aired, distilled water was then opened to the bottom of the specimen; and water was allowed to seep into the soil very slowly, displacing the air in the specimen. When water had completely filled the specimen voids and about 100 cc had been allowed to seep through the soil, the valve in the waterline was closed; the vacuum on the specimen was gradually reduced to zero; and the top line of the specimen was exposed to the atmosphere, while the vacuum on the chamber was simultaneously reduced to zero and a positive pressure of 5 psi was applied to the chamber. Thus, the net effective confining pressure acting on the specimen was still 5 psi. Back-pressure saturation was then used to ensure complete saturation of the specimen. Typically, complete saturation of the soil was obtained with a back pressure ranging from 30 to 80 psi. The degree of saturation for this testing is expressed in terms of Skempton's B-parameter. The

B-parameter is the ratio of the induced change in pore pressure (Δu) to a change in chamber pressure ($\Delta\sigma_c$) in an undrained state, i.e.

$$B = \frac{\Delta u}{\Delta \sigma_c} \tag{1}$$

The value was determined by closing the drainage line, increasing the chamber pressure by 10 psi, and observing the increase in pore water pressure. The B-values of all specimens ranged from 0.94 to 1.00, with the majority being 0.96 or greater.

c. Consolidation. After saturation had been achieved, specimens were consolidated under the effective confining pressures at which they would be tested. Consolidation was accomplished by increasing the chamber pressure, while allowing such drainage that the final difference between the chamber pressure and the back pressure was the desired effective confining pressure. In the monotonic $\bar{R}$ tests at effective confining pressures of 40 and 80 psi, an isotropic compression load-rebound test (ICL-R) was conducted by isotropically loading to a consolidation pressure (σ_3) of 30 and 60 psi, respectively, rebounding to $\sigma_3 = 5$ psi , and reconsolidating to the testing σ_3 of 40 or 80 psi. It was anticipated that the load-rebound portion of the isotropic compression test would not affect specimen behavior when reconsolidated to higher testing pressure. Once the specimens were fully consolidated under the effective confining pressure, the drainage valves were closed, and the desired static or cyclic loads were applied.

PART III: PRESENTATION AND ANALYSIS OF RESULTS

Cyclic Triaxial Tests

Check tests

11. In order to determine the adequacy of the cyclic triaxial test equipment and testing procedures used in this investigation, three cyclic triaxial tests were performed on Monterey No. 0 sand, and the results of these tests were compared with the results of the cyclic triaxial strength of a standard test sand[5,6] (Monterey No. 0). The sand, density, effective confining pressure, and compaction procedures used in these tests were identical to those used to determine the strength of the standard test sand.[16]

12. The results of these tests are summarized in Table 3, along with the results of all cyclic triaxial tests, and are compared graphically in Figures 4 and 5 with the results of the cyclic triaxial strength of a standard test sand.[4,5] These graphs show the relationship between the cyclic stress ratio (R) and the number of cycles of loading required to cause 100 percent pore pressure response and 10 percent peak-to-peak axial strain. The cyclic stress (R) is defined as:

$$R = \frac{\pm\sigma_{cd}}{2\sigma'_o} \qquad (2)$$

where

$\pm\sigma_{cd}$ = cyclic deviator stress, psi

σ'_o = initial effective confining pressure, psi

13. As shown in Figures 4 and 5, the results of the check tests agree very well with the results of the cyclic triaxial strength of a standard test sand, indicating the adequacy of the test equipment and testing procedures used in this investigation.

Cyclic triaxial tests on four sands

14. The results of cyclic triaxial tests on specimens of Reid-Bedford Model, Ottawa, Platte River, and Standard Concrete sands are presented in Table 3 and are shown graphically in Figures 6-8. These

Table 3

Summary of Isotropically Consolidated Cyclic Triaxial Test Results

Material*	γ_d pcf	D_r %	B	σ'_o psi	$\frac{\pm\sigma_{cd}}{2\sigma'_o}$	N_{iL}**	$N_{\pm 2.5}$**	$N_{\pm 5}$**
MO	98.14	58.1	0.95	14.5	0.386	10	10	14
MO	98.78	61.9	0.96	14.5	0.395	8	10	14
MO	98.91	62.6	0.98	14.5	0.370	9	9	11
PR	114.15	61.3	0.94	40.0	0.307	40	39	--‡
PR	114.22	61.7	0.94	40.0	0.356	22	22	--‡
PR	114.63	63.7	0.94	40.0	0.441	10	10	--‡
O	102.00	59.9	0.98	40.0	0.322	3	3	4
O	101.79	58.5	0.98	40.0	0.232	16	16	17
O	101.85	58.8	0.97	40.0	0.261	8	8	9
O	101.81	58.6	0.95	40.0	0.216	25	25	26
SC	109.02	62.9	0.94	40.0	0.358	13	13	18
SC	108.95	62.5	0.97	40.0	0.414	9	9	13
SC	108.99	62.7	0.98	40.0	0.312	20	20	24
RB	98.97	60.4	0.97	40.0	0.401	6	6	9
RB	98.48	57.8	0.98	40.0	0.367	8	8	10
RB	99.03	60.7	0.98	40.0	0.336	9	9	12
RB	99.05	60.8	0.96	40.0	0.301	14	14	17
RB	99.19	61.6	0.94	40.0	0.271	45	45	48
RB	98.87	59.9	0.94	40.0	0.261	47	47	48
RB	98.58	58.4	0.99	10.0	0.402	11	12	15
RB	98.74	59.3	0.96	10.0	0.351	247	250	253
RB	98.76	59.3	1.00	10.0	0.375	48	49	52
RB	98.98	60.6	0.98	10.0	0.412	11	12	15
RB	98.82	59.6	0.96	10.0	0.441	9	11	15
RB	98.78	59.4	0.98	10.0	0.490	7	9	13
RB	98.91	60.1	0.94	20.0	0.466	6	6	8
RB	99.18	64.2	0.94	80.0	0.235	22	21	23
RB	99.16	64.1	0.98	80.0	0.316	5	4	6
RB	99.21	64.4	0.93	80.0	0.214	22	20	22
RB	99.24	64.6	0.98	80.0	0.197	45	43	46
RB	95.46	41.3	0.96	10.0	0.310	6	6	7
RB	95.05	38.9	0.96	10.0	0.282	12	12	13
RB	95.08	39.1	0.95	10.0	0.246	24	23	24
RB	95.13	39.4	0.95	40.0	0.221	11	10	11
RB	95.86	43.5	0.97	40.0	0.172	74	74	75
RB	95.65	42.3	0.95	40.0	0.191	55	54	55
RB	95.16	39.5	0.97	40.0	0.209	18	17	18
RB	95.40	40.9	0.96	40.0	0.275	4	3	4
RB	102.65	79.1	0.95	10.0	0.448	49	60	69
RB	102.61	78.9	0.94	10.0	0.486	37	42	51
RB†	99.27	62.0	0.96	40.0	0.123	--	--	--
RB††	99.08	61.0	0.95	40.0	0.112	--	--	--

* MO = Monterey No. 0; PR = Platte River; O = Ottawa; SC = Standard Concrete; RB = Reid-Bedford.

** N_{iL} = number of cycles to 100 percent pore pressure response; $N_{\pm 2.5}$ = number of cycles to 5 percent axial strain - peak-to-peak; and $N_{\pm 5}$ = number of cycles to 10 percent axial strain - peak-to-peak.

† Sine wave, no liquefaction after 400 cycles.

†† Half-sine wave, no liquefaction after 700 cycles.

‡ Specimen necked prior to ±5 percent strain.

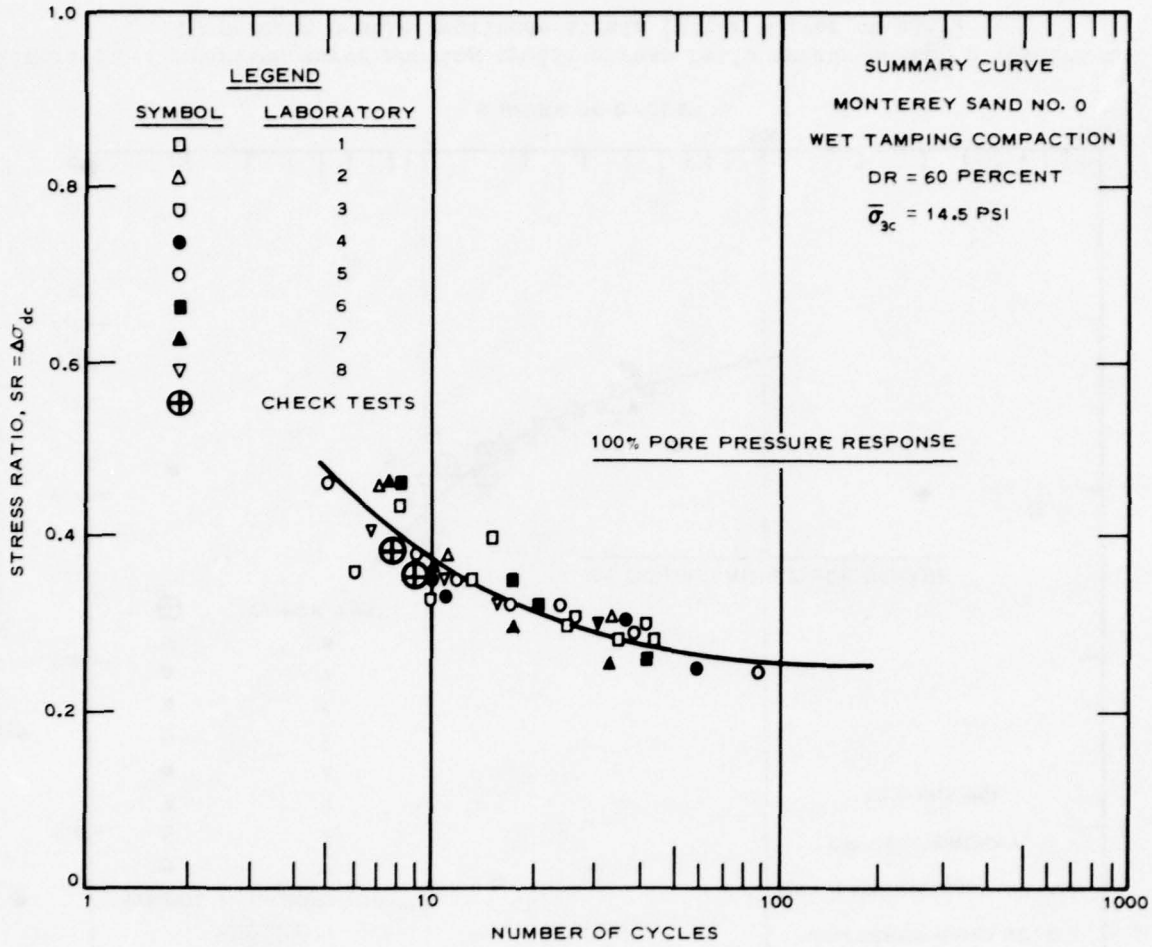

Figure 4. Comparison curve showing cyclic stress ratio versus number of cycles to initial liquefaction (100 percent pore pressure response) (after Silver et al[16])

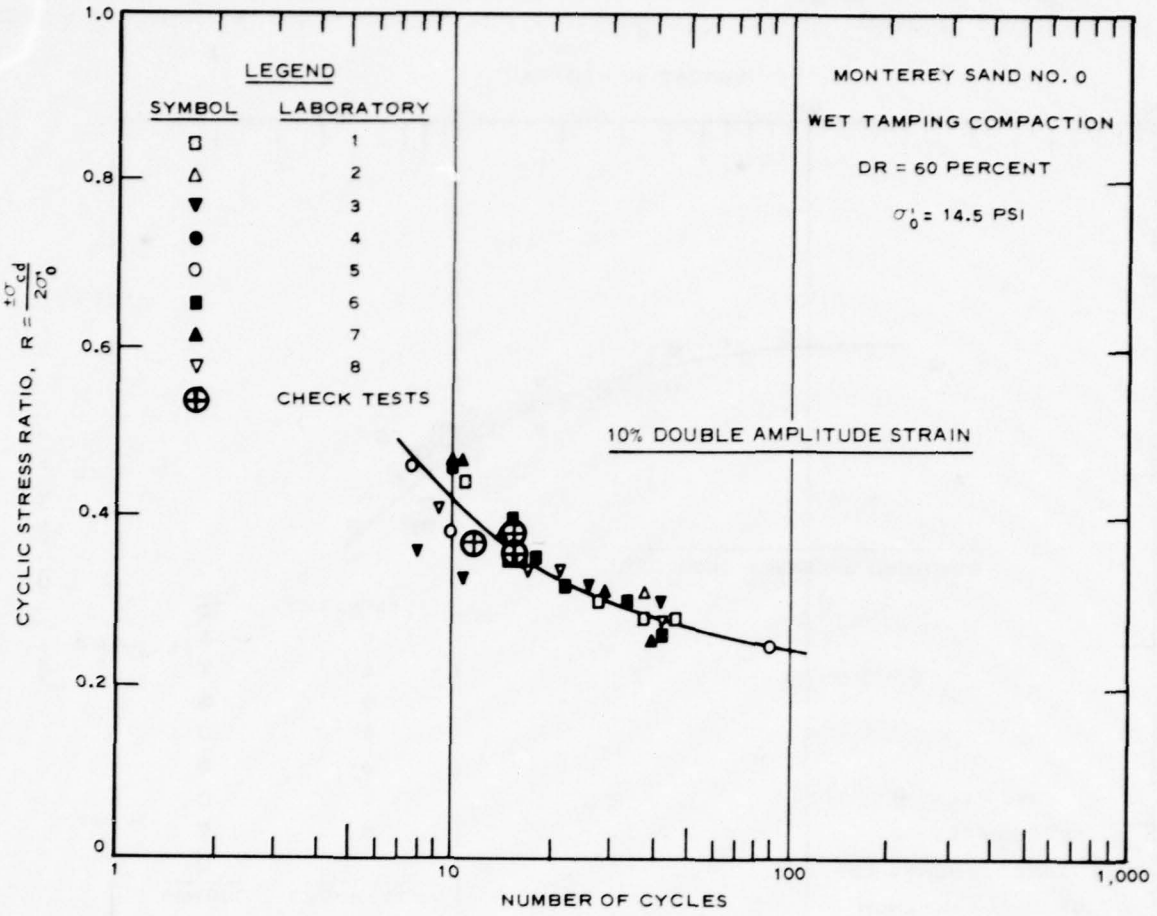

Figure 5. Comparison curve showing cyclic stress ratio versus number of cycles to 10 percent double amplitude strain (after Silver et al[16])

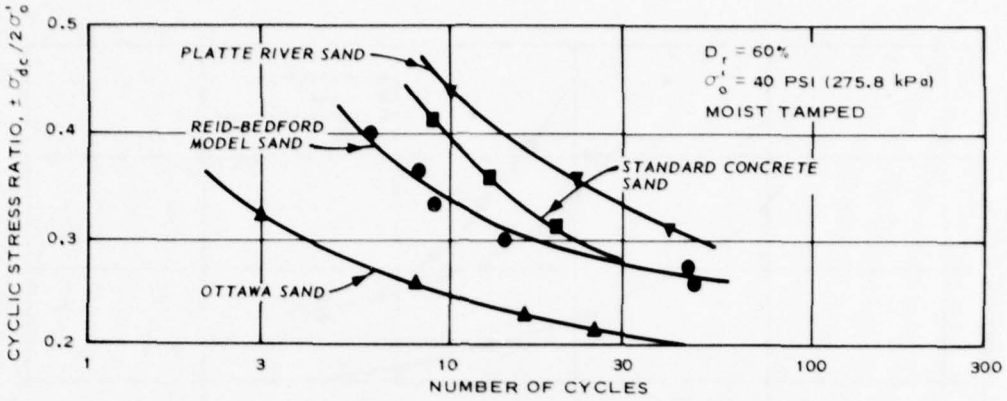

Figure 6. Cyclic stress ratio required to cause 100 percent pore pressure response for four sands at 60 percent relative density and 40-psi confining pressure

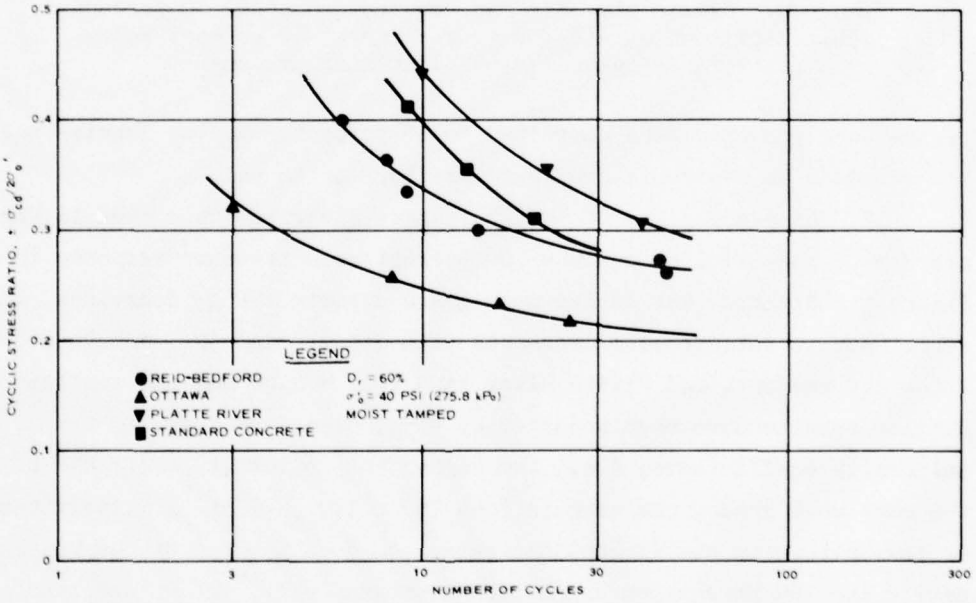

Figure 7. Cyclic stress ratio required to cause 5 percent double amplitude strain for four sands at 60 percent relative density and 40-psi confining pressure

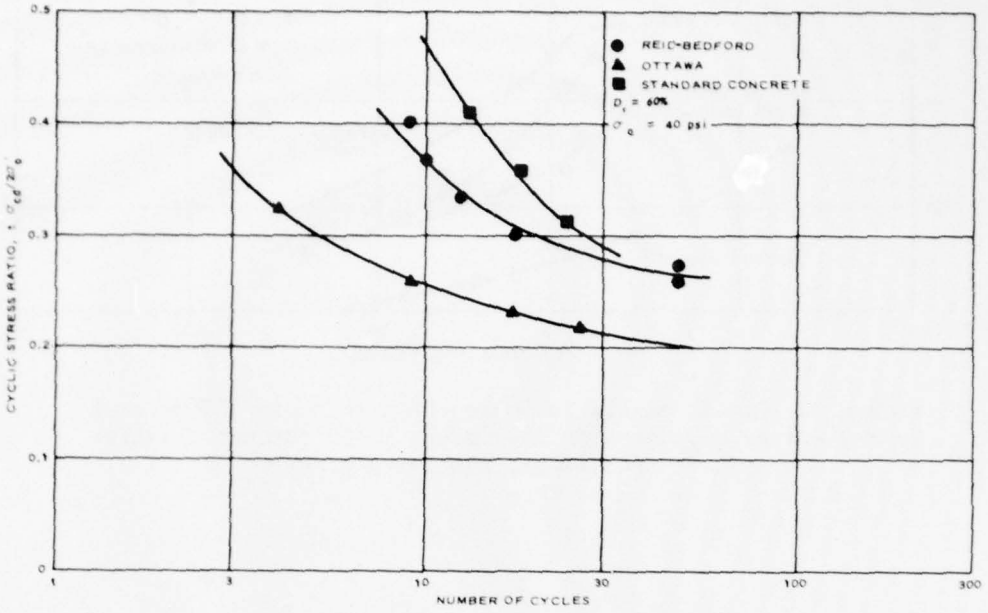

Figure 8. Cyclic stress ratio required to cause 10 percent double amplitude strain for four sands at 60 percent relative density and 40-psi confining pressure

figures are for specimens compacted to 60 percent relative density and tested under an isotropic confining pressure of 40 psi.

15. An examination of the grain-size distribution curves in Figure 3 with potential to achieve 100 percent pore pressure response in Figure 6 indicates that as the mean grain diameter D_{50} decreases, the resistance to failure also decreases with Ottawa sand (D_{50} = 0.20 mm) being the weakest, and Platte River sand (D_{50} = 2.00 mm) the strongest. Similar results have been reported by Wong, Seed, and Chan.[17] Comparing uniformity coefficients, i.e., the higher the uniformity coefficient the more well graded the sand is (see Table 1), suggests similarly that as the uniformity coefficient decreases, so does the resistance to developing 100 percent pore pressure response, e.g., for Ottawa sand C_u = 1.6 , while for Platte River sand, C_u = 5.3 . Both these observations support the general conclusion that fine, uniform sands are the most susceptible to developing 100 percent pore pressure responses in

cyclic triaxial tests. However, Wong, Seed, and Chan,[17] using large diameter tests, have reported that well-graded cohesionless soils tended to be weaker than uniformily graded cohesionless soils.

Supplementary tests on Reid-Bedford Model sand

16. In addition to the cyclic triaxial tests performed on Reid-Bedford Model sand, which were discussed in the previous section, several additional tests were performed on this same sand to investigate the effects of density and confining pressure. The results of these tests are discussed in the following paragraphs.

17. Effects of density. The results of tests performed on specimens remolded to relative densities of 40, 60, and 80 percent and consolidated to 10 psi are listed in Table 3 and presented in Figures 9-11, which show the relationship between the cyclic stress ratio and the number of loading cycles required to cause 100 percent pore pressure, 5 and 10 percent peak-to-peak ($\pm$2.5 to $\pm$5 percent) axial strain. These results are summarized in Figures 12 and 13, which show the relationship between the relative density of the specimens and the cyclic stress ratio required to cause 100 percent pore pressure response and 10 percent peak-to-peak axial strain in 10 cycles of loading. Also shown in these figures are summarized results of tests performed at a confining pressure of 40 psi. The individual test results for this confining pressure are shown in Figures 14, 15, and 16.

18. As shown in Figures 12 and 13, regardless of confining pressure, the cyclic stress ratio required to cause 100 percent pore pressure response and 10 percent peak-to-peak ($\pm$5 percent) axial strain increases with increasing relative density, and the relationship is linear up to a relative density of at least 60 percent for 100 percent pore pressure response and up to approximately 45 percent for 10 percent peak-to-peak ($\pm$5 percent) axial strain. Increasing the relative density from 40 to 60 percent causes an increase in the cyclic stress ratio required to cause 100 percent pore pressure response of approximately 50 percent, independent of the confining pressure. Similar results have been obtained by others (Seed and Lee,[18] DeAlba et al.[19])

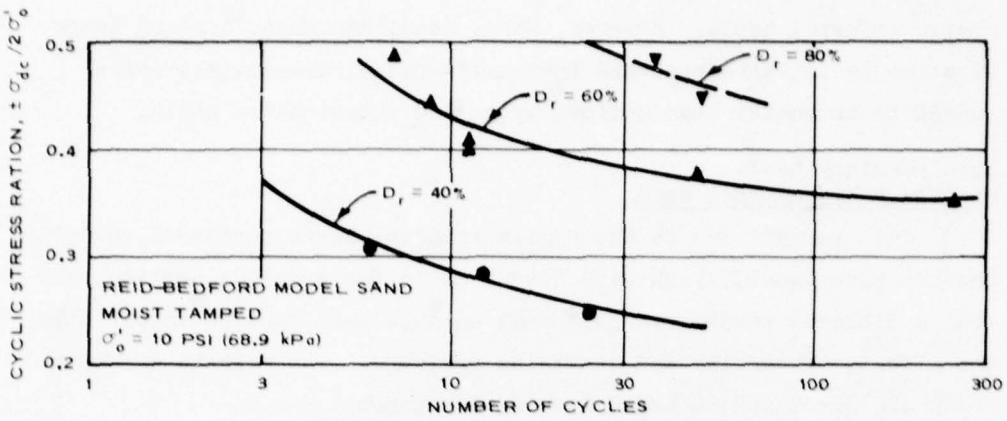

Figure 9. Cyclic stress ratio versus number of cycles to initial liquefaction for specimens of Reid-Bedford Model sand remolded to three different densities

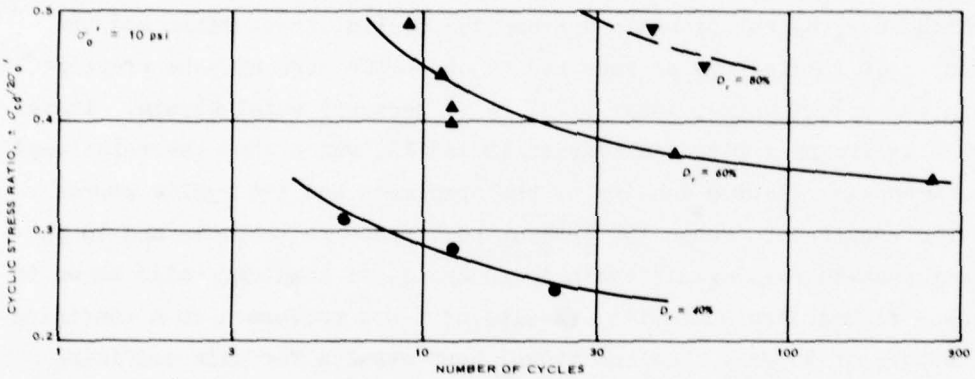

Figure 10. Cyclic stress ratio versus number of cycles to ±2.5 percent axial strain for specimens of Reid-Bedford Model sand remolded to three different densities

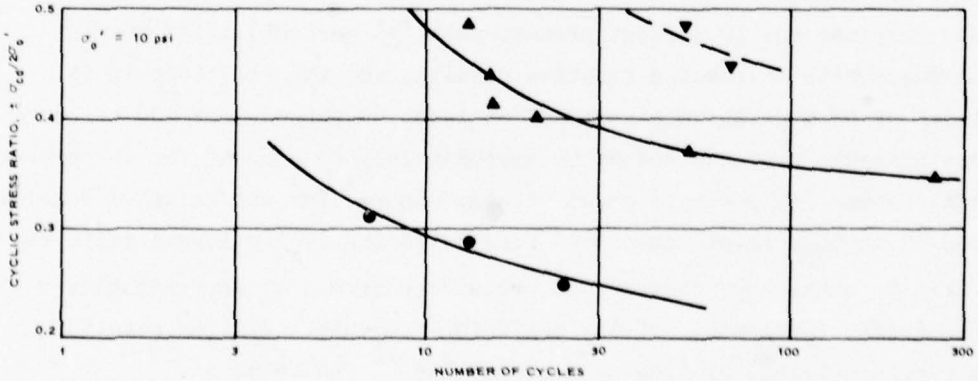

Figure 11. Cyclic stress ratio versus number of cycles to ±5 percent axial strain for specimens of Reid-Bedford Model sand remolded to three different densities

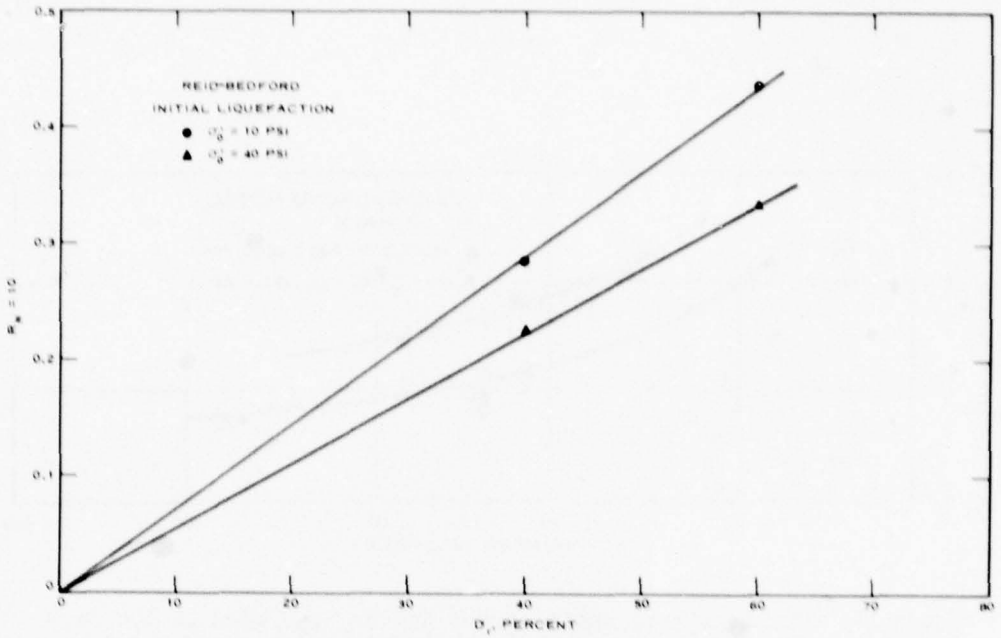

Figure 12. Cyclic stress ratio at 10 cycles for 100 percent pore pressure response versus relative density

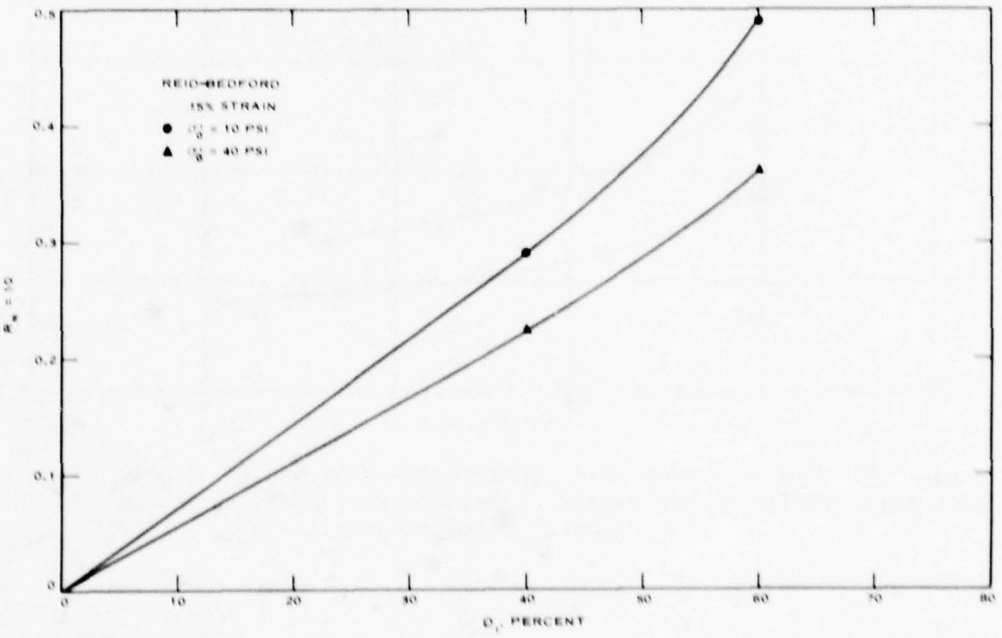

Figure 13. Cyclic stress ratio at 10 cycles for ±5 percent strain versus relative density

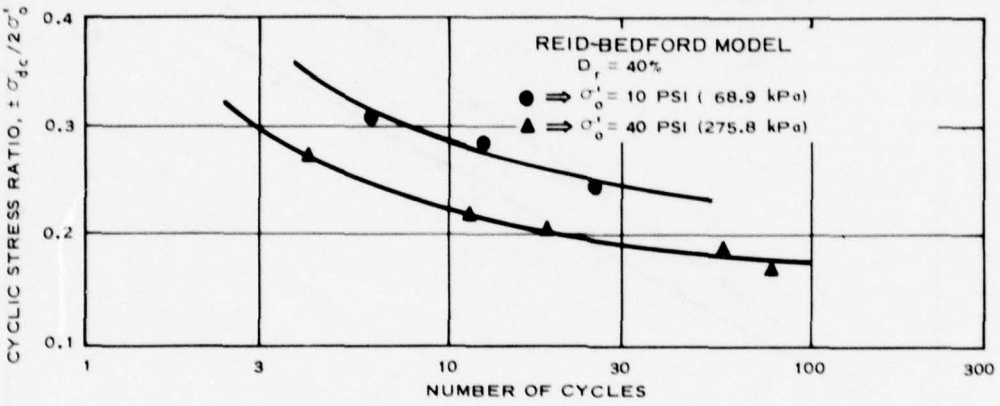

Figure 14. Cyclic stress ratio versus number of cycles to 100 percent pore pressure response for specimens of Reid-Bedford Model sand remolded to 40 percent relative density

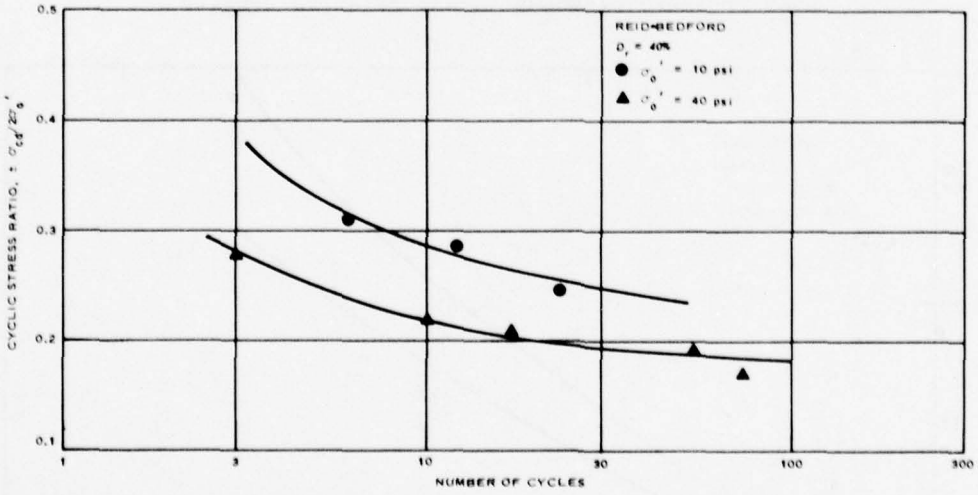

Figure 15. Cyclic stress ratio versus number of cycles to ±2.5 percent axial strain for specimens of Reid-Bedford Model sand remolded to 40 percent relative density

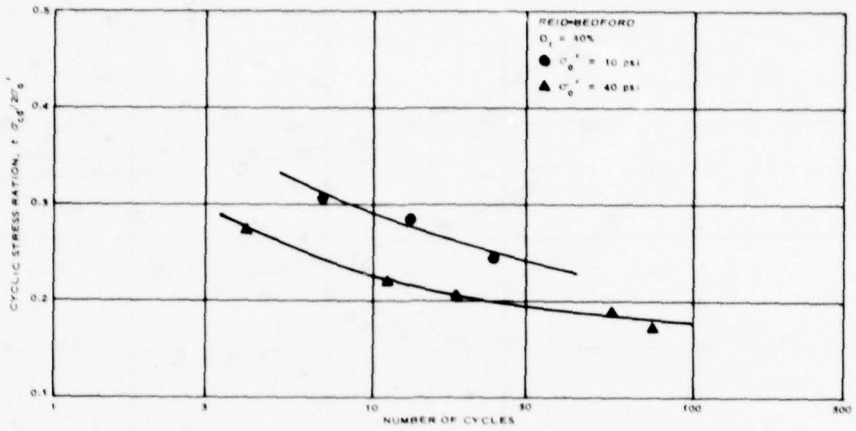

Figure 16. Cyclic stress ratio versus number of cycles to ±5 percent axial strain for specimens of Reid-Bedford Model sand remolded to 40 percent relative density

19. Effects of confining pressure. The results of tests performed to investigate the effects of the initial effective confining pressure on the cyclic stress ratio required to cause 100 percent pore pressure response, 5 and 10 percent (±2.5 and 5 percent) peak-to-peak axial strain are presented in Figures 17-19 and summarized in Figures 20 and 21. Figures 20 and 21 summarize the effects of confining pressure and relative density by expressing the relationship between the initial effective confining pressure and the cyclic stress ratio required to cause 100 percent pore pressure response and 10 percent peak-to-peak axial strain in 10 loading cycles.

20. Figures 20 and 21 show that without respect to the relative density, the cyclic stress ratio required to cause 100 percent pore pressure response and 10 percent peak-to-peak axial strain decreases with increasing initial effective confining pressure. These figures also show that the relationship is linear for relative densities of 40 and 60 percent up to approximately 40 psi. Increasing the confining pressure from 10 to 40 psi causes a decrease in the cyclic stress ratio at 10 cycles of loading, ranging from 27 to 36 percent, depending on the relative density and failure criteria (100 percent pore pressure response or 10 percent peak-to-peak axial strain). Similar results have been reported.[20]

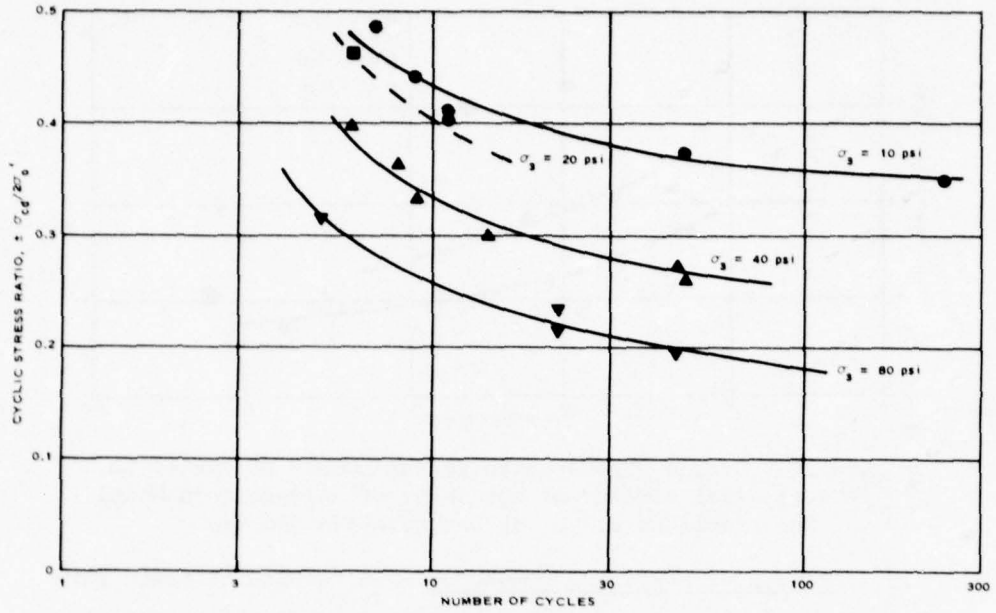

Figure 17. Effect of confining pressure on cyclic stress ratio and number of cycles required to cause 100 percent pore pressure response of Reid-Bedford Model sand at 60 percent relative density

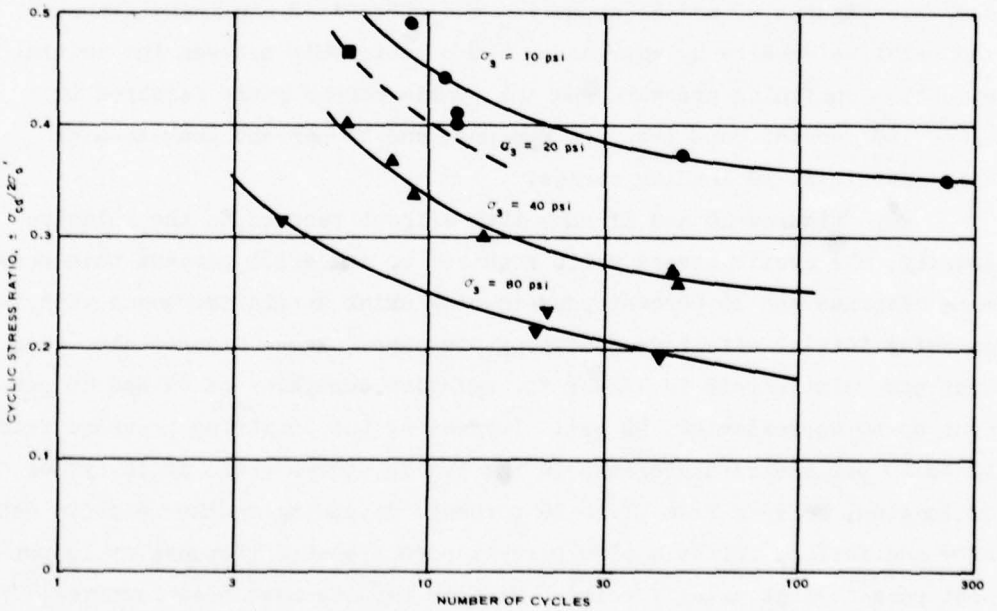

Figure 18. Effect of confining pressure on cyclic stress ratio and number of cycles required to cause 5 percent double amplitude strain for Reid-Bedford Model sand at 60 percent relative density

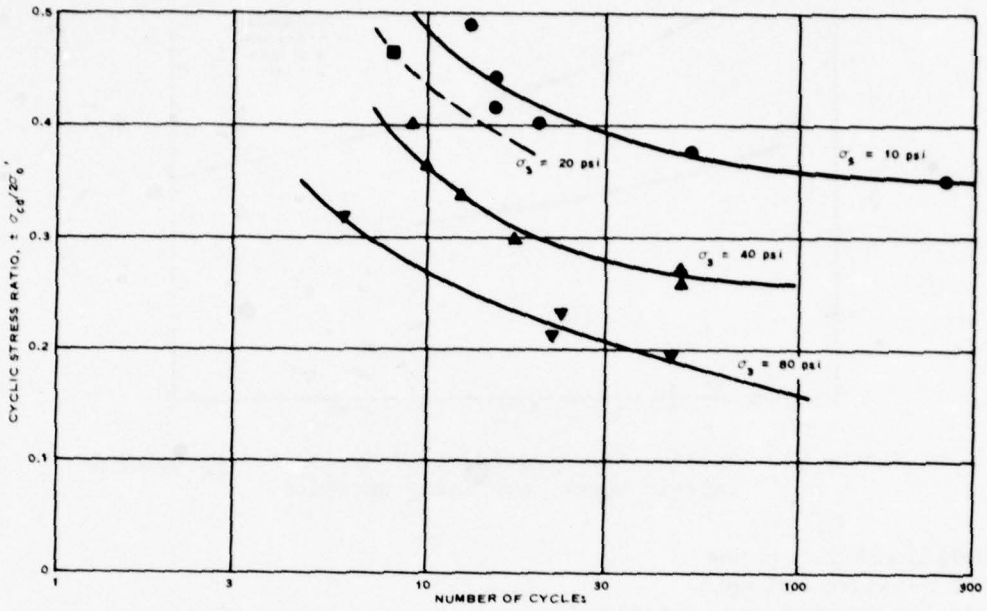

Figure 19. Effect of confining pressure on cyclic stress ratio and number of cycles required to cause 10 percent double amplitude strain for Reid-Bedford Model sand at 60 percent relative density

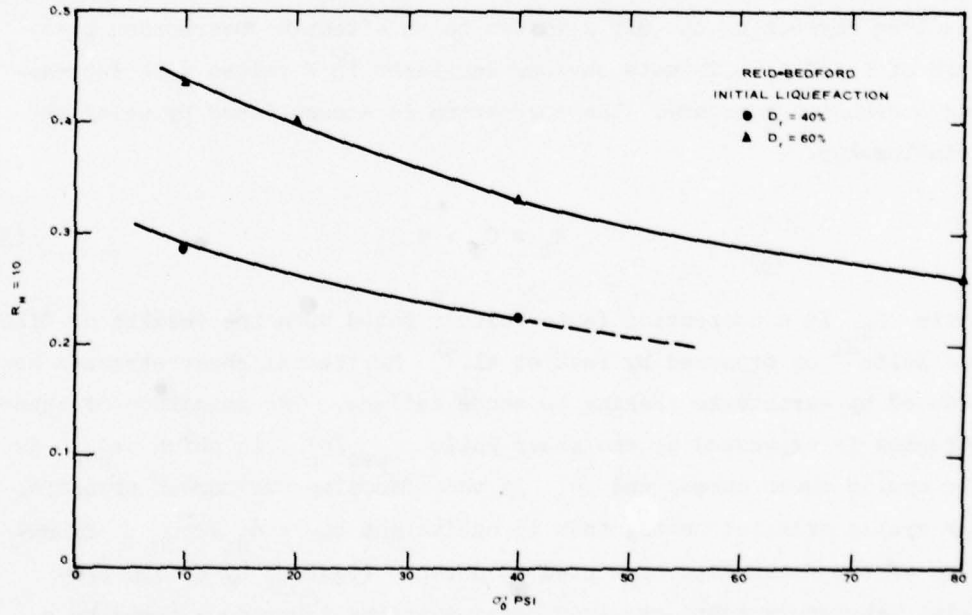

Figure 20. Cyclic stress ratio at 10 cycles for 100 percent pore pressure response versus confining pressure

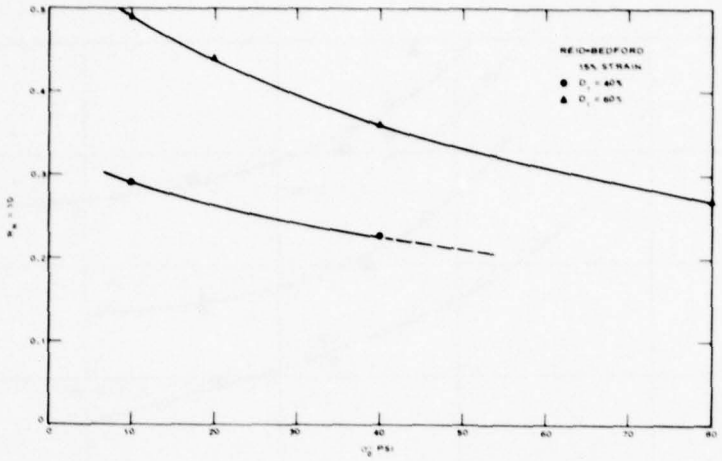

Figure 21. Cyclic stress ratio at 10 cycles for ±5 percent strain versus confining pressure

Relationship between SPT N-values and seismically induced ground failure

21. In Figure 1, Seed[3] has suggested the use of a semiempirical procedure for estimating the seismically induced ground failure, due to cyclic stress applications of level ground deposits. This design chart requires correcting the SPT N-values to an effective overburden pressure of 1 tsf to eliminate obvious increases in N-values with increasing overburden pressure. The correction is accomplished by using the relationship:

$$N_1 = C_N \cdot N \tag{3}$$

where C_N is a correction factor either based upon the results of Gibbs and Holtz[21] or proposed by Peck et al.[22] Horizontal shear stresses are induced by earthquake shaking to cause failure. The magnitude of these stresses is expressed by the shear ratio τ_{ave}/σ'_o, in which τ_{ave} is the cyclic shear stress and σ'_o is the effective overburden pressure. For cyclic triaxial tests, this is equivalent to $\pm \sigma_{dc}/2\bar{\sigma}_{3c}$. Extension of the field data base used to develop Figure 1 by cyclic triaxial laboratory tests requires correcting the laboratory tests by a

correction factor (C_r) to account for differences in K_o conditions and other factors.[8]

22. Based upon the Bureau of Reclamation data, Seed[3] proposed that

$$C_N = 1 - 1.25 \log\left(\frac{\sigma'_o}{\sigma'_1}\right) \tag{4}$$

where

C_N = the correction factor

σ'_o = the effective overburden pressure where penetration resistance is N , tsf

σ'_1 = 1 tsf

22. Alternately, Peck et al.[22] have corrected N-values to an effective overburden pressure of 1 tsf using

$$C_N = 0.77 \log\left(\frac{20}{\overline{P}}\right) \tag{5}$$

where $\overline{P}$ represents the effective overburden pressure in tons per square foot for $\overline{P} \geq 0.25$ tsf.

23. Similarily, C_r-values for correcting stress ratios τ/σ'_o (equal to $\sigma_{dc}/2\sigma_{3c}$) from laboratory cyclic triaxial test to field values are a function of density and number of cycles.

24. Castro[5] recommended a C_r-value of 0.7 to adjust cyclic triaxial test conditions to field conditions. DeAlba et al.[19] showed that for reducing the results of triaxial tests on specimens pluviated (rained) through the air onto a shaking table, the C_r-factor results varied between 0.66 and 0.61 in the 2- to 30-cycle range, which is the range of interest in most earthquake analyses. A reduction of 10-15 percent would further reduce this correction factor to 0.59-0.55 to account for multidirectional shaking.[23] Hence, Seed[3] recommended that $C_r = 0.57$ should be used to correct laboratory cyclic triaxial tests to field behavior.

25. For discussion, however, Seed[3] also emphasizes that correction factors for a variety of conditions would be required to correct

large-scale shaking table data to field in situ conditions. These various conditions: long-term loading, increased pressure, and two-dimensional shaking, will be disturbed to some degree by sampling. Hence, a C_r-value of 1.3 would be required to align shaking table data from pluviated specimens with in situ conditions. If one then attempted to correct cyclic triaxial data to field data via a shaking table test, a C_r of $0.63 \times 1.3 = 0.82$ would be required.

26. Thus, from these considerations, a dilemma exists about what C_N relationship is appropriate and what value of C_r is required for using the relationships in Figure 1, since all the data are plotted against corrected N-values and the magnitudes 6 and 8.25 curves have been extrapolated using corrected shaking table data. An additional quandary, not discussed here, concerns the accuracy of the stress ratio reported for the earthquakes plotted in Figure 1.

27. Results of a laboratory program determining the penetration resistance of these four sands under overburden pressures of 10, 40, and 80 psi have been presented elsewhere;[13,14,24,25] but for convenience they are reproduced as Figure 22. To account for densification due to applied overburden pressures, the relative densities presented are "adjusted" values. Utilizing this data and Equation 1 by interpolating between overburden pressures of 10 and 40 psi for N-values, C_N-values can be obtained for these four sands (Appendix B). Accordingly, Figure 23 (reproduced from Reference 25) plots C_N-values versus effective overburden pressure for relative densities of 40, 60, and 80 percent. Relationships used by Seed (Equation 2, Reference 3) and Peck et al. (Equation 3, Reference 22) are also presented. These results conclusively demonstrate that C_N is not a function of overburden pressure only, but also of soil type, relative density, and, possibly, other unknown variables.

28. Figure 24 compares the cyclic stress ratio required to cause 100 percent pore pressure response in 15 cycles for cyclic triaxial specimens prepared by moist tamping with lower bound magnitude 7.5 field earthquake responses. (Seed et al.[26] have suggested that magnitudes 6, 7.5, and 8.25 earthquakes are represented by 5-6, 15, and

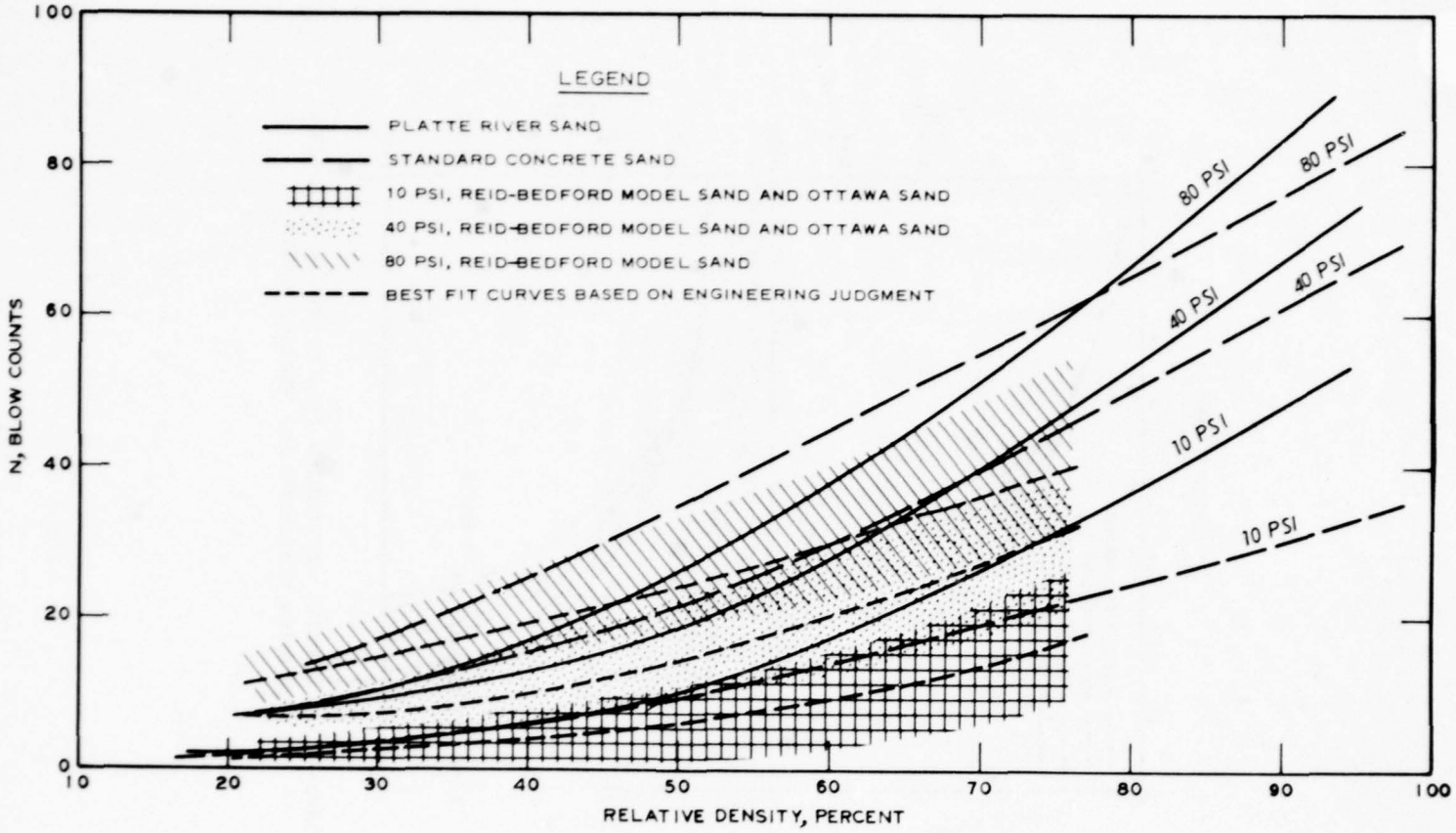

Figure 22. Comparison of Platte River, Standard Concrete, Reid-Bedford Model, and Ottawa sand data (after Bieganousky and Marcuson[14])

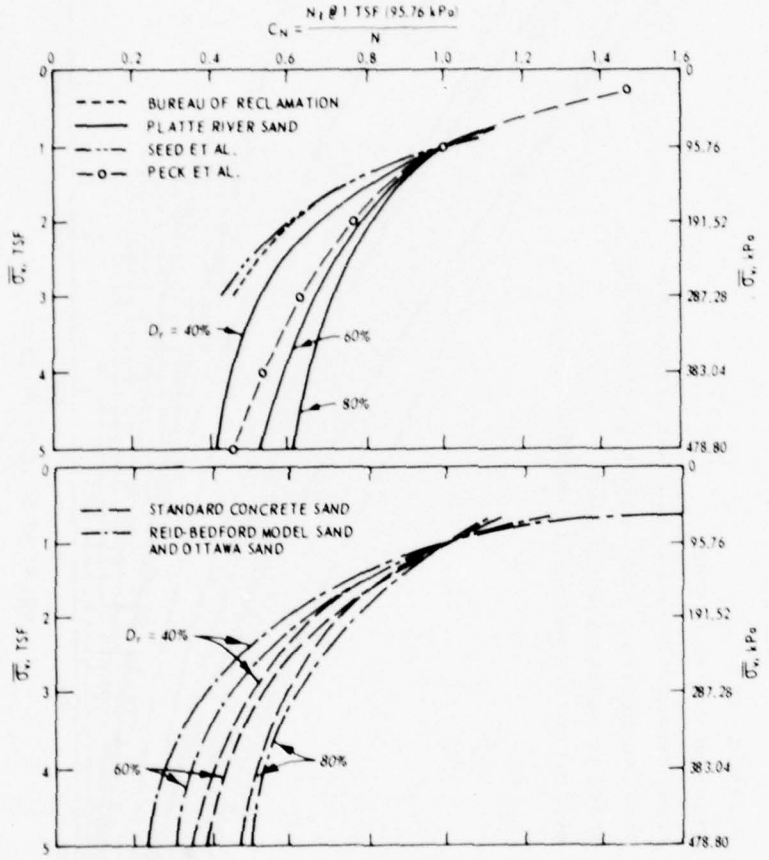

Figure 23. N-value correction factor versus effective overburden pressures for various sands

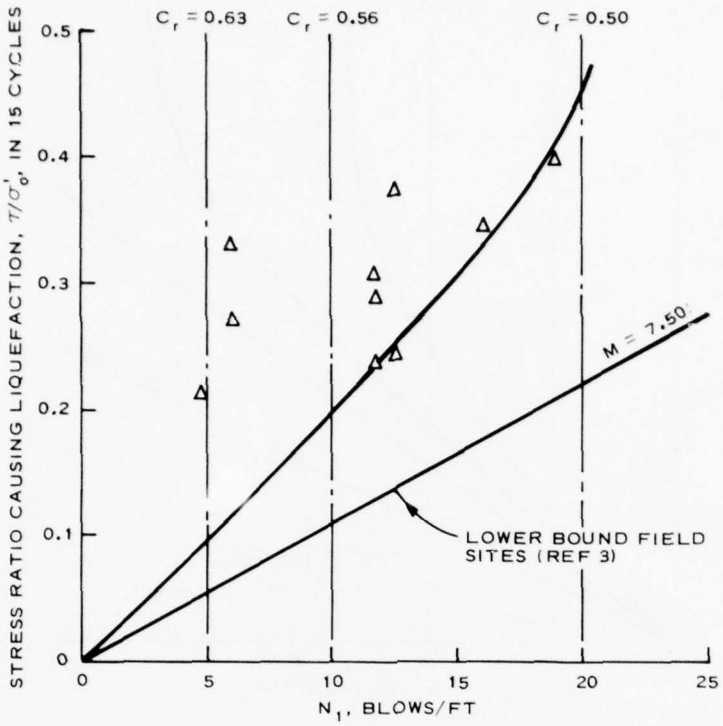

Figure 24. Correction factors for cyclic triaxial tests on moist, tamped specimens for 100 percent pore pressure response in 15 cycles

25 uniform cycles, respectively. This comparison shows that for N-values between 5 and 20 blows/ft the C_r-value ranges from 0.63 to 0.50. Figure 25 is based upon shaking table test results[19] corrected by a factor of 1.3 to obtain estimated field response for magnitudes 6 and 8.25 earthquakes. The figure presents C_r-values corresponding to these earthquake magnitudes for moist tamped cyclic triaxial specimens. These comparisons show C_r-values ranging from 0.41 to 0.43 for magnitude 6 earthquakes and 0.52-0.66 for magnitude 8.25 earthquakes.

29. It must be emphasized that these C_r comparisons are based upon isotropically consolidated cyclic triaxial specimens prepared by moist tamping. Obviously, other methods of specimen preparation would produce different C_r-values. For example, verification of the C_r-values in

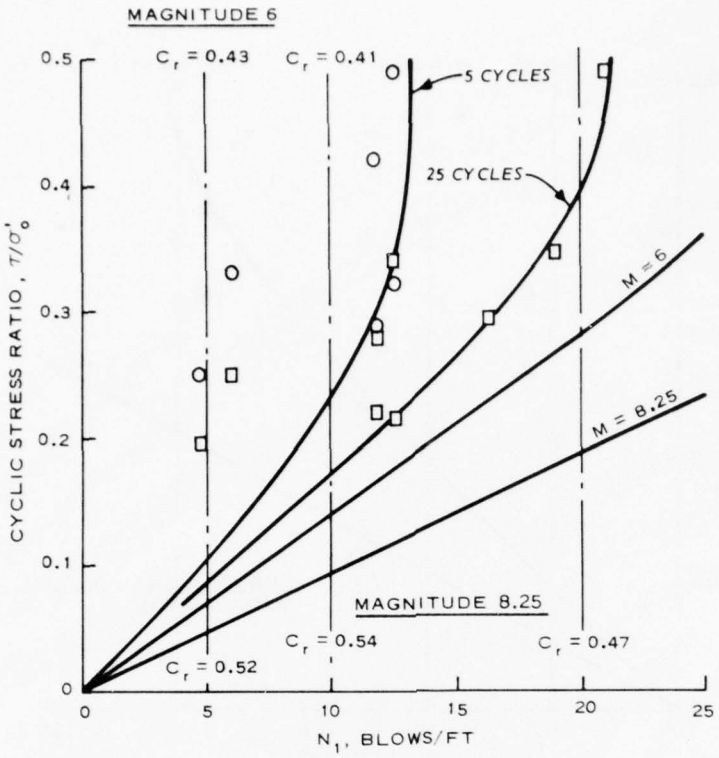

Figure 25. Correction factors for cyclic triaxial tests on moist-tamped specimens for magnitudes 6 and 8.25 earthquakes

Figures 23 and 24 via correlations would produce the following results:

Correction factor - shaking table on pluviated specimens to field	× 1.3 (3)
Correction factor - cyclic triaxial tests pluviated to shaking table pluviated	× 0.63 (19)
Correction factor - cyclic triaxial moist tamped to cyclic triaxial pluviated	× 0.60 (20)
Therefore, cyclic triaxial moist tamped to field	× 0.49

Hence, C_r could be estimated to be 0.49 based upon correlations published for Monterey No. 0 sand, compared with a range of 0.63-0.50 presented in Figure 23. This difference is probably due to the difficulties in comparing four sands with different densities and confining pressures than those used to establish the correlations for Monterey No. 0 sand.

30. Table 4 lists both actual and corrected (C_r = 0.57) values of stress ratio required to cause liquefaction in 5-6, 15, or 25 cycles, as well as actual and corrected N-values which correspond to the cyclic triaxial conditions. A comparison of the corrected SPT N-values shows that a reasonable agreement exists between Equations 2 and 3 and the actual data (listed as column 15), with Equation 3 being slightly better. (C_N-values presented by Seed[4] appear to be an average of C_N-values presented in Figure 23.) Figure 26 compares corrected cyclic triaxial

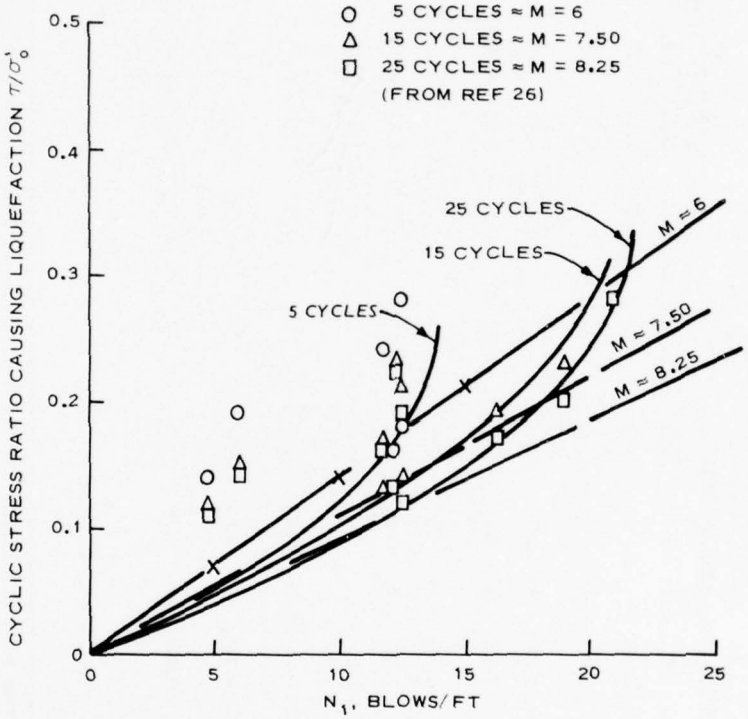

Figure 26. Comparison of laboratory SPT and cyclic triaxial tests with field response (C_N from Figure 23, C_r = 0.57)

stress ratios and N-values for the four sands tested in this investigation with the lower bounds suggested by Seed in Figure 1. As seen up to N-values of 20 blows/ft, the agreement is excellent for magnitudes 6, 7.5, and 8.5 or 8.25 percent earthquakes. However, this agreement is

Table 4

Summary of Actual and Corrected Cyclic Stress Ratios and SPT N-Values for Four Sands

Sand Tested* (1)	Relative Density D_r (2)	Confining Pressure σ_{3c}, tsf (3)	Stress Ratio for 100 Percent Pore Pressure Response in Cycles** 5-6 (4)	15 (5)	25 (6)	Corrected Stress Ratios for 100 Percent Pore Pressure Response in Cycles† 5-6 (7)	15 (8)	25 (9)	SPT N-Values Corresponding to Cyclic Triaxial Test Conditions (10)	C_N-Values Fig 8 (11)	Eq 3†† (12)	Eq 2‡ (13)	Ref 18‡‡ (14)	Corrected SPT N-Values Fig 8 (15)	Eq 3 (16)	Eq 2 (17)	Ref 18 (18)
RBM	60	0.72	--	0.41	0.39	--	0.23	0.22	10	1.20	1.11	1.18	1.12	12.0	11.1	11.8	11.2
RBM	60	1.44	0.49	0.37	0.34	0.28	0.21	0.19	15	0.83	0.88	0.80	0.83	12.5	13.2	12.0	12.5
RBM	60	2.88	0.42	0.305	0.28	0.24	0.17	0.16	22	0.53	0.65	0.43	0.57	11.7	14.3	9.5	12.5
RBM	60	5.76	0.32	0.24	0.215	0.18	0.14	0.12	32	0.39	0.42	0.05	0.38	12.5	13.4	1.6	12.2
RBM	40	0.72	0.33	0.27	0.25	0.19	0.15	0.14	5	1.2	1.11	1.18	1.12	6.0	5.6	5.9	5.6
RBM	40	2.88	0.25	0.21	0.195	0.14	0.12	0.11	11	0.44	0.65	0.43	0.57	4.8	7.1	4.7	6.3
RBM	80	0.72	--	--	0.49	--	--	0.28	20	1.05	1.11	1.18	1.12	21.0	22.2	23.6	22.4
O	60	2.88	0.285	0.235	0.22	0.16	0.13	0.13	22	0.53	0.65	0.43	0.57	11.7	14.3	9.5	12.5
PR	60	2.88	--	0.395	0.345	--	0.23	0.20	28	0.68	0.65	0.43	0.57	19.0	18.2	12.0	16.0
SC	60	2.88	--	0.34	0.295	--	0.19	0.17	30	0.54	0.65	0.43	0.57	16.2	19.5	12.9	17.1

* RBM = Reid-Bedford Model sand; O = Ottawa sand; PR = Platte River sand; SC = Standard Concrete sand.

** Cycles 5-6 correspond to magnitude 6 earthquake, while cycles 15 and 25 correspond to magnitudes 7.5 and 8.25 earthquakes, respectively.

† Corrected using $C_r = 0.57$ to correct cyclic triaxial stress ratio values to field stress ratio values.

†† Reference 22, $C_N = 0.77 \log (20/\overline{p})$.

‡ Reference 3, $C_N = 1 - 1.25 \log (\overline{\sigma}_o/\overline{\sigma}_1)$.

‡‡ Reference 4, Figure 10.

probably fortuitous, considering that the cyclic triaxial specimens were prepared by moist tamping and a C_r-value of 0.57 probably would have produced quite different results had a different specimen preparation procedure been used.

Monotonic $\bar{R}$ Tests

31. Complementary monotonic $\bar{R}$ tests on only Reid-Bedford Model sands were conducted at identical confining pressures as the cyclic triaxial and SPT tests, i.e., 10, 40, and 80 psi. The results of these 12 tests are listed in Table 5 and presented in Figure 27. Considering the response of specimen RB25-80-12, the listed void ratio after consolidation e_c is too low and is probably closer to 0.780 than 0.765, as shown, based upon specimen RB20-80-10's response.

32. The deviator stress and pore pressure response versus axial strain curves, as well as the $q = \left(\sigma_1 - \sigma_3\right)/2$ versus $p = \left(\sigma_1 + \sigma_3\right)/2$ effective stress paths for these $\bar{R}$ tests, are contained in Figures B-1 through B-10 in Appendix B.

Criteria of designating specimen response

33. Column 5 of Table 5 lists the specimen response during shear. In this instance, L refers to liquefaction, D refers to dilation, and LL refers to an intermediate response between L and D, previously termed limited liquefaction.[2] Differentiation between L and LL response is based primarily on the shape of the stress paths. In the case of liquefaction, the stress path always travels down the α line toward the origin; while in the case of a limited liquefaction, the stress path begins to travel down the α line but then reverses itself and travels up the α line, as exhibited by dilative specimens.

34. The effective angle of internal friction ϕ' can be obtained from the slope of the α line in the p-q plots (b. portion of figures in Appendix B) and the relationship $\sin \phi = \tan \alpha$. For all these $\bar{R}$ tests, regardless of specimen response, ϕ' at failure ranged

Table 5

Summary of Monotonic $\bar{R}$ Tests on Reid-Bedford Model Sand

Test No.	σ_{3c} kg/cm^2	D_r %	e_c	Type Failure	$\sigma_{d_{max}}$ kg/cm^2	e_{max} %	σ_{1f} kg/cm^2	σ_{3f} kg/cm^2	Maximum $\bar{\sigma}_1/\bar{\sigma}_3$	Remarks
RB20-40-1	--	--	--	--	--	--	--	--	--	Bad test, no data
RB20-40-2	2.81	24.3	0.791	LL	2.45	22.07	3.20	1.10	2.91	No LVDT clamps used
RB20-40-3	2.81	23.8	0.792	L	2.29	18.44	2.98	1.02	2.92	No LVDT clamps used
RB30-40-4	2.81	34.3	0.760	D	5.21	5.82	7.75	2.54	3.05	No LVDT clamps used
RB20-40-5	2.81	23.9	0.792	LL	2.73	9.77	4.10	1.36	3.00	2 LVDT clamps used, consolidated to 30 psi and rebounded to to 5 psi
RD30-40-6	2.81	34.9	0.759	D	4.77	7.53	7.12	2.34	3.04	2 LVDT clamps used, consolidated to 30 psi and rebounded to 5 psi
RB15-10-7	--	--	--	--	--	--	--	--	--	Bad test, no data
RB15-10-8	0.70	15.3	0.818	L	0.39	16.67	0.53	0.18	2.88	1 LVDT clamp used
RB20-10-9	0.70	22.6	0.796	D	0.99	3.44	1.52	0.53	2.85	1 LVDT clamp used
RB20-80-10	5.62	26.3	0.785	LL	4.24	11.32	7.08	2.47	2.87	1 LVDT clamp used, consolidated to 60 psi and rebounded to 5 psi
RB15-80-11	5.62	23.3	0.794	L	3.35	5.62	4.75	1.43	3.31	1 LVDT clamp used, consolidated to 60 psi and rebounded to 5 psi
RB25-80-12	5.62	32.9	0.765	LL	4.20	6.41	1.12	0.95	2.85	1 LVDT clamp used, consolidated to 60 psi and rebounded to 5 psi; specimen unloaded after failure

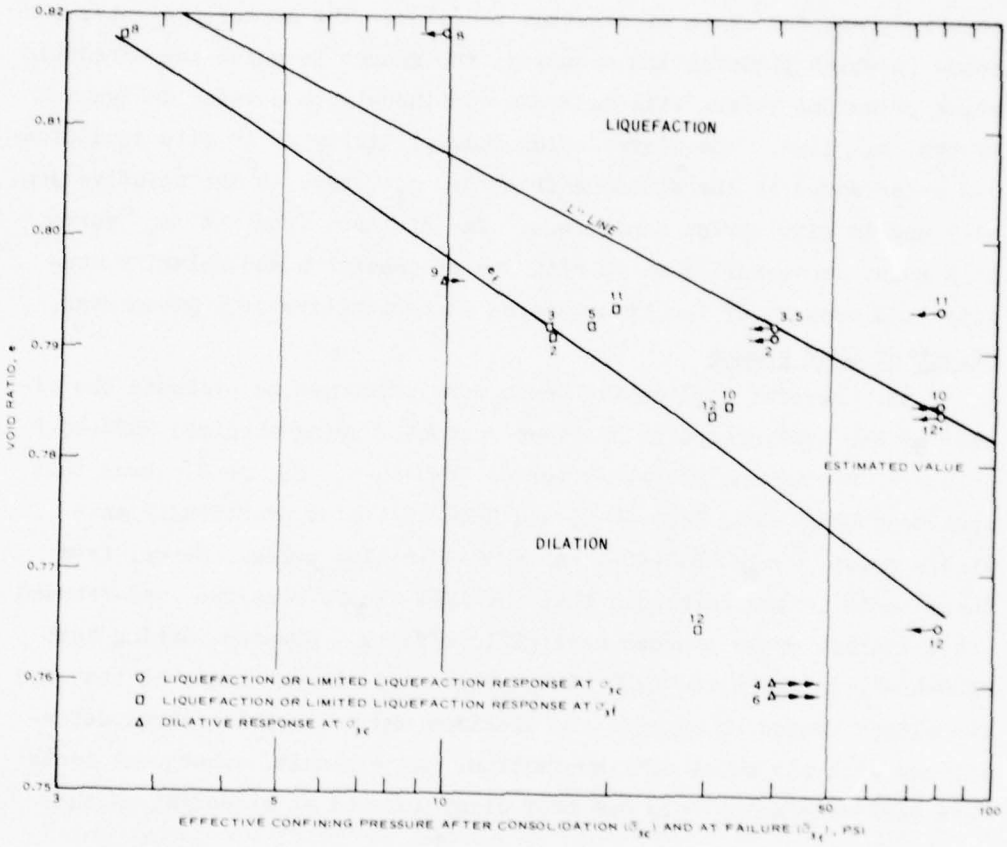

Figure 27. Critical void ratio and L lines for Reid-Bedford Model sand

between 28.4 and 32.5 with an average value of 29.6 deg. The e_f line, or critical void ratio curve, is the relationship between the effective confining pressure at failure (σ_{3f}), column 9, Table 5, and the void ratio after consolidation[2] and is only for cases in which liquefaction occurred, not for cases of dilatant behavior. The arrows indicate, for cases in which liquefaction occurred, the manner in which the effective minor principal stress will decrease continously to a value designated by the e_f line. The liquefaction susceptibility of in situ conditions can be assessed by the distance from the e_f curve to the relative density and in situ stress conditions. The distance from the e_f curve to a point representing an in situ stress condition and relative density is a measure of the liquefaction susceptibility of a given sand.

Effect of LVDT clamps

35. Several duplicative tests were performed to evaluate the effect of the LVDT clamps on specimen response, using specimen RB20-40-2 versus RB20-40-5 and RB30-40-4 versus RB30-40-6. Figure 27 shows that specimens RB20-40-2, RB20-40-3, and RB20-40-5 plot practically as a single point, while RB30-40-4 and RB30-40-6 also agree. Hence, from these tests it was concluded that the LVDT clamps plus the load-rebound consolidation cycle produce negligible effects. However, during test RB20-40-5, in which two LVDT clamps were used, it was observed that the two clamps tended to support the specimen and to restrict large deformations with the onset of liquefaction. As a result, subsequent tests were performed using only one LVDT clamp located at midheight on the specimen.

Relationship between SPT N-values and monotonic $\bar{R}$ triaxial tests

36. Figure 28 presents the relationship between SPT N-values and overburden (confining) pressure separating liquefaction and dilative behavior for two sands. To extend the data base, monotonic $\bar{R}$ data on Ottawa banding sand from Castro[2] are also included with the Reid-Bedford Model sand. Both sands are quite similar in grain-size distribution, and it is believed that SPT data on Reid-Bedford Model sand and Ottawa

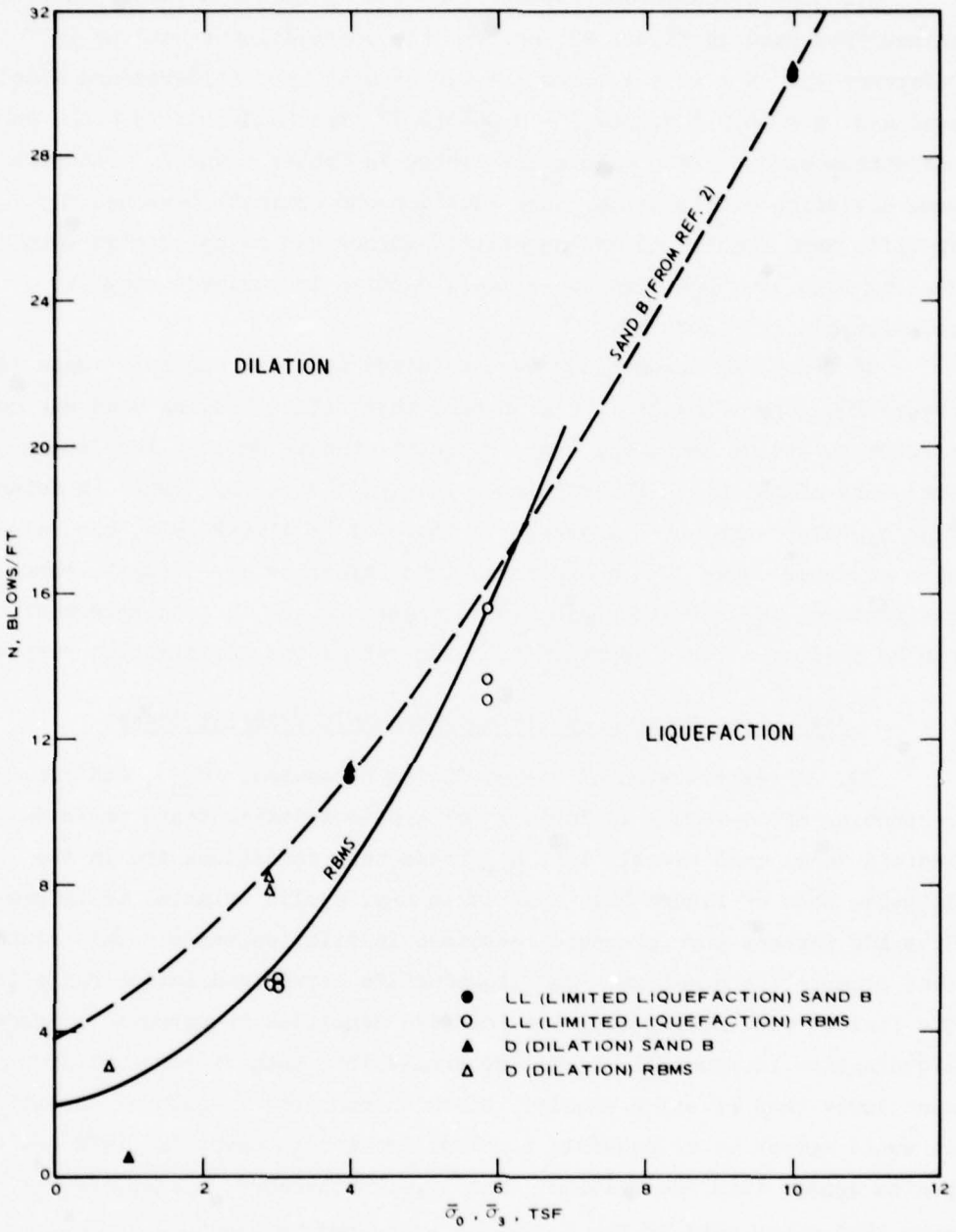

Figure 28. Relationship between liquefaction susceptibility under monotonic loading and SPT N-values for Banding Sand[2] and Reid-Bedford Model sand

sand contained in Reference 13 are appropriate.

37. The N-values corresponding to the monotonic $\bar{R}$ tests can be obtained from data in Figure 22, or from the correlation equations in Reference 13: $N = -5.5 + 0.2(\bar{\sigma}_v) + 0.0046(D_r)^2$ for Reid-Bedford Model sand and $N = -6.5 + 0.23(\bar{\sigma}_v) + 0.0045(D_r)^2$ for Reid-Bedford Model sand and Ottawa sand. These values are listed in Tables 6 and 7. Inasmuch as some deviation exists using these equations to estimate N-values for specific test conditions and negative N-values can be calculated when dealing with low D_r- and σ_o-values, caution is advised using the relationship in Figure 28.

38. Several assumptions were required to adapt Castro's[2] data for Figure 28. Specifically it was assumed that Ottawa Banding sand was comparable to Ottawa sand, and that SPT relationships derived for Ottawa sand were compatible. In addition, since procedures by Castro to determine D_r-values are not comparable to those of EM 1110-2-1906, his values were adjusted using D_r comparisons from Reference 11. Despite these assumptions, the results presented in Figure 28 are in good agreement and can be used as a first approximation for estimating liquefaction response.

Comparison Between Cyclic and Monotonic Triaxial Tests

39. An examination of the confining pressures, σ_{3c}, and corresponding SPT N-values in Table 1 for cyclic triaxial tests on Reid-Bedford Model sand reveals that all these test conditions are in the dilative zone of Figure 28. That is to say, cyclic triaxial tests produce 100 percent pore pressure responses in dilative sands. This statement prompts the question: Can liquefaction occur in dilative sands in the field? Considering that the relative densities required to produce liquefaction in monotonic tests (generally less than 25 percent) are much lower than relative density values encountered in natural deposits, it would appear to be possible for liquefaction to occur in field deposits denser than the critical density. Furthermore, a case may be made that since most of the N_1-values presented by Seed[3] in Figure 1 for field liquefaction range between 10 and 30 blows, and if the relationship in Figure 28 is approximate for these field cases, then

Table 6

Summary of Friction Angle Values and Estimated SPT N-values for Monotonic $\bar{R}$ Tests on Reid-Bedford Model Sand

Specimen No.	α , deg*	ϕ' , deg**	ϕ' , deg†	Estimated SPT N-values††
1	--	--	--	--
2	26.0	29.2	29.2	5.2
3	26.1	29.3	29.3	5.1
4	26.6	30.0	30.4	7.9
5	26.6	30.0	30.0	5.1
6	26.8	30.3	30.3	8.1
7	--	--	--	--
8	25.9	29.1	29.0	-2.4
9	25.4	28.4	28.7	-1.1
10	25.7	28.7	28.9	13.7
11	28.3	32.5	32.4	13.0
12	28.4	28.4	28.7	15.5

* Based upon $\alpha = \tan(q/P)$ at failure.

** Tan α = sin ϕ' .

† Based upon $\bar{\sigma}_1/\bar{\sigma}_3 = \tan^2(45 + \phi'/2)$ at maximum $\bar{\sigma}_1/\bar{\sigma}_3$ value.

†† Based upon Equation $N = -5.5 + 0.2(\bar{\sigma}_v) + 0.0046(D_r)^2$, where σ_v is $\bar{\sigma}_{3c}$ in psi and D_r from Table 5.

Table 7

Estimated SPT N-Values for Castro's[2] Banding Sand

Test No.	$\bar{\sigma}_3$ kg/cm^2	D_{rc} %	Corrected D_{rc} %	SPT N*	Failure
13-3	0.3	29	17.5	-4.14	LL
13-4	0.3	41	28	-1.99	D
1-4	1	37	22	-1.05	LL
1-4	1	43	29	0.56	D
4-7	4	46	31	10.91	LL
4-8	4	47	32	11.2	D
10-5	10	49	34	31.4	LL
10-6	10	53	40	33.41	D

* $N = -6.5 + 0.23(\bar{\sigma}_v) + 0.0045(D_r)^2$, where $\bar{\sigma}_v$ is in psi from Reference 13.

liquefaction will occur in deposits denser than critical. Conversely (and probably more correctly), Casagrande[27] points out that

> in nature, liquefaction will normally start in a lens of particularly loose sand; and from such a nucleus it may spread by a chain reaction also into somewhat denser sand layers....Flow will continue until the driving forces are reduced to the small shearing resistance of the sand in its flow state, then dilation will cause the liquefied mass to 'freeze' again into a solid structure, accompanied by a great reduction in pore pressures, and the mass then stops flowing.

From this viewpoint it is most likely that sand lenses looser than critical existed in the field deposits presented in Figure 1 and were the nucleus for the liquefaction observed. Such lenses could easily have gone undetected in the field investigations or could have been averaged out in summarizing the data.

40. It has been hypothesized[1,27] that in cyclic laboratory tests, the cyclic softening that occurs in dilative sands is the result of density redistributions. Portions of a dense specimen expand to a loose state, flow briefly, and revert by dilation to a solid structure which can momentarily carry the load before the following cycle. This response has been termed "liquefaction-dilation" by Casagrande.[27]

41. Figure 29 presents the load, deformation, and pore pressure responses for specimen RB60-80-1 (Reid-Bedford Model sand at 60 percent D_r and σ_2 = 80 psi) which was tested at a stress ratio of 0.235. A careful examination of the pore pressure trace reveals that for cycles 1-17, a uniform sinusoidal response occurs, with the pore pressures steadily increasing. However, for cycles 17-21 the pattern becomes rectangular, with pronounced "spikes" occurring at instances of zero shear stress; i.e., instant of stress reversal when passing from compression to extension or visa versa. Between these "spikes" in cycles 17-21 a plateau is observed which corresponds with application of the full compressive or extension axial stress, under which the specimen dilates. This pattern corresponds to a "liquefaction-dilation" response, with liquefaction occurring at the instant of stress reversal when the

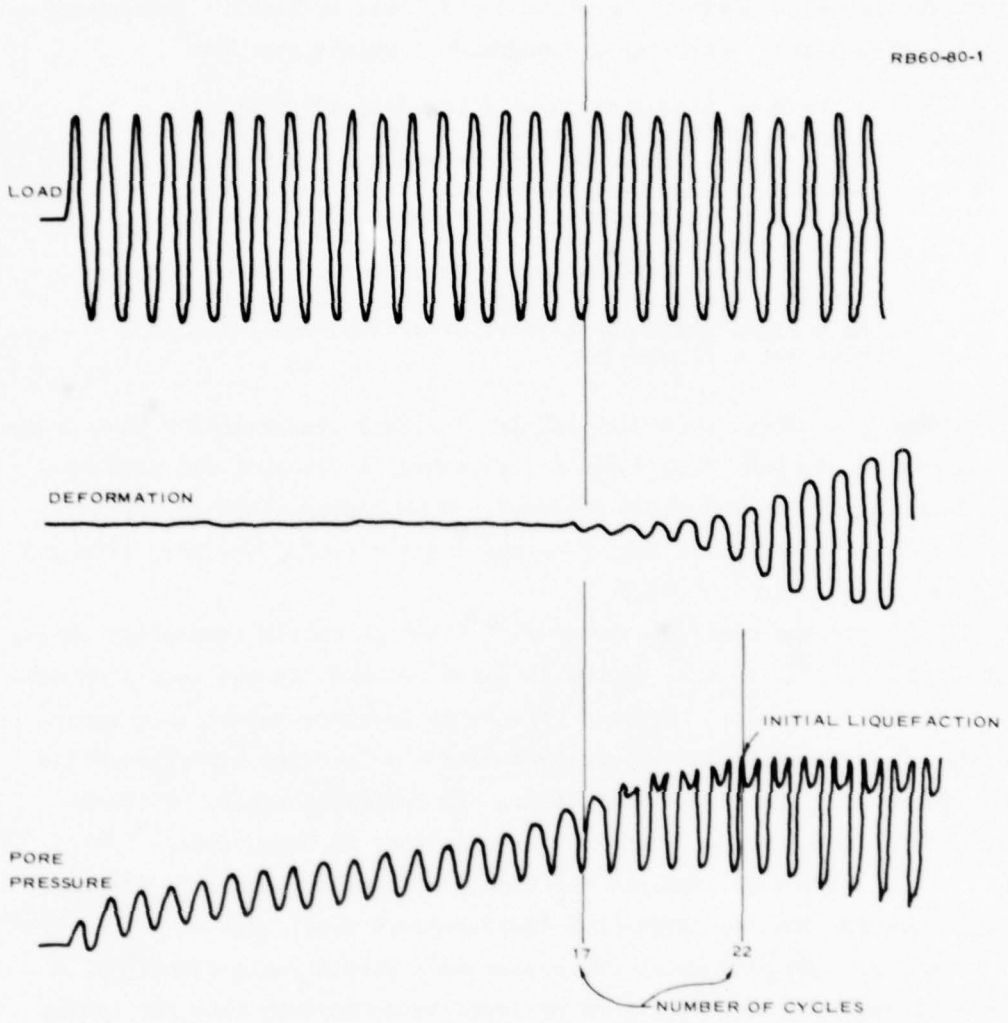

Figure 29. Cyclic triaxial test record of load, deformation, and pore pressure for test RB60-80-1

pore pressure "spikes", and dilation occurring when the full axial compression or extension load is applied and the "plateaus" are formed.

42. An examination of the deformation response reveals that at cycle 17 double amplitude axial strain is less than 1 percent, while at cycle 21 double amplitude strain is 5 percent and occurs just prior to 100 percent pore pressure response (initial liquefaction).

43. Figure 30 presents the corresponding effective stress path followed during cyclic triaxial test RB60-80-1, for which the data are listed in Table 8. This figure shows that failure of the specimen is caused by the stress path marching progressively leftward toward the origin until the extension failure envelope is reached on cycle 17 (point A). Then, the compression failure envelope is reached on cycle 21 (point B). After cycle 21 the effective stress is zero when the shear stress is zero, i.e., the origin and the stress path cycles from point A to origin to B and back.

44. The path followed from cycle 1-2 clearly shows the process by which positive pore pressures are generated in a dilative sand by cyclic testing. In compressional loading on this cycle, a dilative response is observed with 4-psi negative pore pressure induced at the end of the first half of the cycle. Because of the difference in specimen stiffness in compression and extension, however, the extension stress is applied, and a positive pore pressure of 8 psi results, producing a net positive pore pressure increase of 4 psi for this cycle. This pattern persists until cycle 19, in which no induced negative pore pressures are generated on the compressive stroke, and positive pressures are generated in both compression and extension.

45. From these considerations it appears that effective stress parameters are valid for design considerations. The amount of redistribution occurring within cyclic triaxial specimens depends upon the relative density, the cyclic deviator stress, and consolidation stress applied in the test. For the specific case in Figure 30, redistribution becomes significant in cycle 17 and increases with each successive cycle until initial liquefaction is reached on cycle 22.

46. Figure 31 presents the effective compressive stress envelope at 100 percent pore pressure response (initial liquefaction) for all the cyclic triaxial tests conducted on Reid-Bedford Model sand. These results were obtained by using the plateau as the pore pressure response ($\bar{\sigma}_{3f}$) for computing the effective confining stress and $\left(\bar{\sigma}_1 + \bar{\sigma}_3\right)/2$. This $\bar{\sigma}_{3f}$ for the plateau is not valid for deriving an e_f as presented in Figure 27, as this $\bar{\sigma}_{3f}$ corresponds to the point at which the

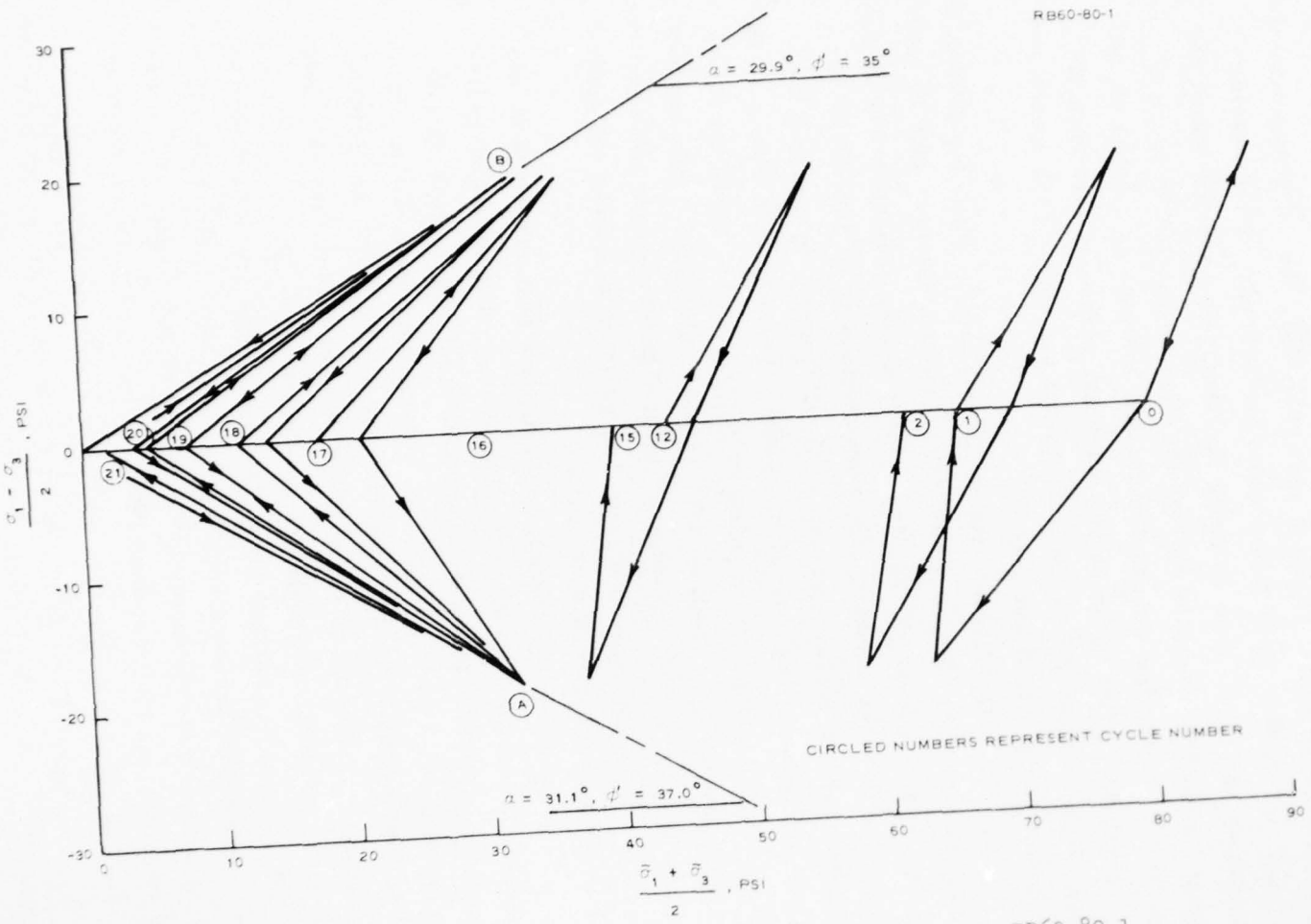

Figure 30. Effective stress path for cyclic triaxial test RB60-80-1

Table 8

Effective Stress Path Points for Cyclic Triaxial

Test RB60-80-1 (Stress Ratio = 0.235)

Cycle No.	Condition*	Pore Pressure Δu, psi	$(\bar{\sigma}_1 + \bar{\sigma}_3)/2$** p, psi	$(\bar{\sigma}_1 - \bar{\sigma}_3)/2$ q, psi
0	O	0	80	0
1/4	C	10	88.8	18.8
1/2	O	0	80	0
3/4	E	-2	63.2	-18.8
1	O	14	66	0
1-1/4	C	20	78.8	18.8
1-1/2	O	10	70	0
1-3/4	E	3	58.2	-18.8
2	O	18	62	0
12	O	36	44	0
12-1/4	C	43	55.8	18.8
12-1/2	O	34	46	0
12-3/4	E	24	37.2	-18.8
13	O	40	40	0
17	O	62	18	0
17-1/4	C	60	38.8	18.8
17-1/2	O	59	21	0
17-3/4	E	30	31.2	-18.8
18	O	68	12	0
18-1/4	C	63	35.8	18.8
18-1/2	O	66	14	0
18-3/4	E	30	31.2	-18.8
19	O	72	8	0
19-1/4	C	65	33.8	+18.8
19-1/2	O	72	8	0
19-3/4	E	30	31.2	-18.8
20	O	75	5	0
20-1/4	C	66	32.8	18.8
20-1/2	O	76	4	0
20-3/4	E	30	31.2	-18.8
21	O	78	2	0
21-1/4	C	66	32.8	18.8
21-1/2	O	80	0	0
21-3/4	E	30	31.2	-18.8
22	O	80	0	0

* O = origin, C = compression, E = extension.

** $(\bar{\sigma}_1 + \bar{\sigma}_3)/2 = (\sigma_d + 2\sigma_3 - 2u)/2 = \sigma_d/2 + (\sigma_3 - u)$.

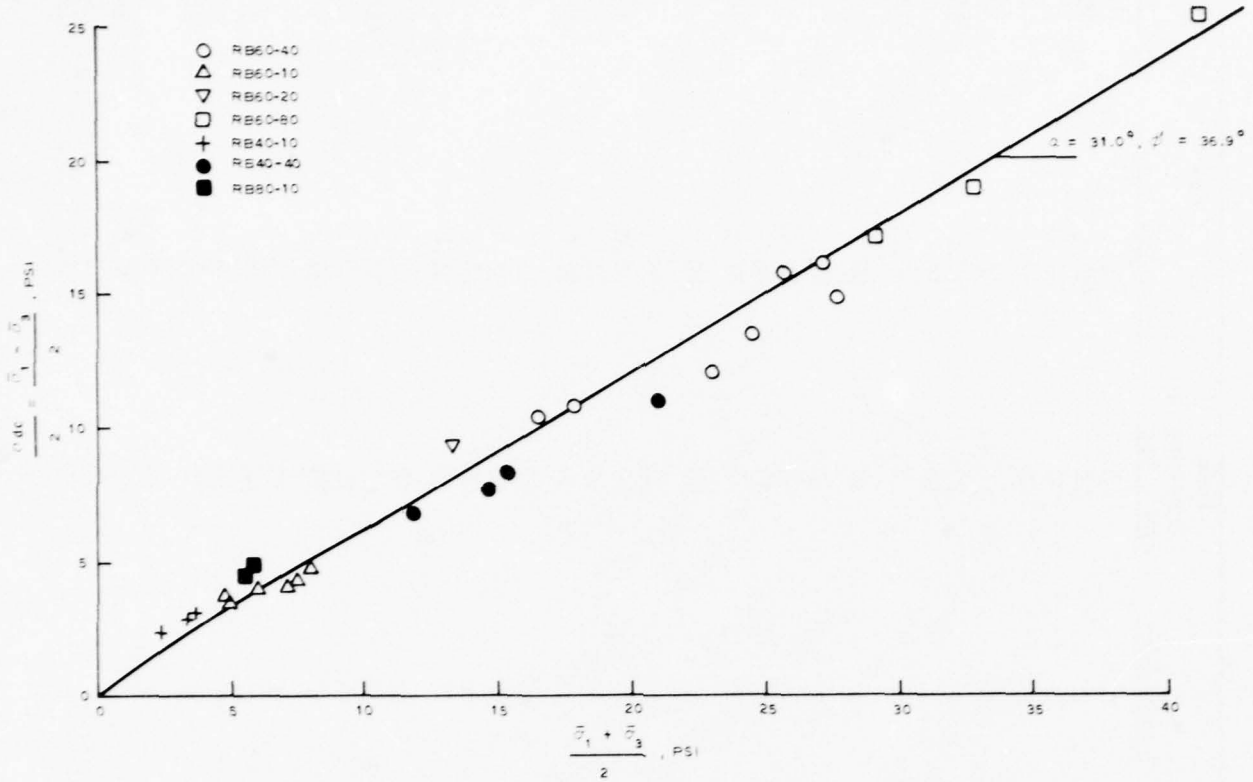

Figure 31. Failure envelope for cyclic triaxial tests on Reid-Bedford Model sand

specimen dilates to carry the load, and the e_f line presents conditions of liquefaction for the point at which the flow structure is developed. Table 9 tabulates the data for Figure 31. The effective friction angle ϕ' for all these tests is 35.0 deg, as compared with the 29.6 deg observed for the monotonic tests. This difference is due to the higher densities of the cyclic tests.

47. It is apparent that for initial liquefaction to occur in cyclic triaxial tests on dense sands, two criteria must be satisfied:

a. A stress reversal through the hydrostatic condition must occur.

b. A sufficient number of cycles must be applied.

Although interpretation of the number of cycles applied during an earthquake has been successfully applied using the concept of an equivalent number of cycles,[28] the stress path during an earthquake is quite different from that followed in the cyclic triaxial test; and a stress reversal through the hydrostatic condition may never occur.

Material Characterization for Elastic-Plastic Constitutive Model

48. As part of the monotonic $\bar{R}$ triaxial tests, an isotropic compression (consolidation) load-rebound (ICL-R), reconsolidation loop was performed on specimens RB20-40-5, RB30-40-6, RB20-80-10, RB15-80-11, and RB25-80-12, as listed in Table 5. Radial measurements by LVDT clamps were made throughout these tests. The objective of using this isotropic compression loop was to obtain material constants to evaluate an elastic-plastic, work-hardening model for fluid-saturated granular materials.[12] Characterization of this elastic-plastic constitutive relationship requires the evaluation of: four material constants, K_i, K_o, $\tilde{K}'$ and K', from the ICL-R portion of the tests; the elastic shear modulus G; the slope of the failure envelope M, as shown in Figure 32.

ICL-R tests

49. The pressure volumetric strain relationships for the five ICL-R tests are presented in Figures 33-37. Shown in these figures are

Table 9

Summary of Effective Stress Condition at 100 Percent Pore Pressure Response for Cyclic Triaxial Tests on Reid-Bedford Model Sand

Material	D_r	e_c	$\frac{\sigma_{dc}}{2}$ psi	$\bar{\sigma}_{3c}$ psi	$\bar{\sigma}_{3f}$ psi	N_i	$\frac{\bar{\sigma}_1 + \bar{\sigma}_3}{2}$* psi
RB60-40	60.4	0.677	16.04	40	11	6	27.04
	57.8	0.686	14.68	↓	13	8	27.68
	60.7	0.676	13.44		11	9	24.44
	60.8	0.676	12.04		11	14	23.04
	61.6	0.673	10.84		7	45	17.84
	59.9	0.679	10.44		6	47	16.44
RB60-10	58.4	0.684	4.02	10	2	11	6.02
	59.3	0.681	3.51	↓	15	247	5.01
	59.3	0.681	3.75		1	48	4.75
	60.6	0.677	4.12		3	11	7.12
	59.6	0.680	4.41		3	9	7.41
	59.4	0.680	4.90		3	7	7.90
RB60-20	60.1	0.678	9.32	20	4	6	13.32
RB60-80	64.2	0.665	18.80	80	14	22	32.80
	64.1	0.665	25.28	↓	16	5	41.28
	64.4	0.664	17.12		12	22	29.12
	64.6	0.664	15.76		10	45	25.76
RB40-10	41.3	0.739	3.10	10	0.5	6	3.60
	38.9	0.746	2.82	10	0.5	12	3.32
	39.1	0.746	2.46	10	0	24	2.46
RB40-40	39.4	0.745	8.84	40		11	--
	43.5	0.732	6.88	↓	5	74	11.88
	42.3	0.735	7.64		7	55	14.64
	39.5	0.744	8.36		7	18	15.36
	40.9	0.740	11.00		10	4	21.00
RB80-10	79.1	0.617	4.48	10	1	49	5.48
	78.9	0.618	4.86	10	1	37	5.86

* $\bar{\sigma}_3 = \frac{\sigma_{dc}}{2} + \sigma'_{3f}$.

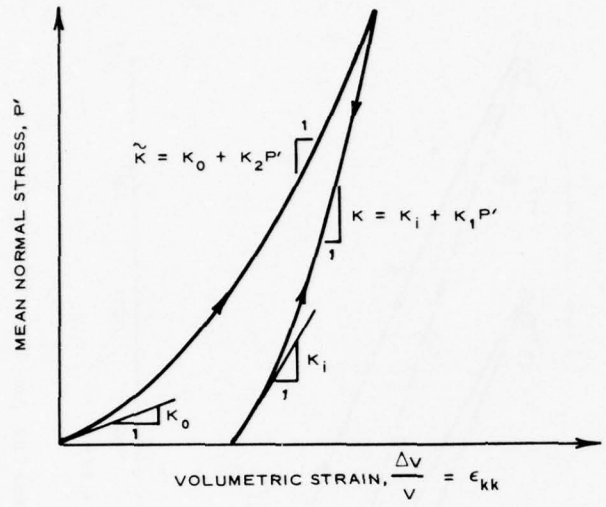

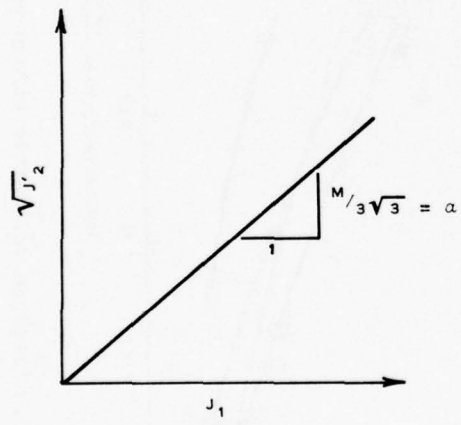

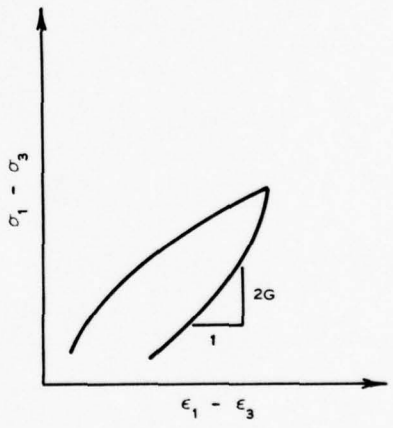

WHERE FOR |X| CONDITIONS:

$$J'_2 = \frac{1}{2}(\sigma_1^2 + 2\sigma_3^2)$$

AND $J'_1 = \sigma_1 + 2\sigma_3$

Figure 32. Definition of material constants for elastic-plastic constitutive equation

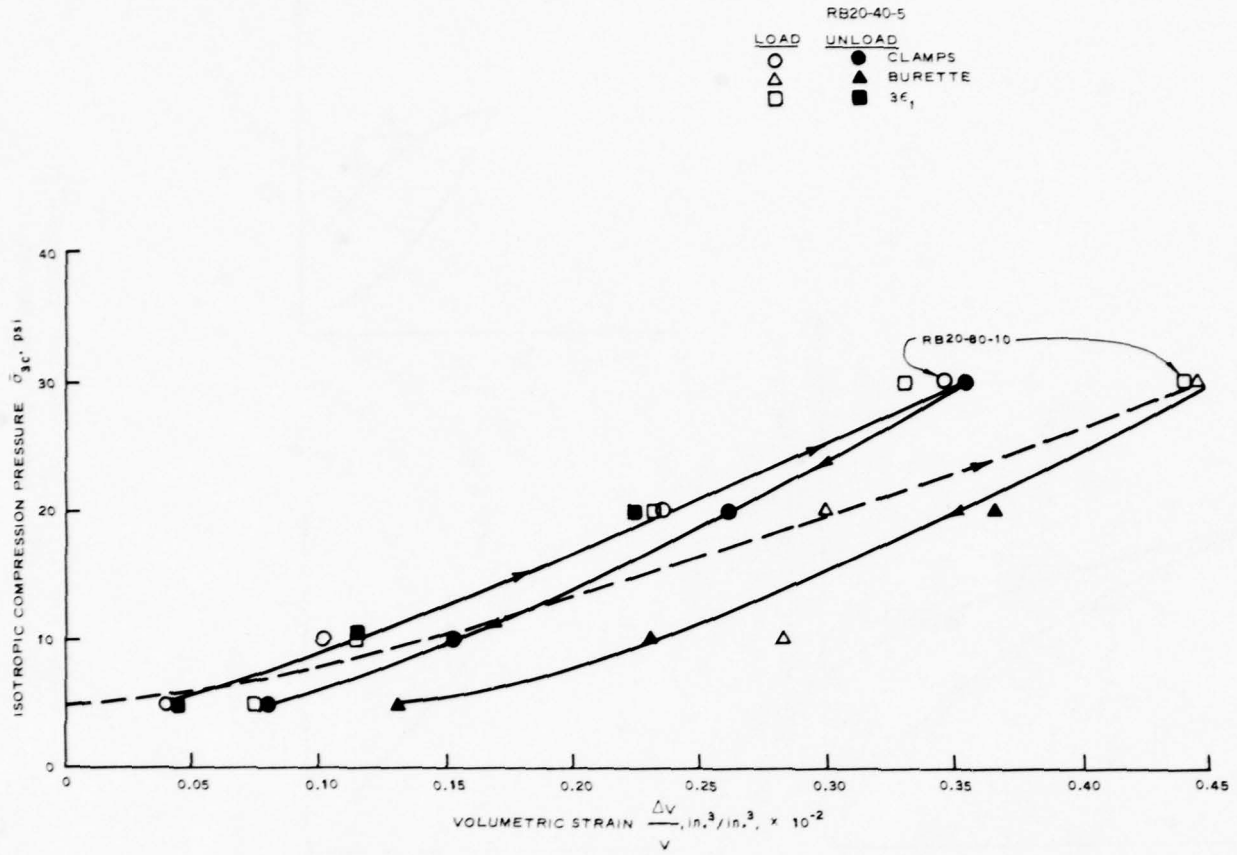

Figure 33. Pressure-volumetric strain relationships for test RB20-40-5

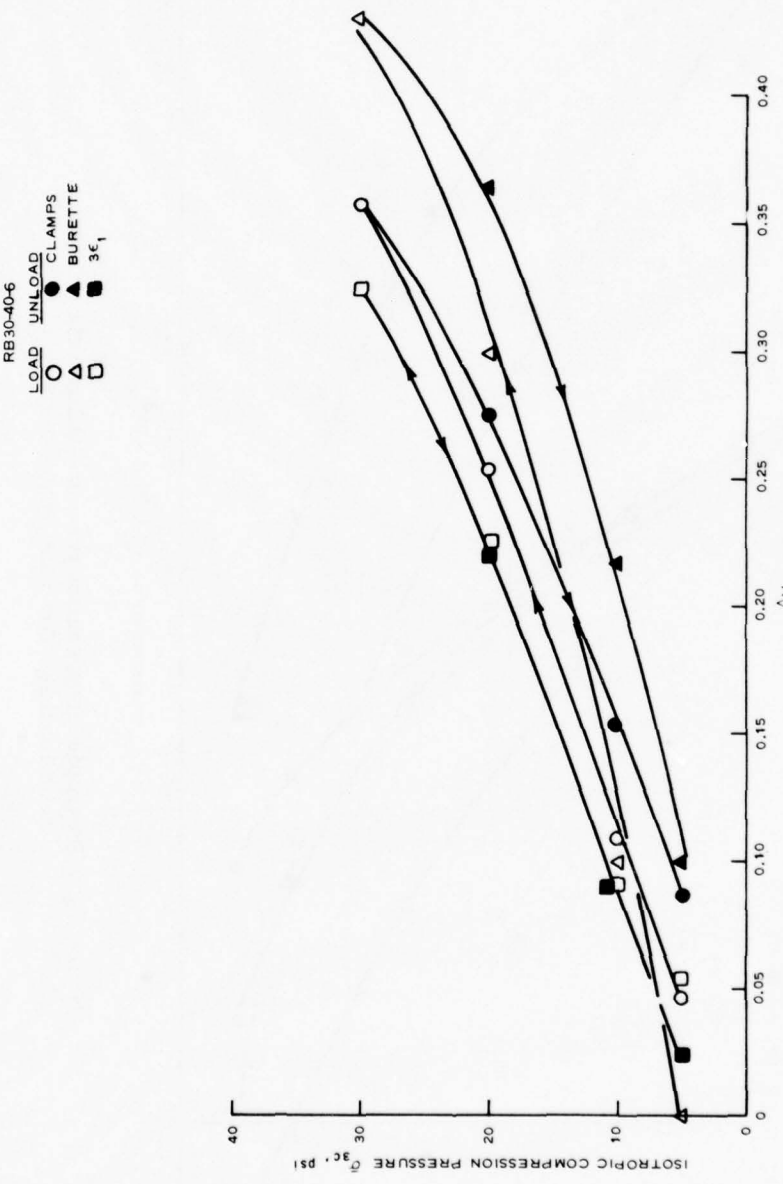

Figure 34. Isotropic compression pressure-volumetric strain relationships for test RB30-40-6

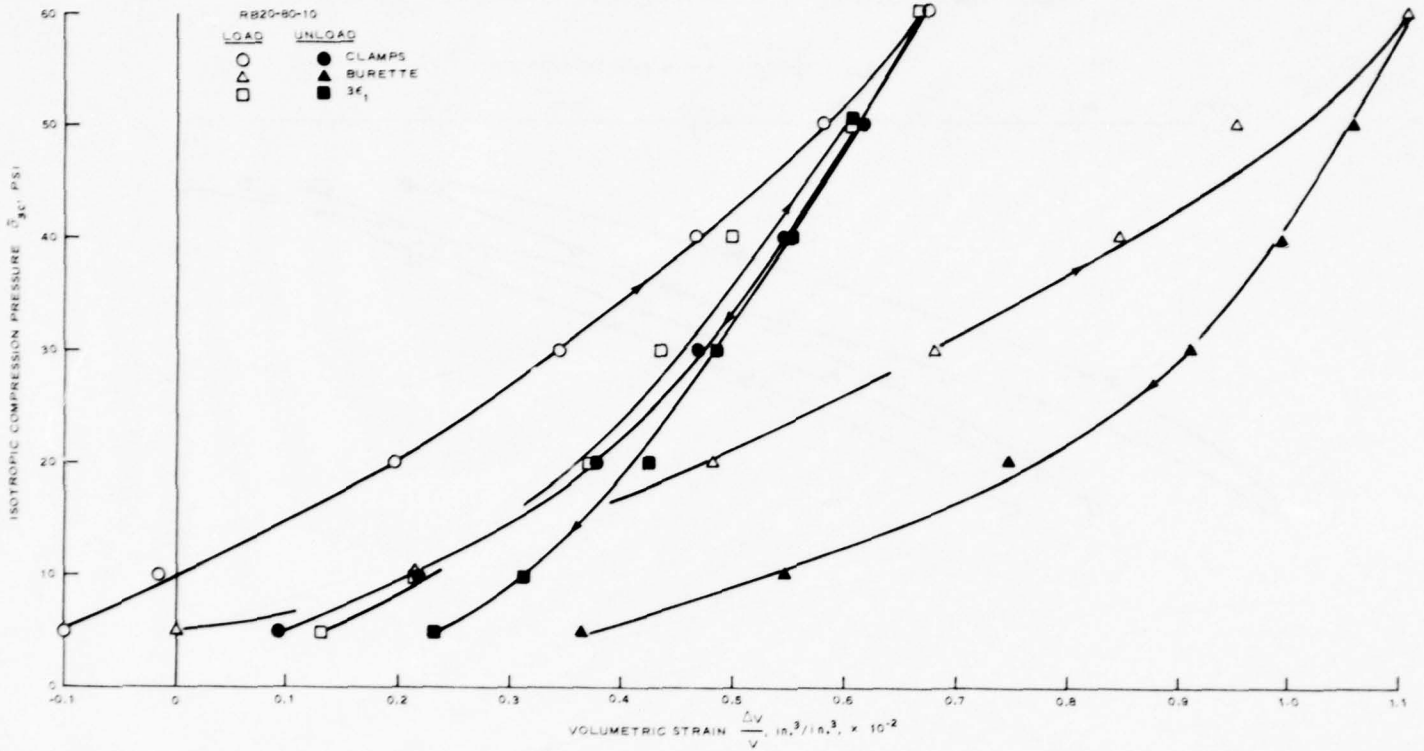

Figure 35. Isotropic compression pressure-volumetric strain relationships for test RB20-80-10

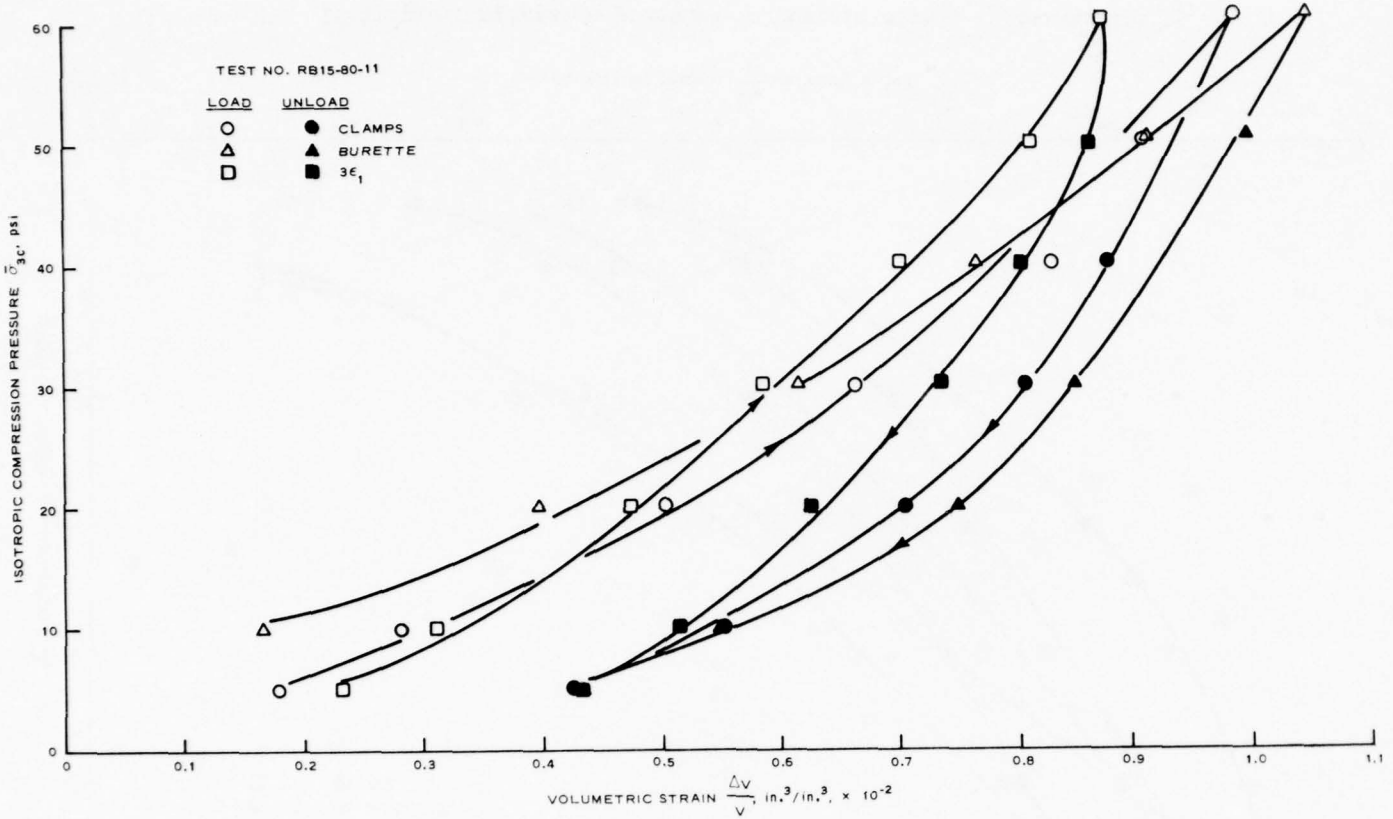

Figure 36. Isotropic compression pressure-volumetric strain relationships for test RB15-80-11

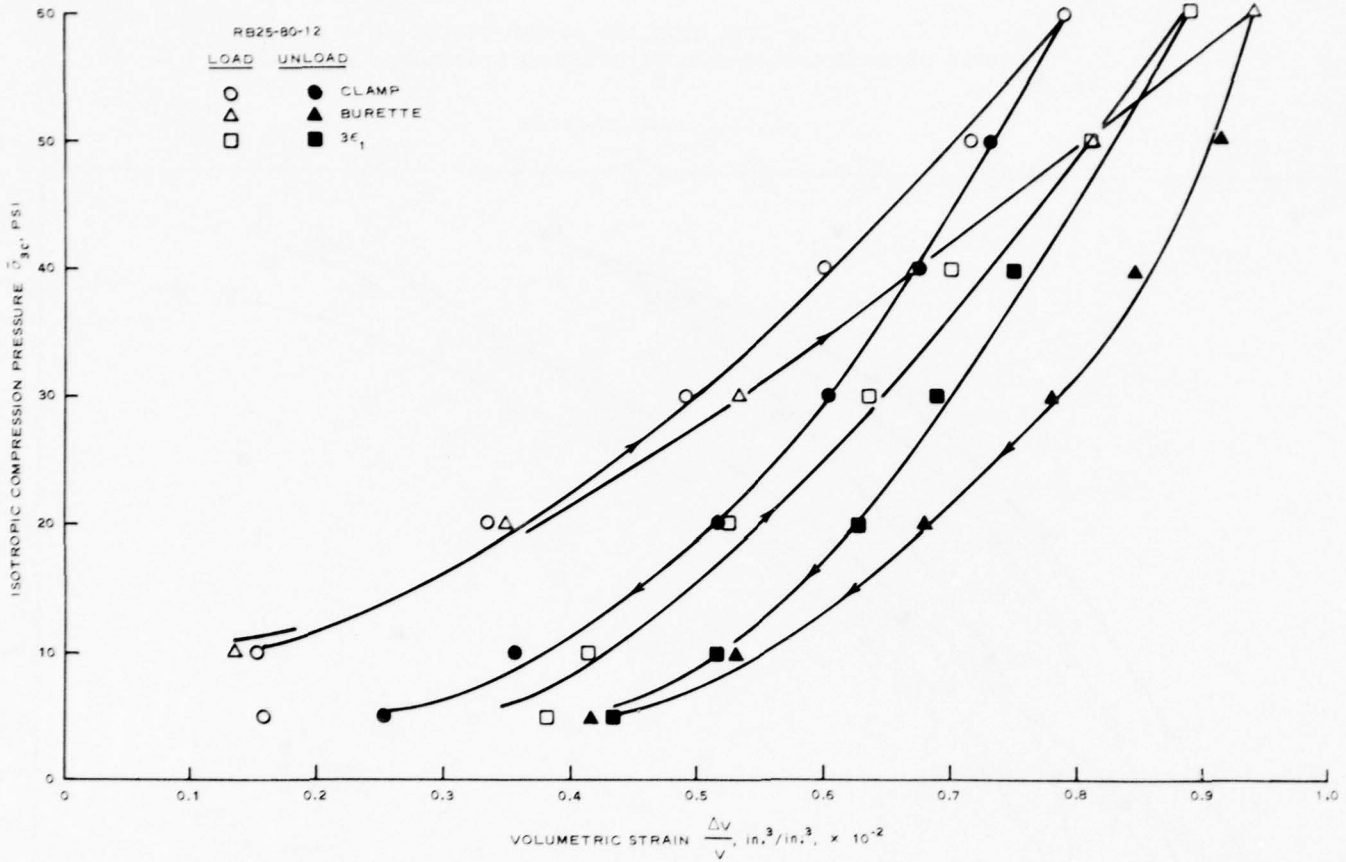

Figure 37. Isotropic compression pressure-volumetric strain relationships for test RB25-80-12

with liquefaction occurring at the instant of stress reversal when

volumetric strains calculated from: (a) measurements of axial and radial deformations, where $\Delta v/v = \varepsilon_1 + 2\varepsilon_3$; (b) burette measurements of water leaving and entering the specimen, Δv burette/Vol of specimen ; and (c) the assumption that the specimens are isotropic, in which case, $\varepsilon_1 = \varepsilon_3$ and $\Delta v/v = 3\varepsilon_1$. A comparison between the volumetric strains determined measurement of the specimen dimensions (Method a) and those determined by burette measurements (Method b) shows the obvious effects of membrane penetration. Table 10 summarizes membrane penetration and lists values of S , which is the membrane penetration in cc per unit area of specimen covered by the membrane, per unit of pressure, kg/cm^2.[29] The range of S-values for loading 0.003-0.005 agree quite well with Frydman et al.[29] value of 0.004, based upon a relationship between D_{50} and S . However, upon unloading, the S-values listed are quite low. Conceivably, membrane penetration values would be independent of loading path and dependent primarily on pressure; hence, the magnitude of membrane penetration measured by this technique may be questioned. The S-values listed are relatively insensitive to D_r for the ranges of values tested.

50. An assumption of isotropy for estimating volume change (Method a versus Method c) typically underestimates the amount of volume change for these five specimens. However, the error in assuming isotropy is about equal to that induced into burette measurements by membrane penetration. Hence, this method of calculating volume changes is reasonably accurate for these test conditions.

Material constants

51. Table 11 lists the material constants experimentally determined for evaluating the elastic-plastic constitutive relationship.[30] The values, K'_o , $\tilde{K}'$, K' and K'_i , were determined from the data presented in Figures 33-37. The ϕ'-values are the same as those listed in Table 6, with α calculated as $\alpha = 2 \sin \phi'/(3 - \sin \phi')\sqrt{3_o}$. Figure 38 presents the undrained deviation stress versus deviation strain relationship during loading. Since the elastic-plastic model requires drained constants, G'-values were estimated from the relationship, $G' = 3K_i (1 - 2\nu')/2(1 + \nu')$, with ν' estimated from

Table 10

Summary of Volumetric Strains and Membrane Penetration for Isotropic Compression-Rebound Tests on Reid-Bedford Model Sand

Test No.	$\sigma_{3\ Max}$ kg/cm^2	σ_{30} kg/cm^2	ϵ_v Clamps	ϵ_v Burette	ϵ_v^* Membrane	ΔV_m ** cm^3/cm^2	S† cm^3/cm^2 kg/cm^2	Remarks
RB20-40-5	2.11	0.35	0.00315	0.00448	0.00133	0.00233	0.003	Load
			0.00275	0.00315	0.00040	0.00070	0.0009	Unload
RB30-40-6	2.11	0.35	0.00312	0.00432	0.0012	0.0021	0.0027	Load
			0.00272	0.00332	0.00048	0.00084	0.001	Unload
RB20-80-10	4.22	0.35	0.00802	0.01111	0.00309	0.00541	0.005	Load
			0.00583	0.00746	0.00163	0.00235	0.0026	Unload
RB15-80-11	4.22	0.35	0.00807	0.01045	0.00238	0.00417	0.0038	Load
				0.00614	0.00054	0.00095	0.00088	Unload
RB25-80-12	4.22	0.35	0.00634	0.00945	0.00311	0.00545	0.005	Load
			0.00539	0.00531	0.0	0.0	0.0	Unload

* $(\epsilon_v)_{membrane} = (\epsilon_v)_{burette} - (\epsilon_v)_{clamps}$.

** $\Delta V_m = (\epsilon_v)_{membrane} \times \frac{V_o}{A\ membrane}$ $V_o \approx 602$ cc $A_m \approx (15.28\ cm)(7.16\ cm) \times \pi = 343.84\ cm^2$; $\therefore \frac{V_o}{A_m} = 1.751\ cm^3/cm^2$.

† $s = \Delta V_m / \log \Delta P$ slope of ΔV_m - log P relationship.

Table 11

Drained and Undrained Material Constants for Elastic-Plastic Model for Reid-Bedford Model Sand

Test Specimen*	LVDT Clamp K'_o** kg/cm^2	$\tilde{K}'$† kg/cm^2	K'†† kg/cm^2	K'_i kg/cm^2	P' kg/cm^2	K_1‡	W‡‡	D_1§ kg/cm^2	ϕ' deg	α§§	G'# Unloading kg/cm^2	E_i## kg/cm^2	Undrained ν¶
RB20-40-5	558	558	696	579	2.11	55	0.0038	0.16	30	0.23	222	4055	0.48
RB30-40-6	567	563	683	581	2.11	48	0.0037	0.16	30.3	0.23	223	1880	0.73
RB20-80-10	311	641	1060	368	4.22	164	0.0066	0.16	28.7	0.22	132	8687	0.59
RB15-80-11	335	653	1166	379	4.22	186	0.0065	0.15	32.5	0.25	155	529	0.61
RB25-80-12	225	703	1116	396	4.22	171	0.0060	0.25	28.4	0.21	162	8364	0.77

* RB20-40-5 = Reid-Bedford Model sand, D_r = 20 percent, $\bar{\sigma}_{3c}$ = 40 psi, Test No. 5 of a series.

** $K_o = 1/3D_1W$.

† $\tilde{K} = (P' - 1/3D_1)/W$.

†† $K = K_i + K_1P'$.

‡ $K_1 = (K - K_i)/P'$.

‡‡ $W = P/\tilde{K} - \frac{1}{K_o} =$.

§ $D_1 = 1/3K_oW$.

§§ $\alpha = \frac{2 \sin \phi'}{(3 - \sin \phi')\sqrt{3}}$.

\# G = drained shear modulus, unloading (elastic) = $3 K_i(1 - 2\nu')/2(1 + \nu')$ $\nu' = K_o/1 + K_o$, where $K_o = 1 - \sin \phi'$.

E_i = initial tangent Young's modulus, undrained loading.

¶ ν = Poisson's ratio $\varepsilon_3/\varepsilon_1$ undrained loading.

n figure 21, as this σ_{3f} corresponds to the point at which the

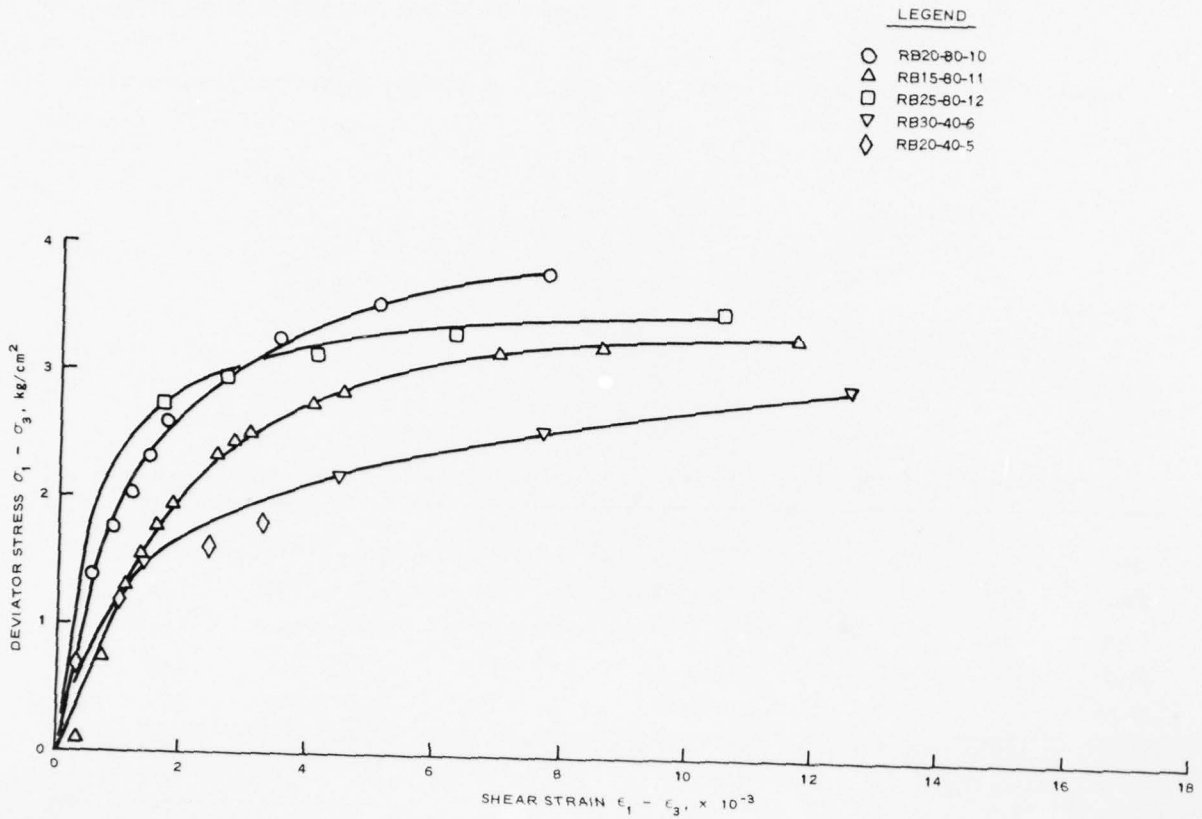

Figure 38. Deviator stress versus shear strain relationships for monotonic $\overline{R}$ tests on Reid-Bedford Model sand

$\nu' = K_o/1 + K_o$, where $K_o = 1 - \sin \phi'$. For comparison, G'-values for Reid-Bedford Model sand at 25 percent D_r were calculated from data contained in Reference 31 and the relationship, $G' = D(1 - 2\nu')/2(1 - \nu')$, where D is the constrained modulus in K_o tests during unloading. G'-values calculated from this data, $D \approx 2743$ kg/cm^2 and $\nu' \approx 0.4$-0.5 , were 566-155 kg/cm^2, which brackets data in Table 11. The undrained parameters, E and ν , from the loading portions of the tests are also listed. Since these are from the loading portions of the tests, the parameters are not truly elastic constants as plastic deformations are included.

Predicted versus observed results

52. The actual model parameters used to compare the model with experimental results of tests RB20-40-5 and RB20-80-10 are listed in Table 12. A comparison of experimental values in Table 11 and assumed values in Table 12 shows that fairly good agreement exists between the two tables, except that experimental K_1-values are lower than assumed values. The parameter R , which is the ratio of the major to minor axis of the elliptical yield surface, must be assumed with contractive materials having R-values $> 1/\alpha$ and dilative materials having R-values $< 1/\alpha$. The two parameters having the greatest effect on the stress-strain pore pressure response are R and α .[30]

53. Figures 39-42 compare behavior predicted by the model with actual test conditions for specimens RB20-40-5 and RB20-80-10. From these figures it is observed that the constitutive model can qualitatively simulate the stress-strain pore pressure response of a contractive sand.[30]

Table 12

Numerical Values of Material Constants for Reid-Bedford Model Sand

Material Constants	Test Series 1 Relative Density 20 percent
K_i kg/cm^2	300.0
K_1	300.0

(Continued)

Table 12 (Concluded)

Material Constants	Test Series 1 Relative Density 20 percent
G kg/cm^2	250.0
α	0.2309
R	4.33
W	0.0074
$D_1 (kg/cm^2)^{-1}$	0.300

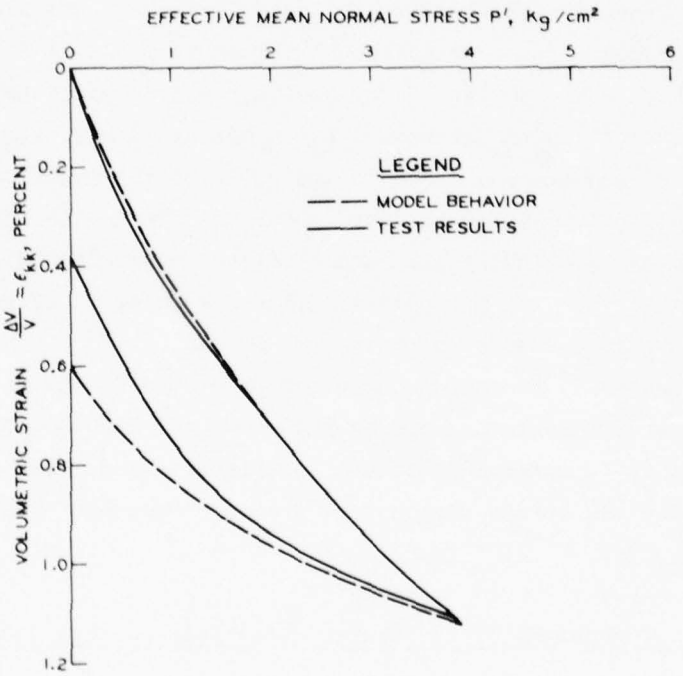

Figure 39. Comparison of experimental effective mean normal stress versus volumetric strain relation with model behavior under isotropic consolidation condition for test RR20-80-10

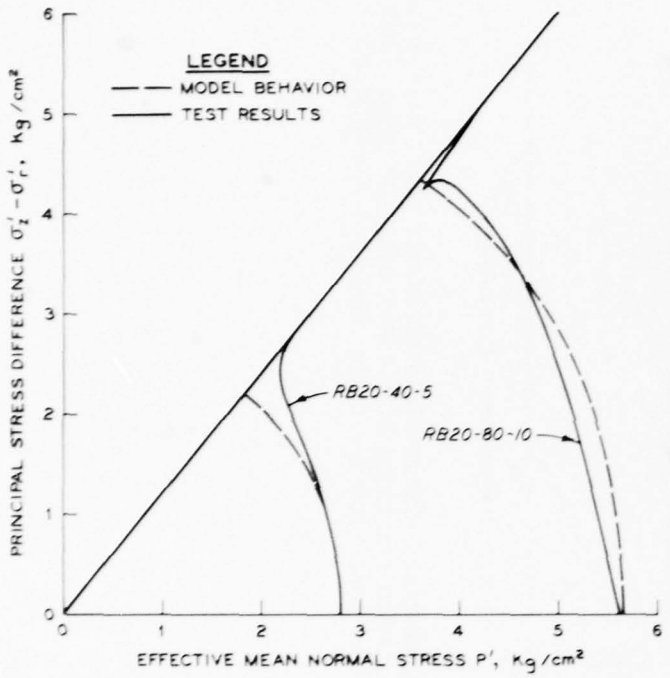

Figure 40. Comparison of experimental effective stress paths with model behavior under undrained triaxial test condition for tests RB20-40-5 and RB20-80-10

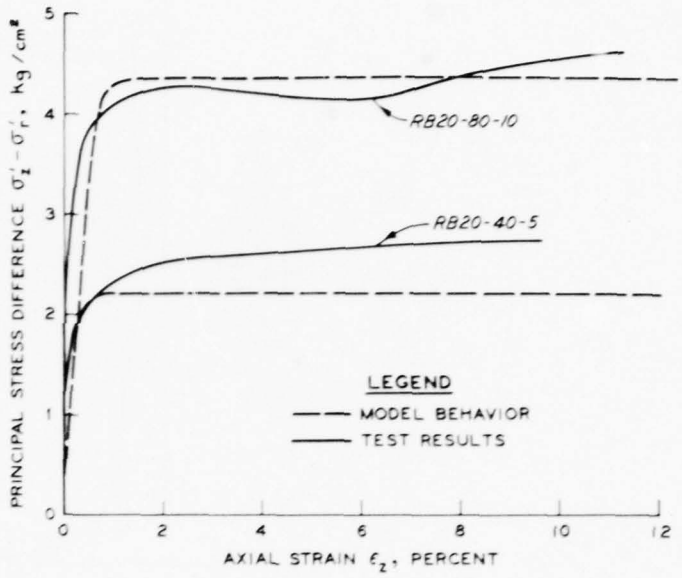

Figure 41. Comparison of experimental stress difference versus axial strain relation with model behavior under undrained triaxial test condition for tests RB20-40-5 and RB20-80-10

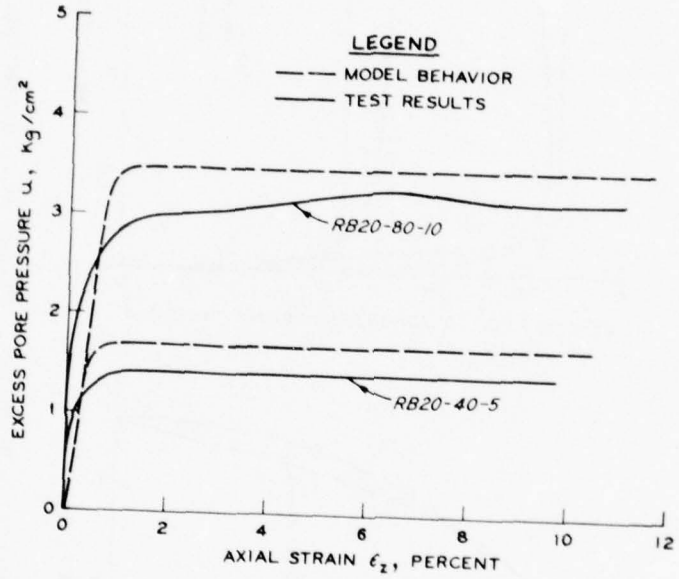

Figure 42. Comparison of experimental excess pore water pressure versus axial strain relations with model behavior under undrained triaxial test condition for tests RB20-40-5 and RB20-80-10

PART IV: CONCLUSIONS AND RECOMMENDED RESEARCH

Conclusions

54. Based upon the materials tested, methods and equipment employed, and information in pertinent literature, the following conclusions are drawn concerning the liquefaction behavior of reconstituted sands under cyclic and monotonic loadings:

a. Cyclic triaxial loadings.

(1) For the four sands tested, as the mean grain diameter D_{50} and uniformity coefficient C_u decrease, so does the resistance to 100 percent pore pressure response. This supports the familiar concept that fine uniform sands are most susceptible to liquefaction.

(2) For Reid-Bedford Model sand, a linear increase in cyclic stress ratio required to cause 100 percent pore pressure response or deformation exists for increasing D_r-values to approximately 60 percent. However, the slope of this relationship depends upon confining pressure. This supports the concept that test results on specimens of different densities can be corrected to a common density for comparison.

(3) For Reid-Bedford Model sand, the cyclic stress ratio required to cause 100 percent pore pressure response or deformation decreases with increasing effective confining pressure. An increase in confining pressure from 10-40 psi decreased the cyclic stress ratio for 10 percent double amplitude strain 27-36 percent, depending upon the D_r.

b. Relationship between SPT N-values and earthquake liquefaction potential.

(1) Values of C_N for correcting SPT N-values to an effective overburden pressure of 1 tsf vary with relative density, sand type, overburden pressure, and possibly additional variables. Nevertheless, the values presented in Figure 23 or Equation 3 can be used as first approximation guides for obtaining C_N-values.

(2) Values of C_r for correcting isotropically consolidated cyclic triaxial test results to estimated field earthquake responses of level ground deposits vary with N_1-values, which are a function of

confining pressure and relative density, and with earthquake magnitude, which is a function of number of cycles. In this context, for the four sands tested, C_r-values vary from 0.41-0.63 for specimens prepared by moist tamping.

(3) For cyclic triaxial specimens prepared by moist tamping procedures and having a C_r-value of 0.57, coupled with the C_N-values in Figure 23, reasonable agreement with published, lower bound field earthquake response is obtained for N_1-values up to 20 blows/ft.

c. Monotonic $\overline{R}$ tests on Reid-Bedford Model sand.

(1) A critical void ratio curve, $\overline{e}_f$, as suggested by Castro,[2] can be fitted to the test results in which liquefaction occurred.

(2) The use of an LVDT clamp to measure radial deformations does not inhibit specimen response.

(3) A relationship, presented in Figure 28, was derived for the critical void ratio in terms of SPT N-values. This relationship permits assessment of liquefaction potential under monotonic loads.

d. Comparison between cyclic and monotonic $\overline{R}$ tests.

(1) Cyclic triaxial tests can produce 100 percent pore pressure response and accompanying deformations on specimens denser than critical, i.e., dilative sands. However, this is attributed to density redistributions occurring within the specimen.[1,2]

(2) A close examination of the cyclic triaxial pore pressure responses reveals that a "liquefaction dilation" pattern develops, with momentary liquefaction occurring at the instant of stress reversal (zero shear stress) and dilation occurring when the full axial stress is applied.

(3) The effective stress path of cyclic tests reveals that compressional loading causes induced negative pore pressures, but extension loading results in greater positive pore pressures, causing a net positive pore pressure and leftward marching of the stress path toward the origin. Hence, for 100 percent pore pressure to occur in dense sands, two criteria must be satisfied:

(a) A stress reversal through the hydrostatic condition must occur.

(b) A sufficient number of cycles must be applied.

(4) Failure occurs during the extension portion of loading for cyclic triaxial tests when the effective stress envelope is reached. After this, because the specimen is stronger in compression, several more cycles must be applied before achieving 100 percent pore pressure response. At 100 percent pore pressure response, the stress path moves up and down the compression and extension envelopes, passing through the origin at each instant of 100 percent pore pressure response.

(5) Failures in cyclic and monotonic tests occur at the same effective stress parameters (conditions). The radical difference between the two tests is the stress path followed to achieve these conditions. Nevertheless, the effective stress parameters are applicable to both types of tests.

e. Material characterization for the elastic-plastic constitutive model.

(1) Membrane penetration in isotropic compression tests can be estimated from Frydman's[29] relationship, using mean grain diameter = D_{50}. For reconstituted specimens of Reid-Bedford Model sand an assumption of isotropy, $\varepsilon_1 = \varepsilon_3$, for estimating volumetric strains is about as accurate as calculating volumetric strains from burette measurements because of membrane penetration affecting burette volumes.

(2) The stress-strain pore pressure response of contractive sand can be accurately predicted by the elastic-plastic constitutive model.[30]

Recommended Research

55. A series of monotonic $\bar{R}$ tests should be performed on the Standard Concrete and Platte River sands to develop a relationship between SPT N-values and critical void ratios similar to Figure 28. In addition, the tests should be performed to gain input parameters for the elastic-plastic constitutive model.[30]

56. A series of cyclic triaxial tests should be performed with LVDT clamps strategically located to monitor axial and radial deformations for calculating nonuniformities and redistribution within cyclic triaxial specimens.

57. A series of monotonic tests should be performed incorporating various total stress paths to verify the uniqueness of the effective stress path.

REFERENCES

1. Casagrande, A., "Liquefaction and Cyclic Deformation of Sands; A Critical Review," Harvard Soil Mechanics Series No. 88, Jan 1976, Harvard University, Cambridge, Mass.; Fifth Panamerican Conference on Soil Mechanics and Foundation Engineering, Buenos Aires, Argentina, Nov 1975.

2. Castro, G., "Liquefaction of Sands," Harvard Soil Mechanics Series No. 81, Jan 1969, Harvard University, Cambridge, Mass.

3. Seed, H. B., "Evaluation of Soil Liquefaction Effects on Level Ground During Earthquakes, Liquefaction Problems in Geotechnical Engineering," Presented at the American Society of Civil Engineers, National Convention, Philadelphia, Pa., Sep 1976.

4. Seed, H. B., Mori, K., and Chan, C. K., "Influence of Seismic History on Liquefaction of Sands," Journal, Geotechnical Engineering Division, American Society of Civil Engineers, Vol 103, No. GT4, Apr 1977.

5. Castro, G., "Liquefaction and Cyclic Mobility of Saturated Sands," Journal, Geotechnical Engineering Division, American Society of Civil Engineers, Vol 101, No. GT6, Proceedings Paper 11388, Jun 1975, pp 551-569.

6. Christian, J. T. and Swiger, W. F., "Statistics of Liquefaction and SPT Results," Journal, Geotechnical Engineering Division, American Society of Civil Engineers, Vol 101, No. GT11, Nov 1975.

7. Ohsaki, Y., "Niigata Earthquakes, 1964, Building Damage and Soil Conditions," Soils and Foundations, Vol 6, No. 2, 1966.

8. Seed, H. B. and Peacock, W. H., "Test Procedures for Measuring Soil Liquefaction Characteristics," Journal, Soil Mechanics and Foundations Division, American Society of Civil Engineers, Vol 97, No. SM8, Aug 1971.

9. Seed, H. B. and Idress, I. M., "A Simplified Procedure for Evaluating Soil Liquefaction Potential," Report No. EERC 10-9, Nov 1970, Earthquake Engineering Research Center, College of Engineering, University of California, Berkeley, Calif.

10. Gilbert, P. A., "Case Histories of Liquefaction Failures," Miscellaneous Paper S-76-4, Apr 1976, U. S. Army Engineer Waterways Experiment Station, CE, Vicksburg, Miss.

11. Durham, G. N. and Townsend, F. C., "Effect of Relative Density on the Liquefaction Susceptibility of a Fine Sand Under Controlled Stress Loading," Evaluation of Relative Density and Its Role in Geotechnical Projects Involving Cohesionless Soils, STP 523, Jun 1972, American Society for Testing and Materials, Philadelphia, Pa.

12. Baladi, G. Y. and Rohani, B., "Liquefaction Potential of Dams and Foundations; Development of an Elastic-Plastic Constitutive Relationship for Saturated Sand," Research Report S-76-2, Report 3, Feb 1977, U. S. Army Engineer Waterways Experiment Station, CE, Vicksburg, Miss.

13. Bieganousky, W. A. and Marcuson, W. F., III, "Liquefaction Potential of Dams and Foundations; Laboratory Standard Penetration Tests on Reid Bedford Model and Ottawa Sands," Research Report S-76-2, Report No. 1, Oct 1976, U. S. Army Engineer Waterways Experiment Station, CE, Vicksburg, Miss.

14. _____, "Liquefaction Potential of Dams and Foundations; Laboratory Standard Penetration Tests on Platte River Sand and Standard Concrete Sand," Research Report S-76-2, Report No. 2, Feb 1977, U. S. Army Engineer Waterways Experiment Station, CE, Vicksburg, Miss.

15. Mulilis, J. P., Townsend, F. C., and Horz, R. C., "The Effects of Cyclic Triaxial Testing Techniques on the Liquefaction Behavior of Monterey No. 0 Sand," Miscellaneous Paper S-76-6, Apr 1976, U. S. Army Engineer Waterways Experiment Station, CE, Vicksburg, Miss.

16. Silver, M. L. et al., "Cyclic Triaxial Strength of Standard Test Sand," Journal, Geotechnical Engineering Division, American Society of Civil Engineers, Vol 102, No. GT5, May 1976.

17. Wong, R. T., Seed, H. B., and Chan, C. K., "Cyclic Loading Liquefaction of Gravelly Soils," Journal, Geotechnical Engineering Division, American Society of Civil Engineers, Vol 101, No. GT6, Jun 1975.

18. Seed, H. B. and Lee, K. L., "Liquefaction of Saturated Sands During Cyclic Loading," Journal, Soil Mechanics and Foundations Division, American Society of Civil Engineers, Vol 92, No. SM6, Nov 1966.

19. DeAlba, P., Chan, C. D., and Seed, H. B., "Determination of Soil Liquefaction Characteristics by Large-Scale Laboratory Tests," Report No. EERC 75-14, May 1975, Earthquake Engineering Research Center, College of Engineering, University of California, Berkeley, Calif.

20. Mulilis, J. P., "Effects of Method of Sample Preparation on the Cyclic Stress-Strain Behavior of Sands," Report 75-18, Jul 1975, Earthquake Engineering Research Center, College of Engineering, University of California, Berkeley, Calif.

21. Gibbs, H. J. and Holtz, W. G., "Research on Determining the Density of Sands by Spoon Penetration Testing," Proceedings, Fourth International Conference on Soil Mechanics and Foundation Engineering, London, Vol 1, 1957.

22. Peck, R. B., Hanson, W. E., and Thornburn, T. H., Foundation Engineering, 2d ed., Wiley, New York, 1974, pp 113-115.

23. Pyke, R., Chan, C. K., and Seed, H. B., "Settlement and Liquefaction of Sands Under Multi-Directional Shaling," Report 74-2, Feb 1974, Earthquake Engineering Research Center, College of Engineering, University of California, Berkeley, Calif.

24. Marcuson, W. F., III, and Bieganousky, W. A., "Laboratory Standard Penetration Tests on Fine Sands," Journal, Geotechnical Engineering Division, American Society of Civil Engineers, Vol 103, No. GT6, Jun 1977.

25. _____, "The SPT and Relative Density in Coarse Sands," Journal, Geotechnical Engineering Division, American Society of Civil Engineers, Vol 103, No. GT11, Nov 1977.

26. Seed, H. B. et al., "Representation of Irregular Stress Time Histories by Equivalent Uniform Stress Series in Liquefaction Analyses," Report 75-29, 1975, Earthquake Engineering Research Center, College of Engineering, University of California, Berkeley, Calif.

27. Casagrande, A. and Rendon, F., "Gyratory Shear Apparatus: Design, Testing Procedure and Test Results on Undrained Sand," Technical Report S-78-15, Oct 1978, U. S. Army Engineer Waterways Experiment Station, CE, Vicksburg, Miss., and Harvard Soil Mechanics Series No. 89, Harvard University, Cambridge, Mass.

28. Annaki, M. and Lee, K. L., "Equivalent Uniform Cycle Concept for Soil Dynamics," Journal, Geotechnical Engineering Division, American Society of Civil Engineers, Vol 103, No. GT6, Jun 1977.

29. Frydman, S., Zeitlen, J. G., and Alpan, I., "The Membrane Effect in Triaxial Testing of Granular Soils of Testing and Evaluation," Journal of Testing and Evaluation, American Society for Testing Materials, Vol 1, No. 1, Jan 1973.

30. Baladi, G. Y. and Rohani, B., "Liquefaction Potential of Dams and Foundations; Development of a Constitutive Relationship for Simulating the Response of Saturated Cohesionless Soil," Research Report S-76-2, Report 5, Aug 1978, U. S. Army Engineer Waterways Experiment Station, CE, Vicksburg, Miss.

31. Al-Hussaini, M. M. and Townsend, F. C., "Investigation of K_o Testing in Cohesionless Soils," Technical Report S-75-16, Dec 1975, U. S. Army Engineer Waterways Experiment Station, CE, Vicksburg, Miss.

APPENDIX A: METHODOLOGY AND DATA FOR OBTAINING C_N VERSUS σ_o

1. The procedure for calculating the C_N versus σ_o relationship presented in Figure 23 (see main text) is as follows:

   a. Utilizing the data presented in Figure 22 (see main text) or contained in RR-76-2, Reports 1 and 2,[13,14*] a figure similar to A-1 comparing N versus σ_o for various D_r-values was prepared.

   b. From Figure A-1, N-values corresponding to σ_o pressure of 1 tsf can be interpolated.

   c. By knowing N_1, one can now calculate C_N for various D_r- and σ_o-values by using the relationship $C_N = N_1/N$, as shown in Figure A-2.

   d. The following tabulation contains values used for preparing Figure 23 (see main text).

Summary of N-Values Used for Calculating C_N

Sand Type	D_r	$N_{0.72}$	$N_{2.88}$	$N_{5.76}$	N_1	$N_1/N_{0.72}$	C_N-Values $N_1/N_{1.88}$	C_N-Values $N_1/N_{5.76}$
Reid-Bedford	40	5	11	21	5	1.0	0.45	0.24
and Ottawa	60	10	22	32	12	1.2	0.55	0.38
	80	20	33	48	22	1.1	0.67	0.46
Platte River	40	6	13	17	8	1.33	0.62	0.47
	60	17	28	37	19	1.12	0.68	0.51
	80	37	54	67	40	1.08	0.74	0.60
Standard	40	6	15	25	8	1.33	0.53	0.32
Concrete	60	14	30	44	16	1.14	0.53	0.36
	80	25	50	75	28	1.12	0.56	0.37

* Raised numbers refer to similarly numbered items in "References" presented on pp 70-72 at end of main text.

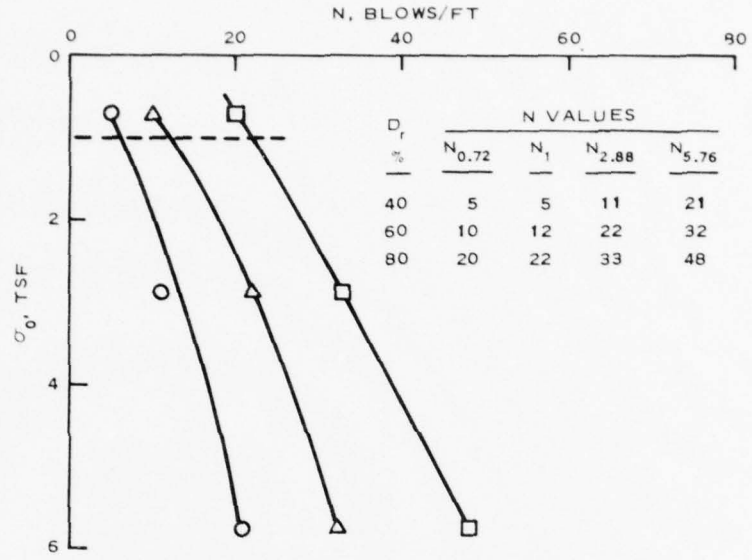

Figure A-1. Relationship between SPT N-values and overburden pressures for Reid-Bedford Model sand

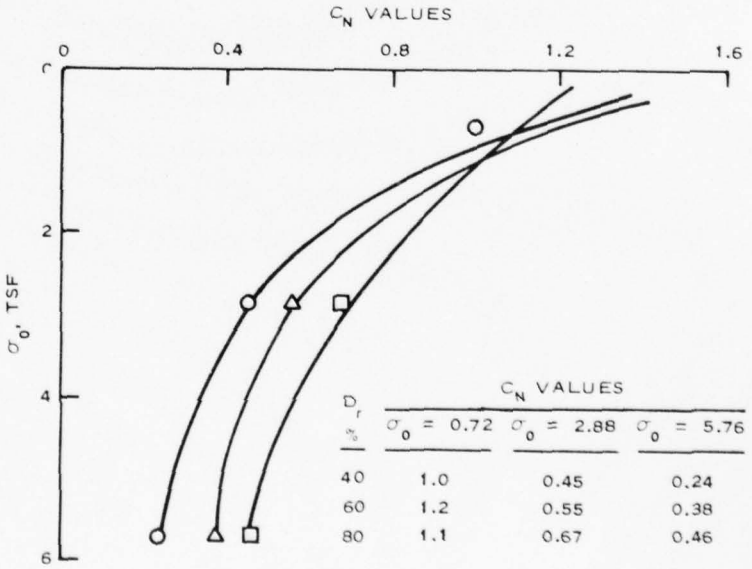

Figure A-2. C_N-values versus overburden pressures for Reid-Bedford Model sand

APPENDIX B: DEVIATOR STRESS AND PORE PRESSURE RESPONSES VERSUS AXIAL STRAIN AND Q-P EFFECTIVE STRESS PATHS

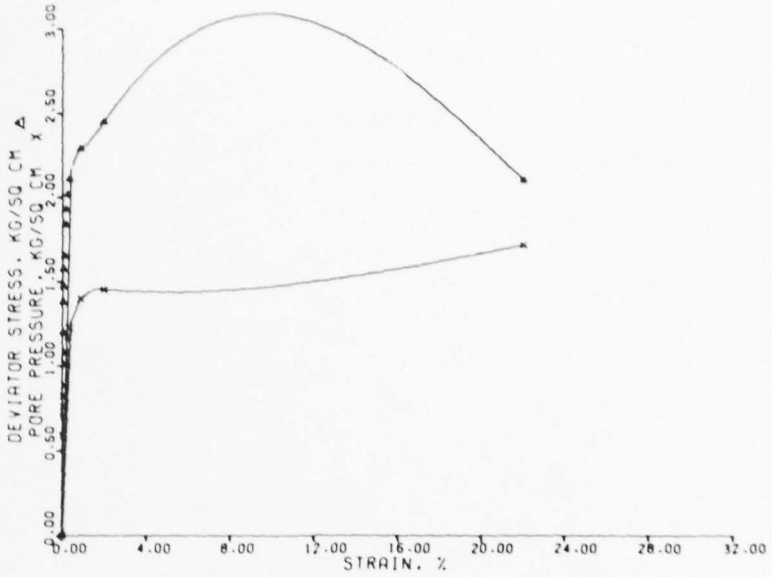

a

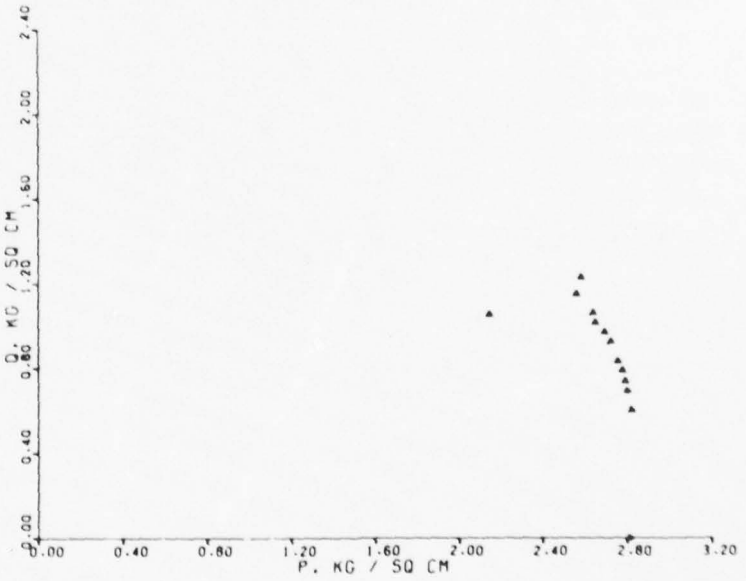

b

Figure B-1. Specimen RB20-40-2 (W = 6%)

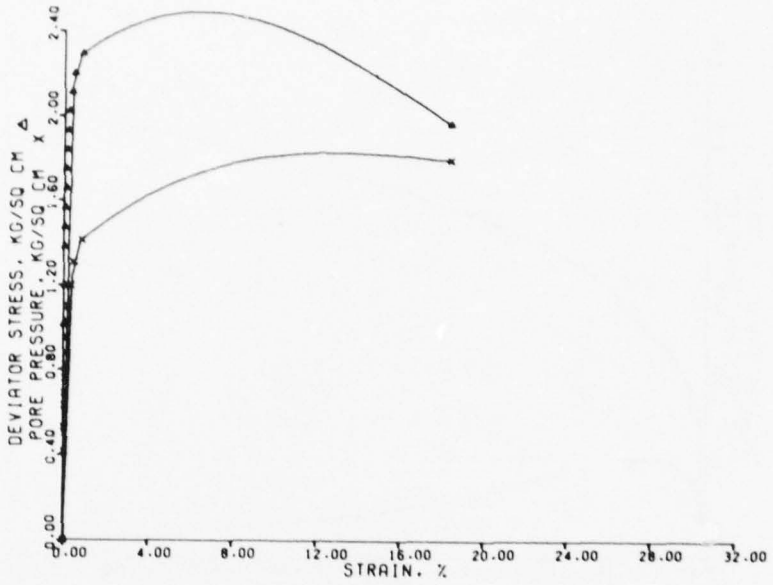

a

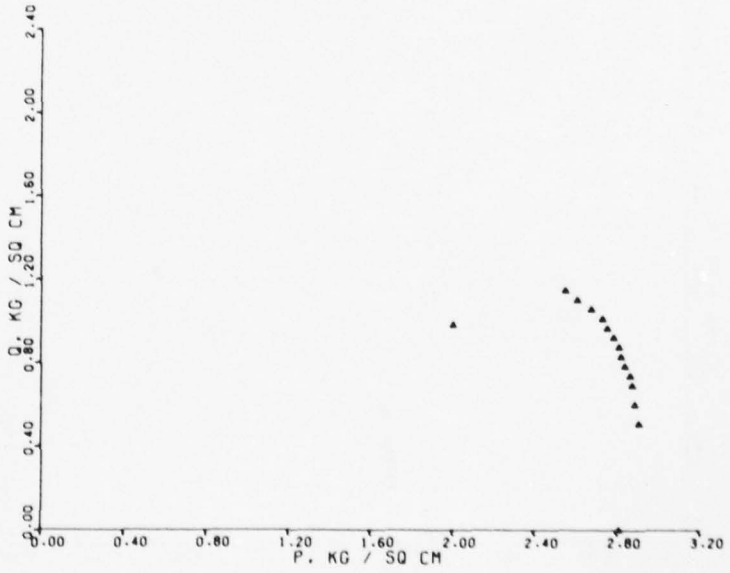

b

Figure B-2. Specimen RB20-40-3 (W = 4%)

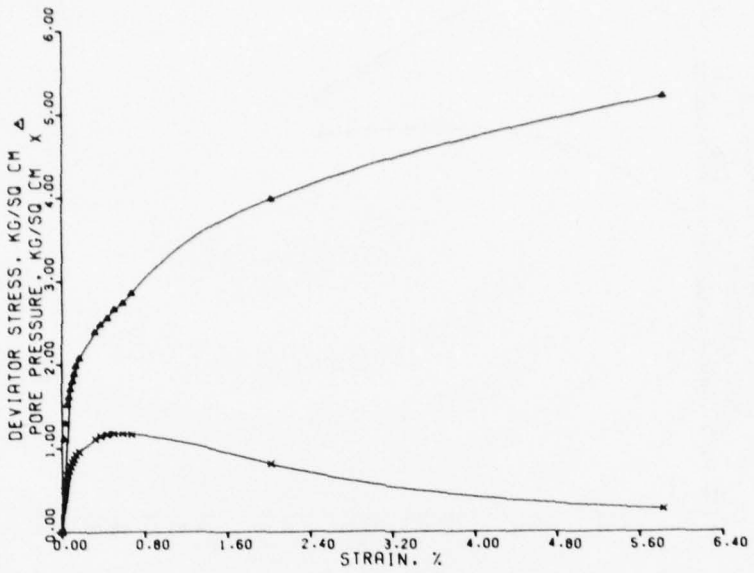

a

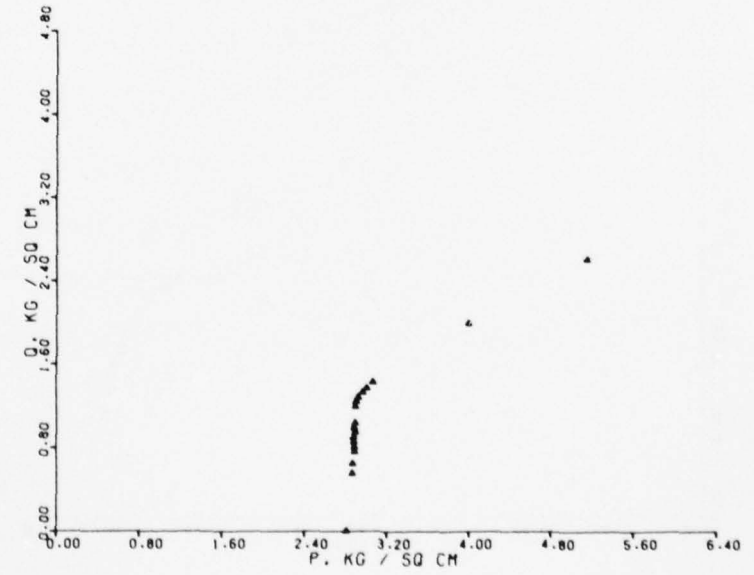

b

Figure B-3. Specimen RB30-40-4 (W = 6%)

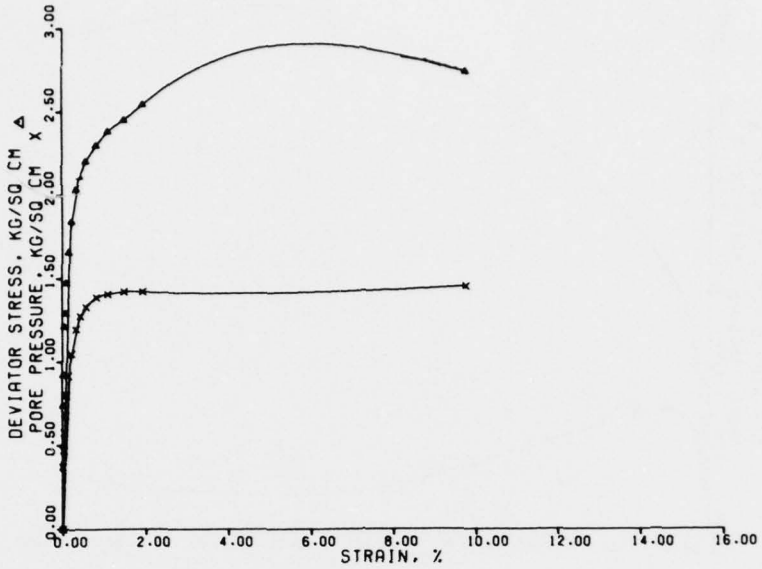

a

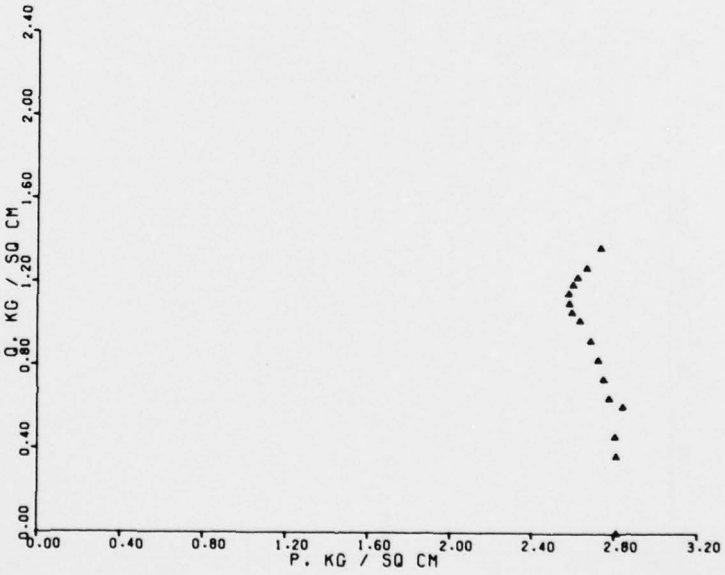

b

Figure B-4. Specimen RB20-40-5 (W = 4%)

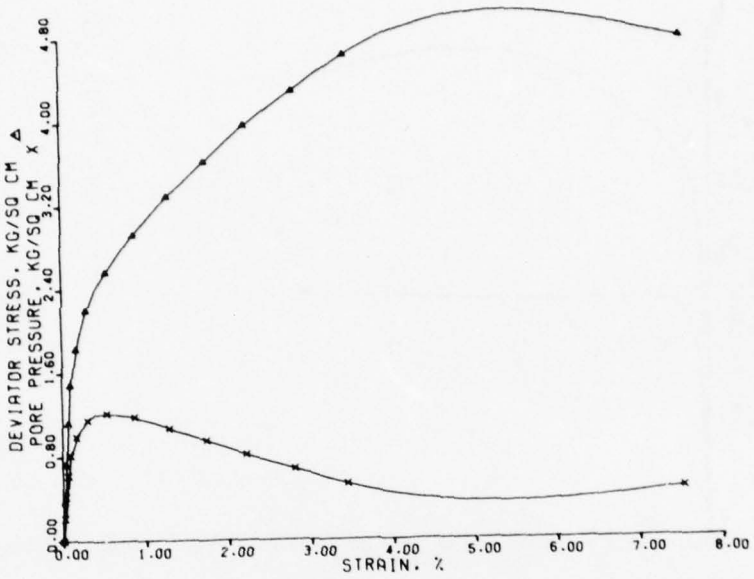

a

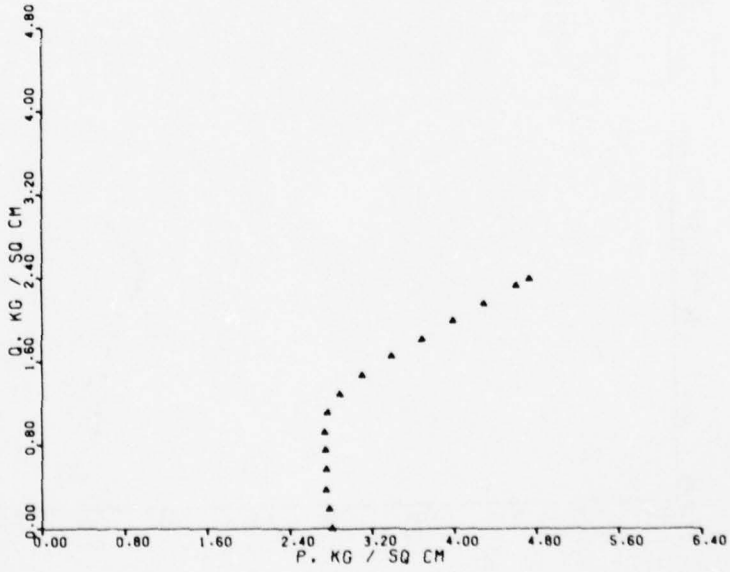

b

Figure B-5. Specimen RB30-40-6 (W = 6%)

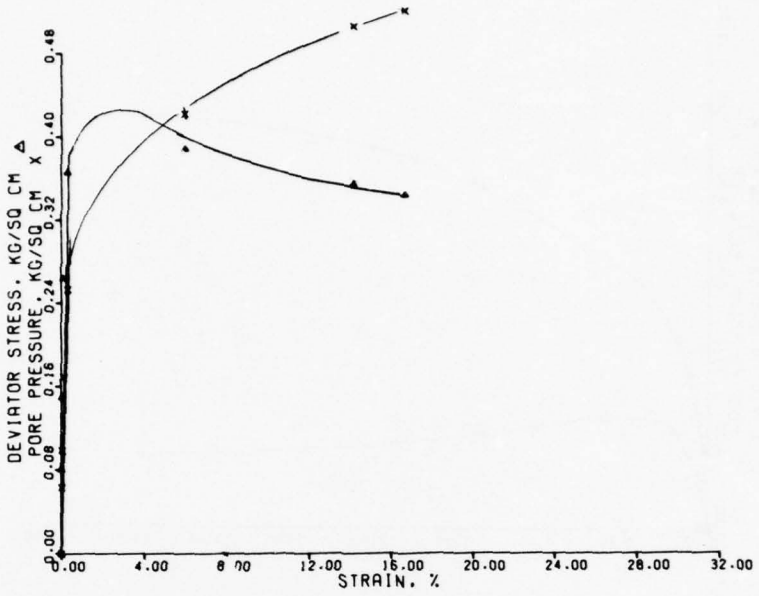

a

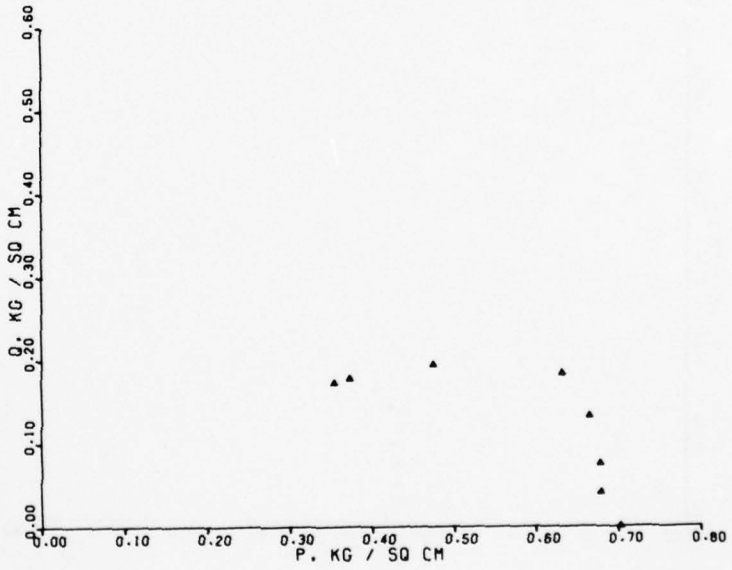

b

Figure B-6. Specimen RB15-10-8 (W = 4%)

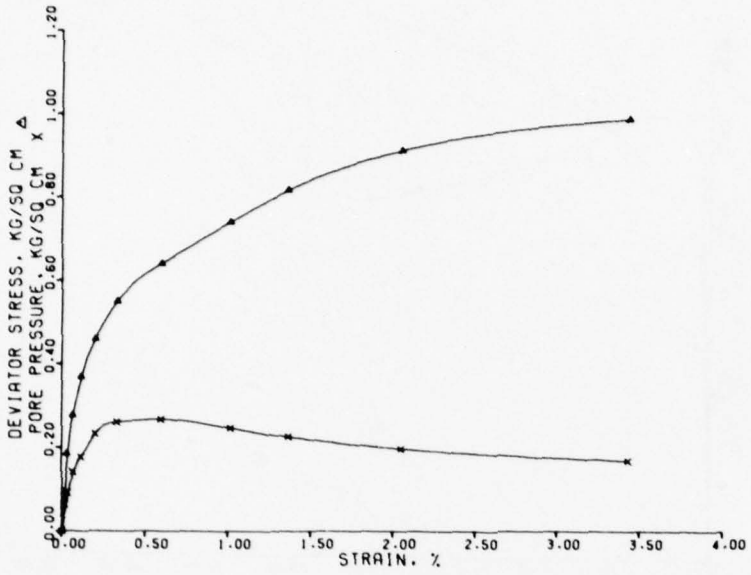

a

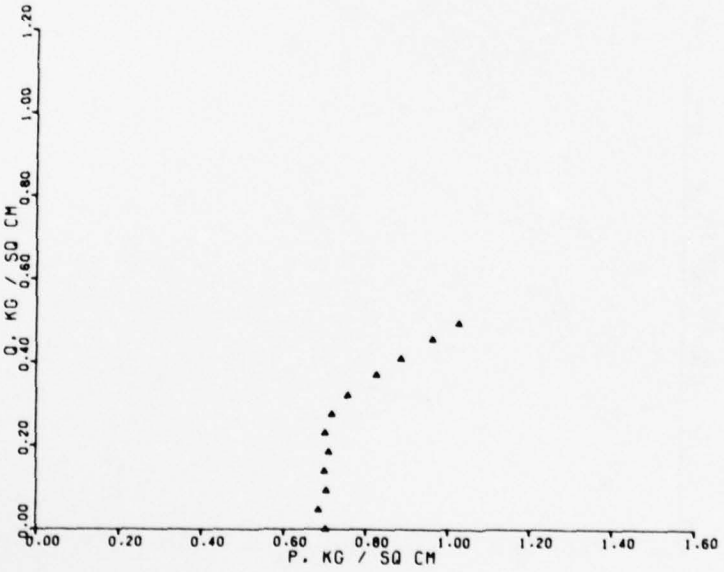

b

Figure B-7. Specimen RB20-10-9 (W = 4%)

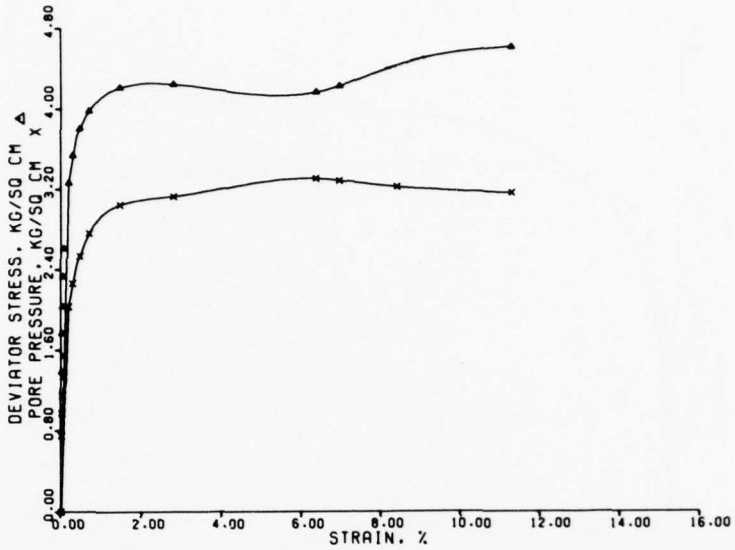

a

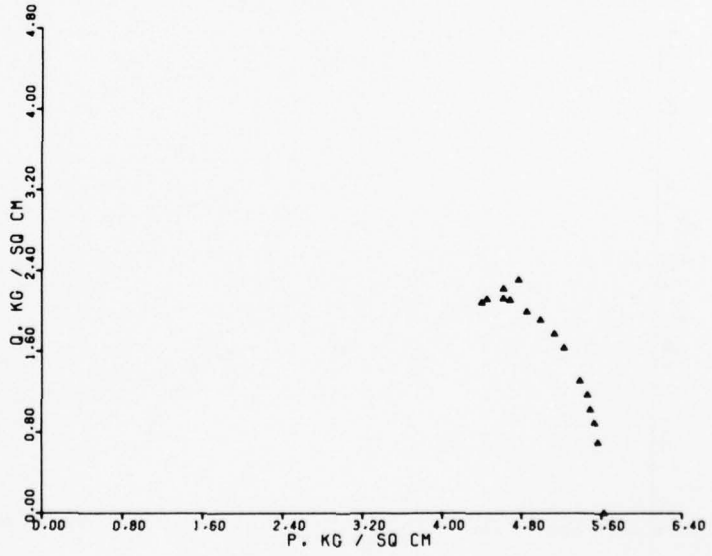

b

Figure B-8. Specimen RB20-80-10 (W = 4%)

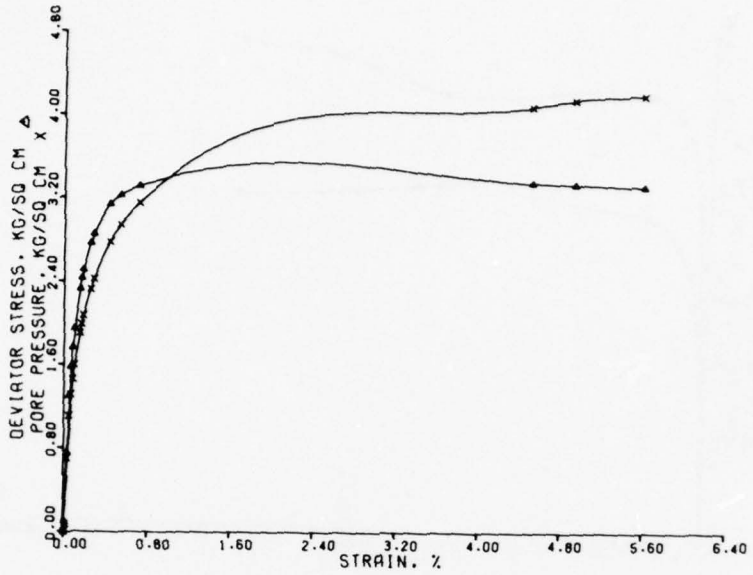

a

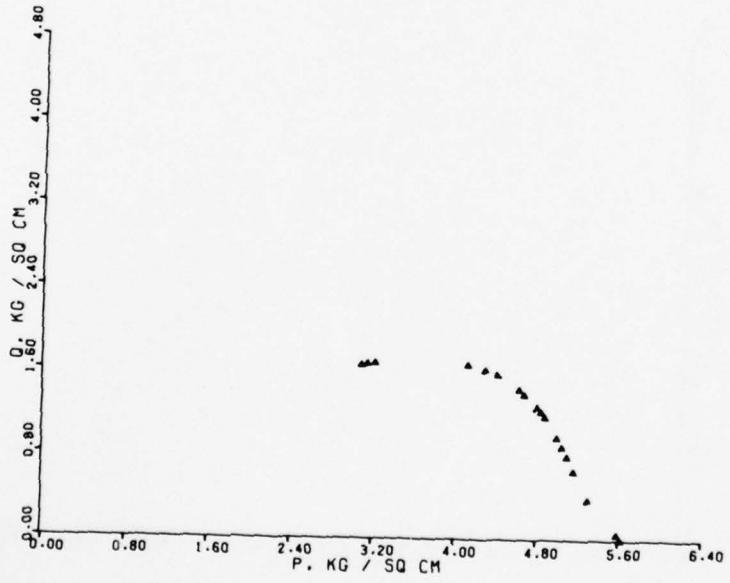

b

Figure B-9. Specimen RB15-80-11 (W = 4%)

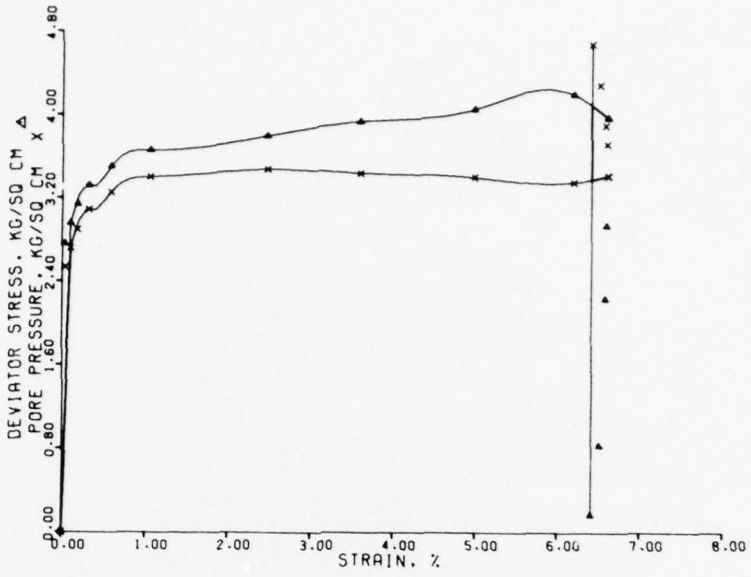

a

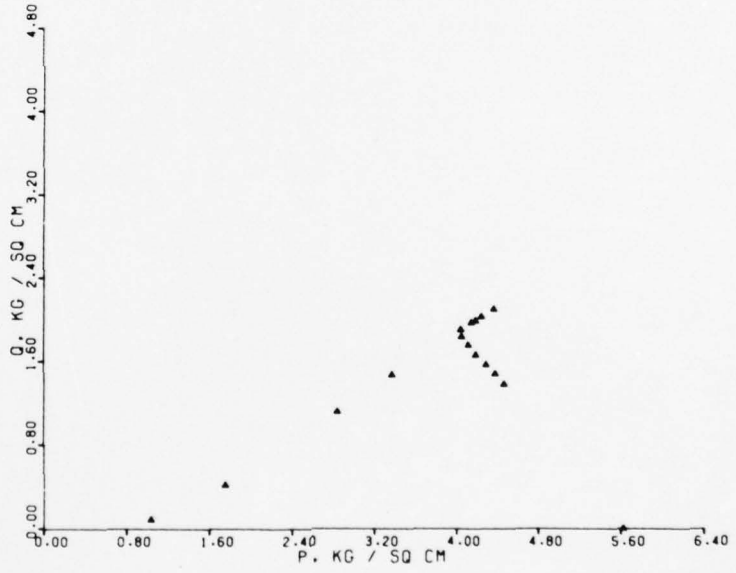

b

Figure B-10. Specimen RB25-80-12 (W = 4%)

APPENDIX C: NOTATION

B	Skempton's parameter
C_N	Correction factor for SPT
C_u	Coefficient of uniformity
D_r	Relative density
D_{50}	Diameter of a soil particle having a size greater than 50 percent (by weight) of the particles
e_c	Critical void ratio
G_s	Specific gravity
K_o	Coefficient of earth pressure at rest
R	Cyclic stress ratio, $\sigma_{cd}/2\sigma'_o$
u	Pore water pressure
γ_d	Dry unit weight
$\pm\varepsilon_a$	Single amplitude cyclic axial strain (i.e. peak-to-peak strain)
σ_c	Chamber pressure
$\pm\sigma_{cd}$	Cyclic deviator stress
σ'_o	Initial effective confining pressure; effective overburden pressure
σ'_3	Consolidation pressure
ϕ'	Effective angle of internal friction

In accordance with letter from DAEN-RDC, DAEN-ASI dated 22 July 1977, Subject: Facsimile Catalog Cards for Laboratory Technical Publications, a facsimile catalog card in Library of Congress MARC format is reproduced below.

Townsend, Frank Charles
Liquefaction potential of dams and foundations; Report 6: Laboratory strength of sands under static and cyclic loadings / by Frank C. Townsend, John P. Mulilis. Vicksburg, Miss. : U. S. Waterways Experiment Station ; Springfield, Va. : available from National Technical Information Service, 1979.
72, [16] p. : ill. ; 27 cm. (Research report - U. S. Army Engineer Waterways Experiment Station ; S-76-2, Report 6)
Prepared for Office, Chief of Engineers, U. S. Army, Washington, D. C., under Project 4A161102B52E, Task 04, Work Unit CWIS 31145.
References: p. 70-72.

1. Cyclic loads. 2. Cyclic triaxial tests. 3. Dams. 4. Foundations. 5. Liquefaction (Soils). 6. R tests (Soils). 7. Sands. 8. Static loads. I. Mulilis, John Paul, joint author. II. United States. Army. Corps of Engineers. III. Series: United States. Waterways Experiment Station, Vicksburg, Miss. Research report ; S-76-2, Report 6.
TA7.W34r no.S-76-2 Report 6